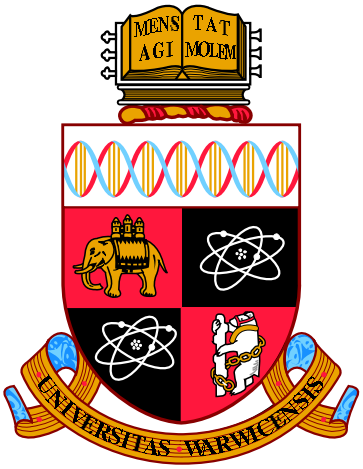

Inclusions in Smectics

by

Christopher Charles Lakey

Thesis

Submitted to the University of Warwick

for the degree of

Doctor of Philosophy

Department of Physics

July 2020

THE UNIVERSITY OF WARWICK

Contents

List of Tables **iii**

List of Figures **iv**

Acknowledgments **vi**

Declarations **vii**

Abstract **viii**

Chapter 1 General Introduction **1**

1.1 Motivation 1

1.2 Overview of Smectic Liquid Crystals 2

1.3 The Smectic Hamiltonian 7

1.3.1 The Moduli of Bending and Compression 10

1.3.2 Modelling Inclusions 15

1.4 Outline 20

Chapter 2 Membrane Microdomains in Lamellae **21**

2.1 Introduction and Motivation 21

2.2 Methodology 24

2.3 Results and discussion 29

2.3.1 A Bulk Geometry 29

2.3.2 A Semi-infinite Slab 34

2.3.3 A Finite Slab Geometry 36

Chapter 3 Swimmers in Smectics **47**

3.1 Introduction 47

3.2 Methods and Theory 49
3.2.1 The Smectic-Mediated Force 49
3.2.2 Swimmer Reorientation 52
3.2.3 A Dimensionless Model 56
3.2.4 Simulation Details 58
3.2.5 Order Parameters 60
3.3 Results and Discussion 63
3.3.1 No Added Noise 63
3.3.2 Noise 79

Chapter 4 Conclusions **82**

List of Tables

2.1 Typical figures for a system with an SM L_o phase and DOPC L_d phase at 24°C and 98% relative humidity [56, 37]. We note that $s_{L_o} \simeq s_{L_d}$. 23
2.2 Dimensions of a columnar L_o inclusion in a finite slab of L_d [57] . . 44

List of Figures

1.1 Comparison of solid crystal, liquid, nematic, and smectic phases of a calamitic. 3
1.2 Representation of nematic and smectic liquid crystal phases. . 4
1.3 The different types of smectic liquid crystal. 5
1.4 The Monge representation of membranes 6

2.1 A liquid-ordered, L_o, domain in a bilayer, surrounded by liquid disordered, L_d material. 22
2.2 Side view of a columnar stack of L_o domains, surrounded by L_d, in a lamellar body. 26
2.3 A protruding column of L_o exerts a force balanced the surface tension at the LC/air interface. 28
2.4 A plot to show the agreement of the expansions for $\tau \ll 1$ and $\frac{1}{\tau} \ll 1$, for $\frac{H}{V}$, with the analytic expression. 33
2.5 Side view of L_o columns in an infinite bulk and semi-infinite slab. 35
2.6 Columnar L_o inclusion, surrounded by L_d, and between two flat, rigid, substrates. 37
2.7 A flat, rigid substrate at a distance h is equivalent to having another, identical inclusion at a distance $2h$. 38
2.8 Energy ($\mathcal{H}$) of an inclusion at different positions in the smectic. 44

3.1 Plot of the interaction potential between two similar inclusions in a smectic phase, as a function of their separation. 50
3.2 Colloidal inclusions in a smectic locally distort the layers resulting in a force, $\mathbf{F}_{\mathrm{Sm}}$. 52

3.3 A torque results if the smectic force acts on a point offset from the swimmer's centre of hydrodynamic stress. 54
3.4 A swimmer moves in the plane as a result of the combination of its own motility ($\mathbf{p}$) and the smectic force ($\tilde{\mathbf{F}}_{\mathrm{Sm}}$). 56
3.5 Centre of mass speed as a measure of the system's orientational order. 61
3.6 System energy as a measure of the system's positional order. . 62
3.7 Rough sketch of the swimmers in smectics phase diagram. . . 65
3.8 Correlation plots and simulation snapshots for realisation of $(S, \tau) = (0, 1)$. 67
3.9 Correlation plots and simulation snapshots for realisation of $(S, \tau) = (0.1, 1)$. 68
3.10 Correlation plots and simulation snapshots for realisation of $(S, \tau) = (1, 10)$. 69
3.11 Correlation plots and simulation snapshots for realisation of $(S, \tau) = (1, 0.1)$. 70
3.12 Correlation plots and simulation snapshots for realisation of $(S, \tau) = (1, 1)$. 71
3.13 Correlation plots and simulation snapshots for realisation of $(S, \tau) = (10, 1)$. 72
3.14 The parameter choices for which we examine change in order with run time, and for which we examine the effect of noise on system order. 73
3.15 Plots of change in system order ($\Phi(t)$ and $\mathrm{H}(t)$) with respect to model run time, for $(\tau, S) \in \{(1, 0.01), (1, 0.1), (1, 1), (1, 10)\}$. . 74
3.16 Plots of change in system order ($\Phi(t)$ and $\mathrm{H}(t)$) with respect to model run time, for $(\tau, S) \in \{(0.01, 1), (0.1, 1), (10, 1), (100, 1)\}$. 75
3.17 Plots of change in system order ($\Phi(t)$ and $\mathrm{H}(t)$) with respect to model run time, for $(\tau, S) \in \{(-1, 0.01), (-1, 0.1), (-1, 1), (-1, 10)\}$. 77
3.18 Plots of change in system order ($\Phi(t)$ and $\mathrm{H}(t)$) with respect to model run time, for $(\tau, S) \in \{(-0.01, 1), (-0.1, 1), (-10, 1), (-100, 1)\}$. 78
3.19 Plots of change in time-averaged system order ($\bar{\Phi}$ and $\bar{\mathrm{H}}$) with increase in orientational noise, for $(\tau, S) \in \{(0.1, 1), (1, 1), (10, 1), (1, 10)\}$. 80

Acknowledgments

I would like to thank foremost, my supervisor, Matthew Turner. Without his enormous and vital guidance, none of the work to follow could have been done.

The office of PS001, and the varied inhabitants thereof must also be acknowledged. It has been a wonderful place to work, and they have often been wonderful people to work in proximity to.

I am grateful to the members of the soft matter and theory groups, for engaging talks, valuable discussion, and entertaining diversion.

To my friends in Warwick, and the members of Warwick Mountains, I am thankful for every pint shared, and every summit conquered. These evenings in pubs and weekends in the hills, have been the butter to this PhD's toast.

Izaak - I shall always remember our flat, with its sweeping views across Kenilworth. Thank you for sharing this sanctuary with me these past years.

Charlotte - you kept me sane.

Finally, I am forever indebted to my parents. Your unwavering support through these 9 years of University, plus the 18 long years beforehand, can never be fully acknowledged, nor repaid.

This thesis was typeset with LaTeX 2$_\varepsilon$[1] by the author.

[1] LaTeX 2$_\varepsilon$ is an extension of LaTeX. LaTeX is a collection of macros for TeX. TeX is a trademark of the American Mathematical Society. The style package *warwickthesis* was used.

Declarations

This thesis is submitted to the University of Warwick in support of my application for the degree of Doctor of Philosophy. It has been composed by myself and has not been submitted in any previous application for any degree.

The work presented (including data generated and data analysis) was carried out by myself.

The material in Chapter 2 will soon be submitted to a journal for publication.

Abstract

Continuum models describe the interactions between inclusions in smectic liquid crystals. We use such models to describe two systems where objects disrupt the layer-spacing in smectics.

Bilayer membranes composed of a mixture of saturated and unsaturated phospholipids can phase-separate, forming liquid-ordered domains rich in saturated lipids. Recent experiments have shown that lamellar stacks of such membranes form columns of liquid ordered domains, aligned across many neighbouring lamellae. Continuum models suggest that such a columnar arrangement is not energetically favourable. Instead, domains would be expected to be laterally offset from those in vertically neighbouring layers, to minimise the cost of their membrane deformation. We provide an explanation for this apparent contradiction by introducing interfacial energies between the phases, for which we provide bounds.

The presence of embedded particles, of diameter comparable to the smectic layer spacing, results in a distortion of the smectic ordering. We consider a system of self-propelling colloidal particles ("swimmers") in a smectic liquid crystal. These swimmers are confined between the smectic layers, but interact with swimmers in other layers via the distortions that they induce in the smectic ordering. We find that the motion of these swimmers is then controlled by a combination of their own motility and the forces that they experience from the smectic mediated interaction potential, giving rise to rich dynamical behaviour.

Chapter 1

General Introduction

1.1 Motivation

Order arises in nature in many ways and across all scales. In this work we seek to understand how order arises in certain microscopic, layered systems - smectic liquid crystals. The two systems we will look at in the coming chapters are quite different, but how their layered structure induces the development of additional order is the common theme that unites them.

Phospholipid bilayers are structures essential to the cellular world. Not only do they form the boundary between cells and their environments, but they are also the site where a multitude of vital processes take place [4]. For all that the structure of cell membranes in the form of the fluid mosaic model has been known for around fifty years [51], much is still unknown. A persistent question is how information passes across membranes via trans-membrane proteins or other means [32].

Under appropriate conditions, it has been observed that bilayers comprised of mixtures of saturated and unsaturated lipids can phase separate into fluid and ordered phases. This results in the formation of roughly circular, liquid-ordered domains, which have been linked to lipid rafts in cell membranes [50]. These rafts are thought to provide more stable platforms in the cell membrane, where functionally trans-membrane proteins may be grouped [7].

Recent work by Parikh and collaborators [56] has shown that ordered domains in stacks of bilayers can align into columnar arrangements spanning

many neighbouring layers. The energetic cost of aligning these microdomains is not yet well understood. Stacked bilayer membranes, so called lamellar bodies, are important in biological systems such as chloroplasts [23, 60], and are widely used in the study of membrane structure by x-ray diffraction or NMR spectroscopy [7]. The potential of aligned domains in lamellar systems for the construction of stable protein assemblies, capable of acting in series across multiple membranes, has many potential applications, and so more information on the stability of these structures would be valuable in realising these [29, 7, 57]. Continuum models of smectic liquid crystals offer a route to better understand the origin of the morphology of these aligned domains.

Lamellar systems occur in many places in nature. There exists work, both theoretical [62, 49] and some experimental [43] looking at the effect of introducing inert foreign particles into such systems. However, there is currently conspicuously little research that has so far explored the possible consequences of introducing auto-motile particles into such a system [21].

Continuum theory suggests that elastic deformation of the layer structure of a stack of membranes by a colloidal inclusion within them might effect a force upon those inclusions, acting to reposition them within the layers [63]. Such a force acting upon swimming micro-organisms has the potential to result in complex dynamics, as the smectic environment of the layered system affects the trajectories of the embedded swimmers. We are particularly interested in whether such a system could produce collective motion of the motile inclusions without the need for explicit co-alignment in the model.

Micro-swimmers live and move in an enormous range of complex natural environments, and in the microscopic world collective motion of organisms can have many advantages [41]. We hope to better understand some of the factors which could induce the emergence of collective motion for swimmers in smectics.

1.2 Overview of Smectic Liquid Crystals

Liquid crystal is the name given to substances with molecular arrangements somewhere between those of liquids and of solid crystals. Unlike solid crystals, they have liquid-like isotropy in at least one spatial dimension; and unlike

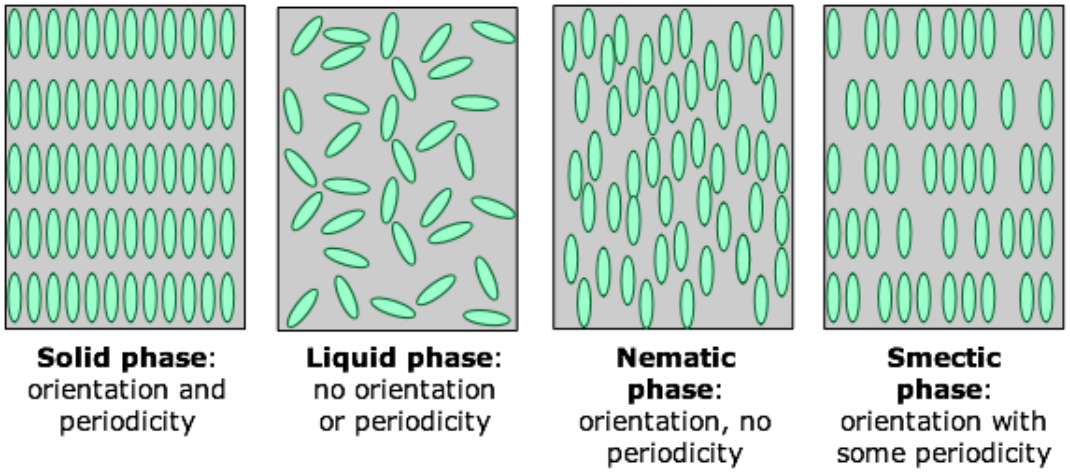

Figure 1.1: Comparison of solid crystal, liquid, nematic, and smectic phases of a calamitic. Note the orientational order preserved through the solid and liquid-crystaline phases is lost in the liquid [54].

isotropic liquids, their molecules exhibit anisotropic orientational ordering as one would see in a crystal. An intermediate phase, they have varied physical properties which one might associate with either solid crystals or liquids. [13]

A broad church, there are many sub-classifications of liquid crystal. Generally they are divided by whether their formation is temperature dependent (so-called thermotropic liquid crystals) or concentration dependent (lyotropic). The former group is further categorised by the molecular shape of the constituent particles: those comprised of rod-like particles are called calamitic, those of disc-like particles called discotic [18]. Thermotropic calamitic liquid crystals are then typically subdivided depending on the geometric arrangement of the molecules. These mesophases include nematics, which have long range orientational order of the molecules but no positional order; cholesterics, where the orientation of the aligned particles changes along one dimension yielding a helical structure; and smectics, whose oriented particles are arranged in discrete layers, typically one or two particles thick, with a uniform spacing between layers. It is this last phase, the smectic, which our work here focusses on.

The originally identified phase and the one given the name *smectic* was what we now call the smectic-A phase. A smectic-A is comprised of on-average flat layers of molecules which are all oriented normal to the plane of the layer.

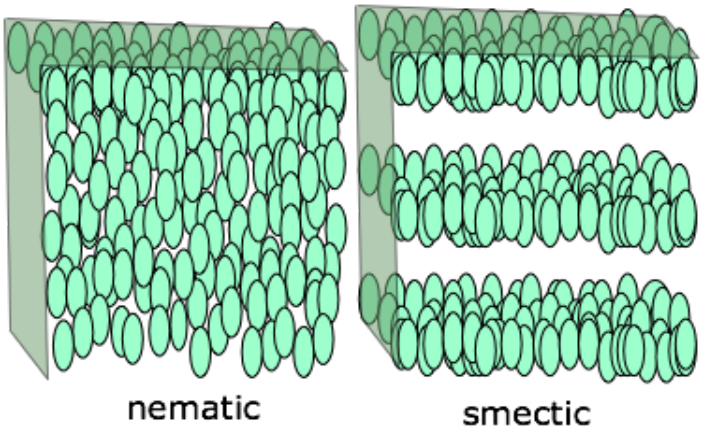

Figure 1.2: Representation of nematic and smectic liquid crystal phases. A smectic liquid crystal is one in which molecules are arranged into layers, comprised of particles with the same orientation. This is like a nematic phase, but with some periodicity. Each layer behaves as a two dimensional fluid [54].

Within each layer the molecules have no long-range positional order and are not fixed in place - indeed each layer behaves much as a two-dimensional liquid [16].

Following the discovery of the original smectic-A phase, a number of other smectic phases were identified. Some of these phases were subsequently determined to actually be crystalline phases, rather than true liquid crystals, however many of them are often still referred to as "smectic". In this work, we focus our attention exclusively on smectic liquid-crystals. The other smectic liquid crystal phases can be grouped into tilted smectics; hexatic smectics; and (necessarily) tilted, hexatic smectics [52].

Whereas smectic-A liquid crystals are composed of molecules aligned with a director normal to their layer, the each of the molecules in a smectic-C phase are tilted at an angle to the normal. This tilt is described by a vector $\mathbf{c} = (\hat{\mathbf{c}}, \omega)$, where $\hat{\mathbf{c}}$ is the projection of $\mathbf{c}$ onto the plane of the layer, and ω is the tilt angle of $\mathbf{c}$ from the layer normal. The $\mathbf{c}$ and $-\mathbf{c}$ states are not equivalent and so there is a loss of symmetry in the smectic-C phase versus the smectic-A. This means that $\mathbf{c}$ can also act as an order parameter between these phases [16, 52].

Both the smectic-A and smectic-C phases are composed of molecules arranged with a liquid-order in their layers. A class of smectics exist wherein

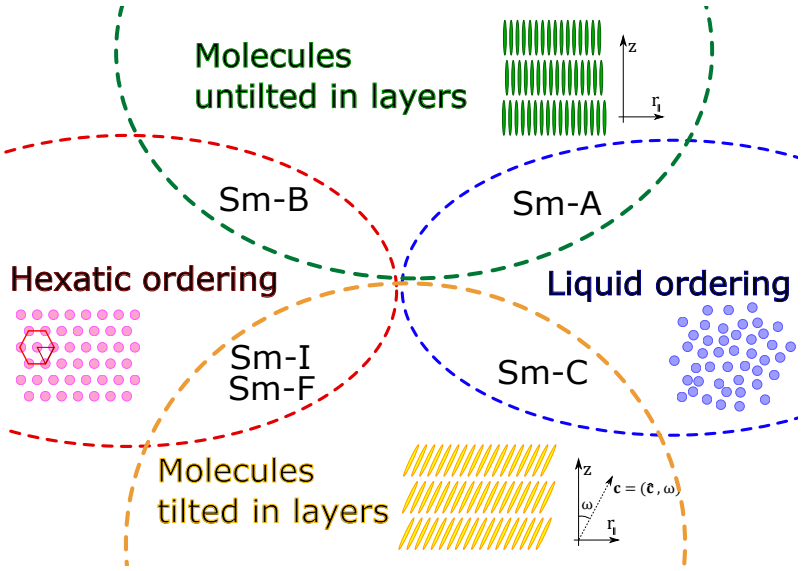

Figure 1.3: The different types of smectics arranged according to their properties: being tilted (Sm-C, Sm-F, Sm-I) or untilted (Sm-A, Sm-B) in layers; and having a liquid order (Sm-A, Sm-C) within the plane of each layer or possessing a hexatic order, with the molecules arranged on a triangular lattice relative to their neighbours (Sm-B, Sm-F, Sm-I).

the molecules are packed with a local hexagonal symmetry in their layers. Known as hexatic smectics, whilst their layers still behave as two-dimensional liquids over long lengthscales, the molecules are locally arranged on a triangular lattice [52]. These hexatics can be made up of layers of untilted molecules - the smectic-B phase; or molecules with a tilt and $\mathbf{c}$ vector - the smectic-F and smectic-I phases. The smectic-F and smectic-I phases differ in the direction of $\hat{\mathbf{c}}$ relative to the triangular lattice, with the smectic-I phase having $\hat{\mathbf{c}}$ parallel to the sides of the triangular lattice, and $\hat{\mathbf{c}}$ orthogonal to those sides in the smectic-F phase [16].

It is worth remarking that tilted smectics composed of chiral molecules exhibit a twist whereby rather than the tilt being uniform across the layers, it instead precesses, altering the direction of $\hat{\mathbf{c}}$ by a fixed angle about the z-axis from one layer to the next. These chiral phases are indicated by the appending of an asterisk to the corresponding tilted phase: sm-C*, sm-F*, sm-I*.

Each of these types of smectic we have mentioned has distinct symmetries, and so behaves in a physically different manner. For our purposes we will see that the smectic-A phase is the most natural candidate to consider,

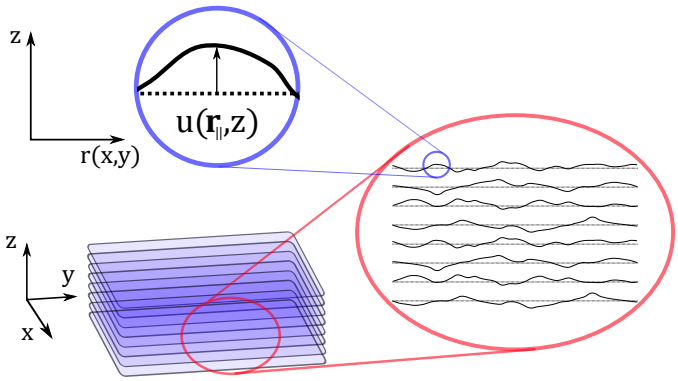

Figure 1.4: The Monge representation gives us a displacement field, $u(\mathbf{r}_{||}, z)$, of membranes from their average flat position within a stack of membranes.

and we will restrict our attention to it alone in this work.

Many smectics are made up of amphiphillic molecules in an aqueous or organic solvent, and their charge-driven attraction to one-another combined with their repulsion from the surrounding medium, results in a very stable layered structure. [1] The fluidity of the layers does afford them some flexibility, however, allowing them to bend and splay. As such, it is often worth thinking of them as being comprised of stacks of fluid membranes [16].

The Monge parametrisation is typically the most used coordinate system used when describing membranes. Assuming the membrane is almost flat, it allows us to easily locate any membrane displacement in a single parameter. We define the flat membrane as resting on an (x, y)-plane, with the other membranes in the stack offset from it in z. The displacement of the membrane, in z, from this flat position, at a given point,$\mathbf{r} = (x, y)$, can be given by the scalar parameter $u(\mathbf{r}, z)$[49, 16]. This proves to be an invaluable quantity when quantifying the energy of a smectic system.

[1] Indeed, the nature of surfactants to form smectic phases is where the phase gets it name, from the latin *smecticus* for something cleansing - a soap, that is.

1.3 The Smectic Hamiltonian

Much of the work that follows considers the energy that arises as a consequence of somehow perturbing the layer structure of a smectic liquid crystal. To best do this, it makes sense to utilise a description of a smectic which quantifies its elastic free energy in terms of the displacement of its layers.

The smectic displacement field is given as $u(r_{||}, z)$.

We can express the variations in u about a point $\mathbf{r}$ by a Taylor expansion [16]

$$\delta u(r_{||}, z) = \nabla u \cdot \delta\mathbf{r} + \tfrac{1}{2}\left(\delta\mathbf{r} \cdot \nabla\nabla u\right) \cdot \delta\mathbf{r} + O(\delta\mathbf{r}^3). \tag{1.1}$$

We can more easily identify those terms which may contribute to the elastic free energy by breaking this down into components in the x, y-plane and perpendicular to the plane, z:

$$\begin{aligned} \delta u(r_{||}, z) \;=\; & \delta z\, \partial_z u \;+\; \delta\mathbf{r}_{||} \cdot \nabla_{||} u \;+\; \frac{1}{4}\,\delta r_{||}^2\, \nabla_{||}^2 u \\ & +\; \frac{1}{2}\left(\frac{\delta x^2 - \delta y^2}{2}\left(\partial_x^2 u - \partial_y^2 u\right) + 2\delta x \delta y\left(\partial_x \partial_y u\right)\right) \\ & +\; \delta z\, \delta\mathbf{r}_{||} \cdot \partial_z \nabla_{||} u \;+\; \frac{1}{2}\,\delta z^2\, \partial_z^2 u \;+\; O(\delta\mathbf{r}^3). \end{aligned} \tag{1.2}$$

Examining the terms in this expansion we identify them as follows: the first term is a dilation (or compression) of the layers, the second term corresponds to a tilt, the third term is the splay of the layers, the fourth term is a saddle-splay deformation of the layers, the fifth as the bend of the layers, and the sixth as the rate of change of the layer dilation [16, 52].

The elastic free energy of a smectic is invarient to actions which amount only amount to a change in co-ordinate system and do nothing to change the organisation of the layers relative to oneanother. That is to say, uniform translations, rotations, and mappings of the form $x_i \to -x_i$. As such, any terms which violate this invariance cannot enter the elastic free energy [10].

The second term in (1.2) corresponds to a tilt. The elastic free energy is only concerned with changes to the layer spacing, which a tilt will preserve. As such the free energy is invarient to such an action and so this term will not

enter [16].

Linear terms are also precluded from the elastic free energy as they change sign under inversion symmetry operations. The lowest order terms allowed, therefore, are those of quadratic order [14]. To obtain the independent terms that will form the elastic free energy we will need to take the scalar square of the remaining terms in (1.2).

The squares of the first, third and sixth terms are straightforward. The square of the fourth term in (1.2), the saddle-splay term, gives

$$\left(\tfrac{\delta x^2-\delta y^2}{2}\left(\partial_x^2 u-\partial_y^2 u\right)+2\delta x\delta y\left(\partial_x\partial_y u\right)\right)^2=\left(\tfrac{\delta x^2-\delta y^2}{2}\right)^2\left(\partial_x^2 u-\partial_y^2 u\right)^2+... \\ ...+2\left(\delta x^2-\delta y^2\right)\left(\partial_x^2 u-\partial_y^2 u\right)\delta x\delta y\left(\partial_x\partial_y u\right)+4\left(\delta x\delta y\left(\partial_x\partial_y u\right)\right)^2. \quad (1.3)$$

Omitting the unacceptable linear second term, we can rewrite this as

$$\left(\tfrac{\delta x^2-\delta y^2}{2}\right)^2\left(\partial_x^2 u-\partial_y^2 u\right)^2+4\left(\delta x\delta y\left(\partial_x\partial_y u\right)\right)^2= \\ \left(\tfrac{\delta x^2-\delta y^2}{2}\right)^2\left(\partial_x^2 u+\partial_y^2 u\right)^2+4\left(\left(\delta x\delta y\left(\partial_x\partial_y u\right)\right)^2-\left(\tfrac{\delta x^2-\delta y^2}{2}\right)^2\left(\partial_x^2 u\partial_y^2 u\right)\right). \quad (1.4)$$

In this form, then, we observe that the first term is a splay term, and so not independent of the square of the third term in (1.2). Meanwhile the second term in (1.4) can be identified via Gauss' Theorem as a surface term and so, consequently, will also not contribute to the bulk elastic energy.

The square of the fifth term, representing a bend, is given by

$$\left(\delta z\,\delta\mathbf{r}_{||}\cdot\partial_z\nabla_{||}u\right)^2=\delta z^2\delta r_{||}^2(\partial_z^2 u)(\nabla_{||}^2 u)+2\delta z^2\delta x\delta y\left(\partial_z\partial_x u\right)\left(\partial_z\partial_y u\right). \quad (1.5)$$

Here, we identify the first term as a product of the splay and rate of change of dilation, whilst the second is, again, a surface term [16, 52].

So we can now construct an expression for the elastic free energy of a smectic by a combination of these permissible terms

$$F_{\mathrm{el}}=\frac{B}{2}\left(\partial_z u\right)^2+\frac{K}{2}\left(\nabla_{||}^2 u\right)^2+\frac{K'}{2}\left(\partial_z^2 u\right)^2+\frac{K''}{2}\left(\nabla_{||}^2 u\right)\left(\partial_z^2 u\right). \quad (1.6)$$

Here we write the moduli (B, K, K', K'') with a factor $\frac{1}{2}$ by convention, and by analogy to Hooke's law. The relative magnitudes of these moduli vary according to the properties of the particular smectic.

The last two terms of (1.6) are often omitted from the elastic free energy. In practice, however, as these terms only contribute if u varies in z, they tend to be unobservable owing to their being dominated by the lower order dilation term, $\frac{B}{2}\left(\partial_z u\right)^2$ for long range distortions [16, 33, 10].

Finally, for completeness, we recall that our free energy contains no terms of the form $\left(\partial_x u\right)^2$ and $\left(\partial_y u\right)^2$. It is important to note that a consequence of this is loss of rotational invariance. A uniform rotation about an axis in the plane of the layer or a bending of the layers (such as could be introduced by an undulation instability) leads to a change in the effective layer spacing in z. This alteration to the arrangement of the material incurs a second order contribution to the free energy[16]. To see this we consider a case where the layers of the smectic are rotated about, say, the y-axis by a small angle, θ:

$$\partial_z u = 0, \tag{1.7}$$

$$\partial_x u = \theta. \tag{1.8}$$

At lowest order we see no change in u with respect to z, but the true distance between the layers has increased from an unperturbed separation of a to $a^* = \delta a$, where

$$\delta a = a\left(1 - \cos\theta\right) \approx -\frac{a}{2}\left(\partial_x u\right)^2. \tag{1.9}$$

So we have a small second-order change. And for a general rotation about an axis in the x, y-plane, we have

$$\delta a = -\frac{a}{2}\left(\left(\partial_x u\right)^2 + \left(\partial_y u\right)^2\right) = -\frac{a}{2}\left(\nabla_{||} u\right)^2. \tag{1.10}$$

The thickness change resulting from such a rotation, would result in a small increase to the free energy of $\frac{1}{2}a^{*2}B$ that our linear elastic free energy does not capture. A change to the compression term in (1.6) restores rotational invariance, though at the cost of solubility [16, 11, 10]:

$$\frac{B}{2}\left(\partial_z u\right)^2 \rightarrow \frac{B}{2}\left(\partial_z u - \tfrac{1}{2}\left(\nabla_{||} u\right)^2\right)^2. \tag{1.11}$$

Whilst it is true that this omitting the anharmonic correction fails to strictly preserve the invariance of the free energy under rigid rotations, its inclusion often precludes the finding of an analytical solution to the energy [46].

For our purposes, we will neglect the higher order terms in (1.6) as well as the non-linear correction (1.11). Their inclusion would make our analysis unwieldy at best and intractable at worst, whilst the error due to their omission should be very small, as we shall see the deformations we examine in our work are small relative to the layer spacing of the smectic [33, 8].

An integral of our linear free energy over the volume of the system yields the so-called Landau-de Gennes Smectic Hamiltonian [16]:

$$\mathcal{H} = \frac{1}{2}\int d^3\mathbf{r} B(\partial_z u)^2 + K(\nabla_{||}^2 u)^2 \tag{1.12}$$

This captures the elastic energy of the bulk system.

We will define the variable λ, here:

$$\lambda := \sqrt{\frac{K}{B}}. \tag{1.13}$$

This is the smectic penetration length. A quantity typically of the order of the layer spacing of the smectic, and which is the length scale over which the bending of the layers is comparable to their compression [62].

1.3.1 The Moduli of Bending and Compression

The bending modulus is straightforwardly given by

$$K = \frac{\kappa}{s}, \tag{1.14}$$

where s is the mean layer spacing in the smectic stack (the water gap in Figure 2.1), and κ is the rigidity of a single layer, typically $\sim 20\mathrm{k_B T}$ [55].

A self-consistent expression for B can be obtained following Helfrich (1978) [28, 45].

First, we must recognise that this compression modulus, B, is a bulk modulus for the smectic. By definition, the bulk modulus is given by $B = -V\frac{dP}{dV}$, for volume V and pressure P. Given that at a constant temperature, the rate of change of Helmholtz free energy with respect to volume is proportional to pressure ($\left(\frac{\partial F_{\mathcal{H}}}{\partial V}\right)|_T = -P$), the bulk modulus at constant temperature can be written as

$$B = V\frac{\partial^2 F_{\mathcal{H}}}{\partial V^2}. \tag{1.15}$$

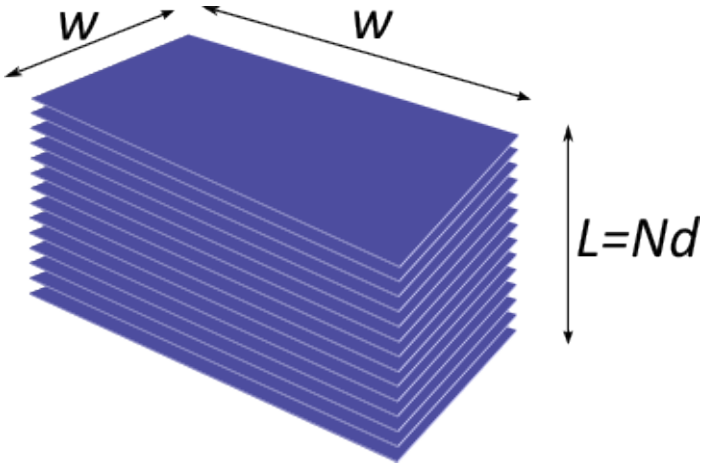

$V = LA$, is the volume of a smectic composed of N layers where $L = Nd$ is the height of the stack, and A is the surface size, or area of each membrane. Smectics are invariant in the plane, thus any change in volume is going to be due to a change in the layer spacing d. If we let $w = \sqrt{A}$ be a factor of length inverse to surface size, then we can write

$$B = \frac{d}{Nw^2}\frac{\partial^2 F_{\mathcal{H}}}{\partial d^2}. \tag{1.16}$$

As the value of B does not depend on system size (so long as we are in the bulk), from here on, rather than considering the whole stack, we will consider only a typical single membrane in the stack (so setting $N = 1$. This will have the advantage of making calculation easier.

We identify that the mean membrane separation, d, is going to be of the order of the membrane displacement, $u(\mathbf{r})$. Since the membranes in a smectic cannot overlap, the membrane displacement cannot exceed the membrane separation, indeed we suggest that the mean membrane separation be equal

to the root mean squared membrane displacement:

$$\sqrt{\langle u(\mathbf{r})^{\mathbf{2}}\rangle} = d. \tag{1.17}$$

We now want an expression for $\sqrt{\langle u(\mathbf{r})^{\mathbf{2}}\rangle}$. For a single membrane we have a Hamiltonian composed of terms describing a harmonic potential, ku^2 (with k a spring constant); the deformation of the surface against tension, $\sigma\left(\nabla u\right)^2$ (σ being the tension); and the bending of the membrane, $\kappa\left(\nabla^2 u\right)^2$ (where κ is the membrane rigidity):

$$\mathcal{H} = \frac{1}{2}\int d^2\mathbf{r}\left(ku^2 + \sigma\left(\nabla u\right)^2 + \kappa\left(\nabla^2 u\right)^2\right). \tag{1.18}$$

Our membrane is confined, as it is in a smectic, it is also tensionless ($\sigma = 0$) as it is assumed to be at equilibrium:

$$\mathcal{H} = \frac{1}{2}\int d^2\mathbf{r}\left(ku^2 + \kappa\left(\nabla^2 u\right)^2\right). \tag{1.19}$$

Defining forward and reverse Fourier transformations as follows, we move to Fourier space.

$$u_{\mathbf{q}} = \frac{1}{w^2}\int d^2\mathbf{r} e^{i\mathbf{q}\cdot\mathbf{r}} u(\mathbf{r}) \tag{1.20}$$

$$u(\mathbf{r}) = \frac{w^2}{(2\pi)^2}\int d^q\mathbf{r} e^{-i\mathbf{q}\cdot\mathbf{r}} u_{\mathbf{q}} \tag{1.21}$$

Which gives the Hamiltonian in terms of $u_{\mathbf{q}}$,

$$\mathcal{H} = \frac{w^2}{(2\pi)^2}\int d^2\mathbf{q}\left(\frac{w^2}{2}\left(k + \kappa q^4\right)|u_{\mathbf{q}}|^2\right). \tag{1.22}$$

We take the ensemble average of $\mathcal{H}$, which we know is equal to $\frac{k_B T}{2}$, by equipartition of energy,

$$\langle\mathcal{H}\rangle = \frac{w^2}{2}\left(k + \kappa q^4\right)\left\langle|u_{\mathbf{q}}|^2\right\rangle = \frac{k_B T}{2} \tag{1.23}$$

$$\implies \left\langle|u_{\mathbf{q}}|^2\right\rangle = \frac{1}{w^2}\frac{k_B T}{k + \kappa q^4}. \tag{1.24}$$

We return to real space by means of Parseval's Theorem:

$$\begin{aligned}
\left\langle u(\mathbf{r})^2 \right\rangle &= \frac{w^2}{(2\pi)^2} \int d^2\mathbf{q} \left\langle |u_{\mathbf{q}}|^2 \right\rangle && (1.25)\\
&= \frac{1}{(2\pi)^2} \int d^2\mathbf{q} \frac{1}{w^2} \frac{k_B T}{k + \kappa q^4} && (1.26)\\
&= \frac{k_B T}{2\pi} \int \frac{q dq}{k + \kappa q^4} && (1.27)\\
&= \frac{k_B T}{2\pi\sqrt{k\kappa}} \int \frac{x dq}{1 + x^4} \left(\text{ with } \; x^2 = q^2 \sqrt{\frac{\kappa}{k}} \right) && (1.28)\\
&= \frac{k_B T}{2\pi\sqrt{k\kappa}} \frac{\pi}{4} \quad (\text{ GR } 3.241(\text{ii}))\,, && (1.29)
\end{aligned}$$

so

$$\left\langle u(\mathbf{r})^2 \right\rangle = \frac{k_B T}{8\sqrt{k\kappa}} = d^2. \tag{1.30}$$

Now that we have an expression for d in terms of the spring constant, k, we want to find an expression for the free energy, F_H.

The free energy is well known to be given by the log of partition function for the system:

$$F_{\mathcal{H}} = -k_B T \log(Z). \tag{1.31}$$

This partition function, Z, is the exponential of the Hamiltonian (1.22), in terms of the the displacement field, $u_{\mathbf{q}}$, integrated over all such fields:

$$Z = \int e^{-k_B T \mathcal{H}(u_{\mathbf{q}})} D u_{\mathbf{q}}. \tag{1.32}$$

Taking the logarithm of Z allows us to bring down the integral in the Hamiltonian as follows

$$\begin{aligned}
\log(Z) &= \log\left(\int e^{-k_B T \frac{w^2}{(2\pi)^2} \int d^2\mathbf{q} \left(\frac{w^2}{2} \left(k + \kappa q^4 \right) |u_{\mathbf{q}}|^2 \right)} D u_{\mathbf{q}} \right) && (1.33)\\
&= \frac{w^2}{(2\pi)^2} \int d^2\mathbf{q} \left(\log\left(\int e^{-k_B T \left(\frac{w^2}{2} \left(k + \kappa q^4 \right) |u_{\mathbf{q}}|^2 \right)} D u_{\mathbf{q}} \right) \right). && (1.34)
\end{aligned}$$

We can compute the functional integral by GR 3.461(iii)[24],

$$\log(Z) = \frac{w^2}{(2\pi)^2}\int d^2\mathbf{q}\left(\log\left(\frac{2\pi k_B T}{w^2\left(k+\kappa q^4\right)}\right)\right) \tag{1.35}$$

$$= -\frac{w^2}{(2\pi)^2}\int d^2\mathbf{q}\left(\log\left(w^2\left(k+\kappa q^4\right)\right) - \log\left(2\pi k_B T\right)\right). \tag{1.36}$$

We evaluate the integral in the plane, and also note that as we are only interested in the free energy differences, we can neglect the constant component.

$$F_{\mathcal{H}} = -k_B T\log(Z) \tag{1.37}$$

$$= k_B T\frac{w^2}{2\pi}\int qdq\left(\log\left(w^2\left(k+\kappa q^4\right)\right)\right) + const. \tag{1.38}$$

So the free energy per membrane area is

$$\frac{F_{\mathcal{H}}}{w^2} = \frac{k_B T}{2\pi}\int qdq\left(\log\left(w^2\left(k+\kappa q^4\right)\right)\right). \tag{1.39}$$

We now have an expression for the free energy of a confined tensionless membrane, but it is in terms of the spring constant, k, rather than the mean layer spacing, d. However, from (1.30), we know that

$$k = \frac{\left(k_B T\right)^2}{64\kappa d^4}. \tag{1.40}$$

Ergo,

$$\frac{\partial}{\partial d} = \frac{\partial}{\partial k}\frac{\partial k}{\partial d} = -\frac{\left(k_B T\right)^2}{16\kappa d^5}\frac{\partial}{\partial k}. \tag{1.41}$$

We are now in a position to determine B from the free energy: We begin by using (1.41) to determine $\frac{\partial}{\partial d}$ of (1.39),

$$\frac{\partial \frac{F_{\mathcal{H}}}{w^2}}{\partial d} = -\frac{(k_B T)^2}{16\kappa d^5}\frac{\partial}{\partial k}\frac{k_B T}{2\pi}\int q dq \left(\log\left(w^2\left(k+\kappa q^4\right)\right)\right) \tag{1.42}$$

$$= -\frac{(k_B T)^3}{32\pi\kappa d^5}\int q dq \frac{\partial}{\partial k}\left(\log\left(w^2\left(k+\kappa q^4\right)\right)\right) \tag{1.43}$$

$$= -\frac{(k_B T)^3}{32\pi\kappa d^5}\int \frac{q dq}{k+\kappa q^4}. \tag{1.44}$$

We evaluate this integral as before to yield,

$$\frac{\partial \frac{F_{\mathcal{H}}}{w^2}}{\partial d} = -\frac{(k_B T)^3}{32\pi\kappa d^5}\frac{\pi}{4\sqrt{k\kappa}} = -\frac{(k_B T)^3}{128\kappa^{\frac{3}{2}} d^5\sqrt{k}} \tag{1.45}$$

$$= -\frac{(k_B T)^2}{16\kappa d^3}, \text{ recalling (1.40).} \tag{1.46}$$

Computing the second derivative with respect to d is then easily done,

$$\frac{\partial}{\partial d}\left(\frac{\partial \frac{F_{\mathcal{H}}}{w^2}}{\partial d}\right) = \frac{\partial}{\partial d}\left(-\frac{(k_B T)^2}{16\kappa d^3}\right) = \frac{3(k_B T)^2}{16\kappa d^4}. \tag{1.47}$$

So from (1.16), (and recalling that we have set $N = 1$ by considering the free energy associated with only a single membrane), we have

$$B = \frac{3(k_B T)^2}{16\kappa d^3}. \tag{1.48}$$

1.3.2 Modelling Inclusions

To model the effect of inclusions, be they colloids or ordered phases, which disrupt the layer spacing of the smectic, requires us to include an additional term in the Landau-de Gennes Smectic Hamiltonian, (1.12). The simplest way to do this is a term of the form $\rho\partial_z u$ [62, 49, 48, 63], where $\rho(\mathbf{r})$ is a term which describes the distribution of the inclusions.

The presence of the inclusion at a position $\mathbf{r}_i$ serves to locally fix the layer spacing in the smectic at some value, d^*. This constraint can be expressed in the continuous limit as [49]

$$\partial_z u|_{\mathbf{r}_i} = \frac{d - d^*}{d}, \tag{1.49}$$

where d is the layer spacing of the unperturbed smectic, away from the inclusion.

The constraint can then be included in the Hamiltonian by means of a Lagrange multiplier, β. This β serves as the coupling constant between the fluid membranes and the inclusions. The effect of this term is to have the inclusion act as a spring between the membranes with β in the role of a spring constant [49, 64]. This is the lowest order term, quadratic in ρ and u, which couples the layer compression to the presence of an inclusion, and preserves symmetry in z. As our interest is in the effect of inter-inclusion interactions mediated by the smectic, we omit terms of higher order in ρ which would correspond to direct inter-inclusion interactions.

The complete Hamiltonian is given by

$$\mathcal{H} = \frac{1}{2} \int d^3\mathbf{r} \left(B \left(\partial_z u\right)^2 + K \left(\nabla_{||}^2 u\right)^2 + 2\beta\rho\partial_z u \right). \tag{1.50}$$

The Hamiltonian may be written as a convolution integral over all the interactions between infinitesimal parts of the smectic,

$$\mathcal{H} = \int d^3\mathbf{r} \int d^3\mathbf{r}' G(\mathbf{r} - \mathbf{r}')\rho(\mathbf{r})\rho(\mathbf{r}'). \tag{1.51}$$

Let us calculate the Green's function, given by $G(\mathbf{r})$, which is the interaction potential between those inclusions in the smectic. To proceed most easily with our analysis, we will transition into Fourier space. We define the three dimensional forward Fourier transform as follows,

$$f_{\mathbf{q}} = \int d^3\mathbf{r} f(\mathbf{r}) e^{i\mathbf{q}\cdot\mathbf{r}}; \tag{1.52}$$

with the reverse transform

$$f(\mathbf{r}) = \frac{1}{(2\pi)^3} \int d^3\mathbf{q} f_{\mathbf{q}} e^{-i\mathbf{q}\cdot\mathbf{r}}. \tag{1.53}$$

Under this transformation, the layer displacement, u, can be written as

$$u(z) = \frac{1}{(2\pi)^3}\int d^3\mathbf{q} u_{\mathbf{q}} e^{-i\mathbf{q}\cdot\mathbf{r}}, \tag{1.54}$$

and in turn:

$$\partial_z u(z) = \frac{-i}{(2\pi)^3}\int d^3\mathbf{q} u_{\mathbf{q}} q_z e^{-i\mathbf{q}\cdot\mathbf{r}}, \tag{1.55}$$

$$\nabla^2_{||} u(z) = \frac{-1}{(2\pi)^3}\int d^3\mathbf{q} u_{\mathbf{q}} q^2_{||} e^{-i\mathbf{q}\cdot\mathbf{r}}, \tag{1.56}$$

$$\rho(\mathbf{r}) = \frac{1}{(2\pi)^3}\int d^3\mathbf{q} \rho_{\mathbf{q}} e^{-i\mathbf{q}\cdot\mathbf{r}}. \tag{1.57}$$

Consequently, we can rewrite (1.50) as follows

$$\begin{aligned}\mathcal{H} = &\int d^3\mathbf{r}\int d^3\mathbf{q}\int d^3\mathbf{q}' \frac{1}{2(2\pi)^6}\times \\ &\times\left(\left(Kq^2_{||}q'^2_{||} - Bq_z q'_z\right) u_{\mathbf{q}} u_{\mathbf{q}'} - i\beta\left(\rho_{\mathbf{q}} u_{\mathbf{q}'} q'_z + \rho_{\mathbf{q}'} u_{\mathbf{q}} q_z\right) e^{-i(\mathbf{q}+\mathbf{q}')\cdot\mathbf{r}}\right).\end{aligned} \tag{1.58}$$

Considering the $d^3\mathbf{r}$ integral first, we see that the exponential term, $e^{-i(\mathbf{q}+\mathbf{q}')\cdot\mathbf{r}}$ integrates to the delta function $(2\pi)^3\delta^3(\mathbf{q}+\mathbf{q}')$. This delta function allows us to sift $\mathbf{q} = -\mathbf{q}'$ when we take the $d^3\mathbf{q}'$ integral. This gives us

$$\mathcal{H} = \frac{1}{2(2\pi)^3}\int d^3\mathbf{q}\left(\left(Bq_z^2 + Kq^4_{||}\right) u_{\mathbf{q}} u_{-\mathbf{q}} + i\beta q_z\left(\rho_{\mathbf{q}} u_{-\mathbf{q}} - \rho_{-\mathbf{q}} u_{\mathbf{q}}\right)\right). \tag{1.59}$$

This Hamiltonian can be minimised, as seen in Sens et al. [49], to yield a Green's function which describes the interaction potential between two infinitesimal parts of the smectic.

To minimise the Hamiltonian, we choose

$$u_{\mathbf{q}} = \frac{-i\beta}{2q_z\varkappa}\rho_{\mathbf{q}}, \tag{1.60}$$

where $\varkappa = \frac{Bq_z^2 + Kq^4_{||}}{2q_z^2}$. This minimisation gives

$$\mathcal{H} = \frac{1}{2(2\pi)^3}\int d^3\mathbf{q}\frac{-\beta^2}{\varkappa}\rho_{\mathbf{q}}\rho_{-\mathbf{q}}. \tag{1.61}$$

From (1.61), we extract the Green's function in reciprocal space:

$$G_{\mathbf{q}} = \frac{-\beta^2}{2B} \frac{q_z^2}{q_z^2 + \lambda^2 q_{||}^4}. \tag{1.62}$$

We have calculated the Green's function for our problem in Fourier space, (1.62). For completeness, we will now attempt to obtain an expression for it in real space.

Our inverse Fourier Transform is given by (1.53). Applying this transformation to (1.62) will yield $G(\mathbf{r})$.

$$G(\mathbf{r}) = \frac{-\beta^2}{2(2\pi)^3 B} \int_0^{2\pi} d\phi \int_0^{\infty} q_{||} dq_{||} \int_{-\infty}^{\infty} dq_z \frac{q_z^2}{q_z^2 + \lambda^2 q_{||}^4} e^{-i\mathbf{q}\cdot\mathbf{r}}. \tag{1.63}$$

The Green's function is radially symmetric, therefore we can make use of a Hankel Transform to compute the $d\phi$ integral:

$$G(\mathbf{r}) = \frac{-\beta^2}{2(2\pi)^2 B} \int_0^{\infty} q_{||} dq_{||} \int_{-\infty}^{\infty} dq_z J_0(q_{||} r_{||}) \frac{q_z^2}{q_z^2 + \lambda^2 q_{||}^4} e^{-izq_z}. \tag{1.64}$$

We will now focus on the dq_z integral. We observe that

$$\frac{q_z^2}{q_z^2 + \lambda^2 q_{||}^4} e^{-izq_z} = -\frac{\partial^2}{\partial z^2} \frac{e^{-izq_z}}{q_z^2 + \lambda^2 q_{||}^4}, \tag{1.65}$$

which allows us to write the dq_z integral as

$$I_z = -\int_{-\infty}^{\infty} \frac{\partial^2}{\partial z^2} \frac{e^{-izq_z}}{q_z^2 + \lambda^2 q_{||}^4} dq_z. \tag{1.66}$$

This is easily computed using Gradshteyn and Ryzhik 3.389(v)[24],

$$I_z = -\frac{\partial^2}{\partial z^2} \left(\frac{\pi}{\lambda q_{||}^2} e^{-\lambda |z| q_{||}^2} \right); \tag{1.67}$$

and applying the derivative operator,

$$I_z = -\pi \lambda q_{||}^2 e^{-\lambda |z| q_{||}^2} + 2\pi \delta(z). \tag{1.68}$$

We recall that by the definition of the Dirac delta function, we can set the

second term in the above expression equal to 0, conditional on $z \neq 0$.

We now have

$$G(\mathbf{r}) = \frac{\beta^2}{2(2\pi)^2 B} \int_0^\infty q_{||} dq_{||} J_0(q_{||} r_{||}) \left(\pi \lambda q_{||}^2 e^{-\lambda |z| q_{||}^2} - 2\pi \delta(z) \right). \tag{1.69}$$

Using Gradshteyn and Ryzhik 6.631(i) [24] to compute the $dq_{||}$ integral gives us an expression for $G(\mathbf{r})$, valid for $z \neq 0$.

$$G(\mathbf{r}) = \frac{\beta^2}{16\pi\lambda B z^2} {}_1F_1 \left(2; 1; -\frac{r_{||}^2}{4\lambda |z|} \right), \tag{1.70}$$

where ${}_1F_1(\alpha; \gamma; z) = \sum_{k=0}^{\infty} \frac{(\alpha)_k}{(\gamma)_k} \frac{z^k}{k!}$ [Lebedev 9.14.2] [17] is a confluent hypergeometric function.

Writing the confluent hypergeometric function in the Series notation given by Lebedev, and expressing the Pochhammer symbol in terms of Gamma functions, as given in Abramowitz and Stegun 6.1.22 [1], $(x)_n = \frac{\Gamma(x+n)}{\Gamma(x)}$, we can attempt to evaluate ${}_1F_1(2; 1; x)$ in terms of elementary functions:

$${}_1F_1(2; 1; x) = \sum_{k=0}^{\infty} \frac{\Gamma(2+k)\Gamma(1)}{\Gamma(2)\Gamma(1+k)} \frac{x^k}{k!}. \tag{1.71}$$

Using $\Gamma(1) = \Gamma(2) = 1$, and $\Gamma(x+1) = x\Gamma(x) = x!$, allows us to simplify (1.71):

$$\begin{aligned} {}_1F_1(2; 1; x) &= \sum_{k=0}^{\infty} \frac{(k+1)x^k}{k!} = \sum_{k=0}^{\infty} \frac{\partial}{\partial x} \frac{x^{k+1}}{k!} \\ &= \frac{\partial}{\partial x} \left(x \sum_{k=0}^{\infty} \frac{x^k}{k!} \right) = \frac{\partial}{\partial x} \left(x e^x \right) \\ &= (1+x) e^x. \end{aligned} \tag{1.72}$$

So, with an expression for the confluent hypergeometric function, we have

$$G(\mathbf{r}) = \frac{\beta^2}{16\pi\lambda B z^2} e^{-\frac{r_{||}^2}{4|z|\lambda}} \left(1 - \frac{r_{||}^2}{4|z|\lambda}\right), \tag{1.73}$$

for $z \neq 0$.

1.4 Outline

In this work, we approach two very different problems which nonetheless share a common theme: the physics of inclusions in smectic liquid crystals.

In Chapter 2, we were motivated by the work of Tayebi et al. (2012) [56]. Here they observed that a lamellar stack of phospholipid bilayers, composed of a mixture of saturated and unsaturated phospholipids, would undergo phase separation leading to the formation of aligned liquid-ordered domains, spanning many layers. By treating the aligned domains as a single columnar inclusion in a smectic liquid crystal, we could determine an expression for it's free energy, and so give a plausible candidate for an interfacial energy that could favour the existence of such aligned structures. We began by considering such an inclusion in an infinite bulk system, before extending our model to look at an inclusion in a finite slab geometry. As well as providing some bounds for the interfacial energy necessary for the formation of such inclusions, we also sought to explain why the aligned structures observed should seem to initially form at the boundary of the lamellar stack.

In Chapter 3, we examine a system in which small, motile, colloidal inclusions are placed between the layers of a smectic liquid crystal. Using the physics of liquid crystals to understand how small inclusions embedded in a smectic might interact with one-another via their disruption of the smectic layer structure, and how this interaction combined with their own motion and body shape might affect their direction of travel, we develop equations of motion for the inclusions. With these equations of motion, we observe a system capable of exhibiting orientational and positional order of motile particles - a rare example of such a phenomenon arising without the explicit addition of co-alignment to the model. We examine the robustness of the order to the addition of noise, noting an order-disorder transition in the fashion of Vicsek et al. (1995) [66].

Chapter 2

Membrane Microdomains in Lamellae

2.1 Introduction and Motivation

The formation of rafts in phosopholipid bilayers has been well known since the work of Dietrich et al. (2001) [19], motivated by investigations in biological systems [59, 50], demonstrated their existence on model membranes. Suspensions of phospholipids (molecules typically composed of a pair of hydrophobic fatty acid "tails" attached to a hydrophilic phosphate "head") readily self-organise into structures which minimise contact between molecule tails and the aqueous solvent. The organisational geometry of most interest to us here is that of bilayer sheets. These are of particular biological significance as they reflect the structure of biological membranes.

Bilayers in a suspension of water are arranged with phosphate heads on the opposite surfaces of the sheet, and the fatty tails in the space between them forming a two dimensional fluid. Some phospholipids, such as sphingomyelin (SM), are termed "saturated", having tails with no doublebonded carbons, those with double bonds in thier lipid tails, such as dioleoylphosphatidylcholine (DOPC), are termed "unsaturated". Bilayers composed of an inhomogeneous mixture of cholesterol, saturated and unsaturated phosopholipids have been observed to phase-separate into liquid-disordered (L_d), containing mostly unsaturated lipids, and liquid-ordered (L_o), containing higher levels of saturated

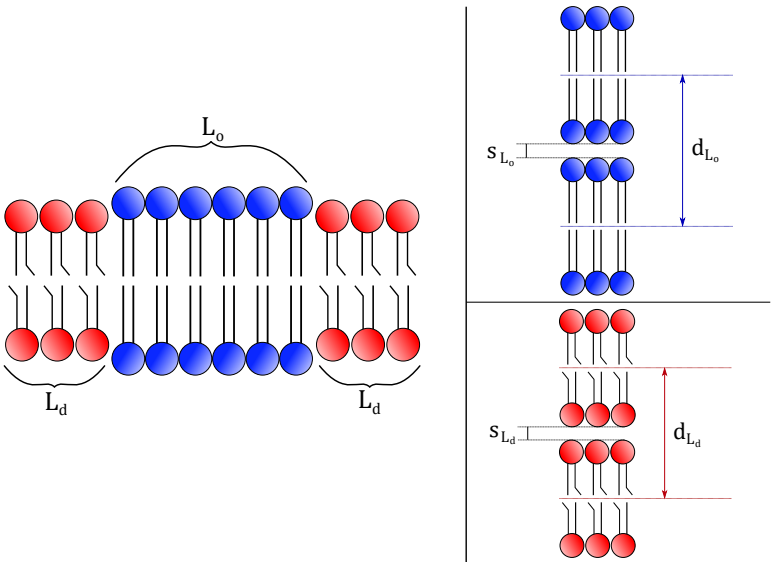

Figure 2.1: A liquid-ordered, L_o, domain in a bilayer, surrounded by liquid disordered, L_d material. The L_o is comprised of phospholipids with saturated tails, these can pack more closely together than the unsaturated lipids comprising the L_d. The L_o domain is slightly thicker than the surrounding L_d phase: $d_{L_o} > d_{L_d}$, where these are the lamellar repeat distances for each phase. The water gaps between neighbouring bilayers are s_{L_o} and s_{L_d}.

lipids and cholesterol, phases, which coexist[5, 29]. Driven by the line tension of the interface between liquid-ordered and liquid-disordered regions, the liquid-ordered domains tend to aggregate to form large circular "rafts" [56].

Unlike the surrounding L_d material, the L_o regions are denser and more rigid. The straighter, saturated fatty acids that make up their tails allow them to be packed more closely together than their unsaturated counterparts in the more fluid regions [34]. The bilayer is therefore thicker in liquid ordered regions, which is to say that the distance between complementary phosphate head-groups on either side of the bilayer is greater (by around 1nm) between the saturated lipids in an L_o raft, than it is between the unsaturated lipids in the L_d phase [44].

Multi-lamellar stacks of phospholipid membranes appear in many living organisms (e.g. in plant chloroplasts) [65], however most of the experimental work on them has been done in a laboratory context. In a recent paper, Taybei et al. [56] examined a system of a stack of raft-forming lipid bilayer mixtures. They observed that when phase-separation occurred, the liquid-ordered rafts

d_{L_o}	d_{L_d}	s_{L_o}	$\simeq s_{L_d}$
62.7 (Å)	54.6 (Å)	6.7 (Å)	6.9 (Å)

Table 2.1: Typical figures for a system with an SM L_o phase and DOPC L_d phase at 24°C and 98% relative humidity [56, 37]. We note that $s_{L_o} \simeq s_{L_d}$.

that formed aligned across neighbouring layers, forming connected columns spanning hundreds of layers.

Given the slight layer thickness difference between L_o and L_d phases, this alignment of rafts across multiple layers tends to distort the lamellae, with the stack of rafts developing an increasingly significant height mismatch with the surrounding fluid phase. Indeed, evidence of this distortion was observed by Tayebi et al. with AFM imaging of the upper surface of the bilayer stack revealing distinct swelling above columns. The height difference was greater for larger columns, but it is worth noting that, from their data, the height difference does not appear to scale linearly with overall stack height. Smaller stacks showed a proportionally greater height mismatch than larger ones.

The height mismatch resulting from the difference in layer thickness has been noted in other papers. Ma et al. [37] observed that whilst the height mismatch in a lipid multilayer was present at partial hydration of the system, at 100% relative humidity, the spacing between the layers in the L_d phase would increase, and those regions would swell until the entire stack was of more or less uniform height with the L_o columns.

Lamellar bodies such as these represent a form of smectic-phase liquid crystals. We will need to treat L_o lipid rafts, with their higher density and greater rigidity than the surrounding L_d phase smectic, as a form of continuous inclusion in the smectic. Inclusions such as these deform the arrangement of layers within the lamellar body by locally influencing the spacing between neighbouring membranes.

Sens et al. [49, 62] used continuum theory to examine the behaviour of inclusions in a smectic phase liquid crystal. By first considering the influence of a single particle on the smectic displacement field, they were able to show that the presence of a particle locally fixing the layer-spacing, results in a paraboloid deformation in the smectic order. The interaction between two or more particles depends on their relative positions, and has the following broad

character: that particulate inclusions are repulsive within the parabola, and attractive outside it. Inclusions in closely neighbouring layers interact more strongly, offsetting themselves, to find a minimum in the interaction potential. In short, this would seem to imply that columnar stacking of rafts, as seen in Tayebi et al. are not merely an energetically unfavourable arrangement, but actually *the least* favourable arrangement, at least from the point of view of Helfrich-inspired, membrane mediated interactions.

In this chapter, we will attempt to quantify the energetic cost of forming a columnar arrangement of L_o domains. Firstly we will address an inclusion in an infinite smectic, similar to the approach in Sens et al. We will then extend our investigation to columns in a slab-like geometry, to better reflect the conditions of the experimental work carried out by Tayebi et al. [56].

2.2 Methodology

We are interested in why denser domains in lamellar bodies should form columnar structures, given that there are reasons to suspect that this would not be the natural minimum energy state of such a system [49, 62, 57]. To address this question, we must describe the energy of the system.

Constructing a Hamiltonian for the total free energy of the system, we include a volume integral for the elastic energy associated with layer deformation in the bulk ($E(\mathbf{r})$), another to account for any inter-layer interaction that might occur ($\mu(\mathbf{r}, \rho)$), and a surface integral for inter-facial energy in the lamellar body. The complete expression, therefore reads

$$\mathcal{H}_{Tot} = \int_V d^3\mathbf{r} \left(E\left(\mathbf{r}\right) + \mu\left(\mathbf{r}, \rho\right)\right) + \int_{\partial V} d\mathbf{S} \cdot \left(\hat{r}\sigma_r + \hat{z}\sigma_z\right). \tag{2.1}$$

We first address the $E(\mathbf{r})$ term. To do this, we make use of the Landau-de Gennes Hamiltonian for a smectic liquid crystal [16]. This description is concerned with the displacement, u, in the direction normal to the plane (which we will henceforth refer to as the z direction, with the layers parallel to the x, y-plane) of layers from an unperturbed, average flat state. We will employ the linearised version of the smectic Hamiltonian. This is comprised of energy densities associated with compression or dilation of layers ($\frac{B}{2}(\partial_z u)^2$), and bending

of layers ($\frac{K}{2}(\nabla_{||}^2 u)^2$). The non-linear elastic free energy contains an anharmonic correction to the compression term, $\frac{B}{2}\left(\partial_z u\right)^2 \rightarrow \frac{B}{2}\left(\partial_z u - \frac{1}{2}\left(\nabla_{||} u\right)^2\right)^2$. This essentially allows the system to respond to a large deformation in z by a non-zero contribution of $\left(\nabla_{||} u\right)^2$, essentially creating undulations in the layers to respond to the increase in the layer spacing [10]. Although the liquid-ordered structures we examine are very large relative to the layers in the system, the deformation fields they generate are small, with the local increase in the layer size of the L_o being an order of magnitude smaller than the mean layer repeat distance (see Table 2.1)[56]. In this small deformation regime using the linear form affords us a significant advantage in terms of the solubility of our equations [46] and still allows us to draw meaningful conclusions from our model[8, 49].

The effect of the ordered domains distorting layers is introduced by means of the term $\mu\left(\mathbf{r}, \rho\right)$ [49, 63]. It applies the deformation due to the increased layer thickness by a coupling between a field describing the size and shape of the L_o domain, $\rho\mathbf{r}$, and the local layer dilation, $\partial_z u$. The lowest order such coupling is $\beta\rho(\mathbf{r})\partial_z u$, which fixes the layer size in the ordered domain via choice of the Lagrange multiplier, β [49, 63, 62].

Our Hamiltonian, therefore, reads:

$$\mathcal{H} = \frac{1}{2}\int d^3\mathbf{r}\left(B\left(\partial_z u\right)^2 + K\left(\nabla_{||}^2 u\right)^2 + 2\beta\rho(\mathbf{r})\partial_z u\right) \tag{2.2}$$

where B (dimensions of energy length^{-3}) and K (dimensions of energy length^{-1}) are respectively the compression and bending moduli, ρ is the density of the smectic phase. β is a coupling constant which determines the size of the layer deformation caused by the ordered raft.

The bending modulus is straightforwardly given by

$$K = \frac{\kappa}{s}, \tag{2.3}$$

where s is the mean layer spacing in the smectic stack (the water gap in Figure 2.1), and κ is the rigidity of a single layer, typically $\sim 20 k_B T$ [55].

Consider a column of rafts spanning the entire height of the lamellar stack, as in Tayebi (2012), Figure 5 [56]. Its base rests upon a solid, flat, rigid substrate; its top is at the smectic-air interface. Due to the height mismatch

between the thicker L_o rafts and the thinner L_d surrounding them, the mean height of the stacked rafts is $H + \delta H$, slightly greater than the height of the L_d smectic surrounding them, H.

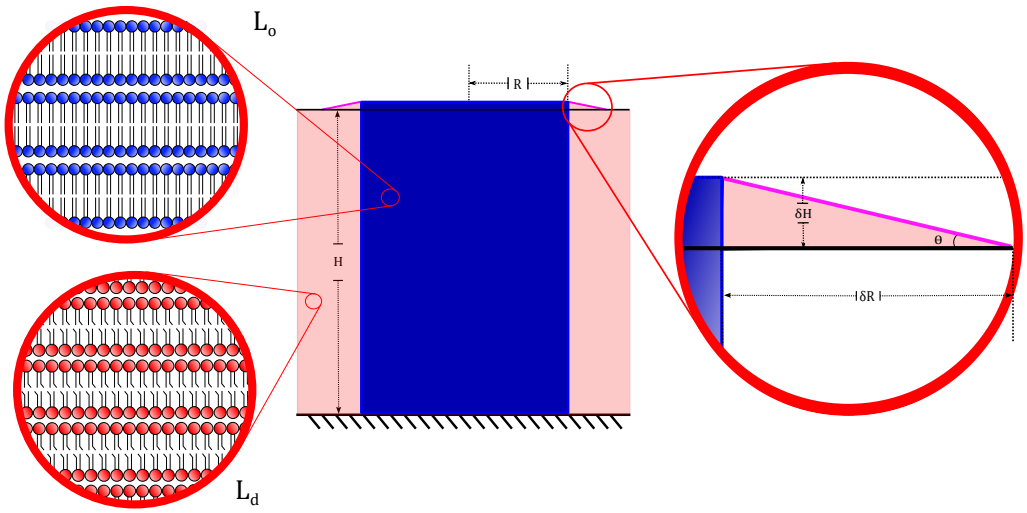

Figure 2.2: A side view of a columnar stack of L_o domains (blue), surrounded by L_d (red), in a lamellar body. The lamellar body rests on a substrate and has some interface above it. The greater layer thickness of the L_o domains result in a height mismatch between the column and the surrounding L_d, so that it protrudes a small distance above the rest of the lamellar body, dragging some of the surrounding L_d layers up with it. The height of the lamellar body above the substrate is given by H, the additional height of the L_o column is δH, the radius of the column is R, and the length over which the L_d layers perturbed by the height mismatch return to the height of the surrounding lamellar body is given by δR.

Around the top of our columnar inclusion, the surrounding L_d layers are dragged up, increasing the surface area around the inclusion. Surface tension seeks to prevent this. The force which results in the increase in interface surface area is that which pushes the column of L_o phase layers up, relative to the surrounding smectic. This force is therefore

$$F_{\text{up}} := \frac{\partial \mathcal{H}}{\partial (\delta H)}. \tag{2.4}$$

The additional height, δH, comes about by the additional layer dilation, $\partial_z u$, found in the L_o phase smectic, versus the L_d phase. Ergo, $\delta H = H \cdot \langle \partial_z u \rangle$, and so

$$\frac{\partial \mathcal{H}}{\partial (\delta H)} = \frac{1}{H} \frac{\partial \mathcal{H}}{\partial \langle \partial_z u(\mathbf{r}, z) \rangle}. \tag{2.5}$$

We are only interested in the column, so we set $\rho = 1$ for the L_o stack, and $\rho = 0$ outside, and and integrate the Hamiltonian only for the volume of L_o inclusion. Neglecting curvature energies ($K = 0$) we see that $\mathcal{H} = \frac{V}{2}\left(B\left(\partial_z u\right)^2 + 2\beta \partial_z u\right)$, where $V = \pi H R^2$ is the volume of the column. And so,

$$\begin{aligned} F_{\mathsf{up}} &= \frac{1}{H} \frac{\partial \mathcal{H}}{\partial \left(\partial_z u\right)} \bigg|_{\partial_z u = 0} = \frac{V}{H} \left(B \partial_z u + \beta\right) \bigg|_{\partial_z u = 0} \\ &= \pi R^2 \beta, \end{aligned} \tag{2.6}$$

where we have evaluated at $\partial_z u = 0$ so that we only obtain the force from the L_o-induced layer swelling, but for layers which are otherwise unperturbed. Meanwhile, surface tension, γ, is acting down the slope of the aberrant surface produced by this up force. The component of γ acting downwards, must balance our previously calculated up force, F_{up}, ie $\gamma \sin\theta$. Because $\delta R \gg \delta H$, we may employ the small angle approximation, and so,

$$F_{\mathsf{down}} = \gamma \sin\theta \cdot A_{\mathsf{surface}} = 2\pi R \frac{\delta H}{\delta R} \gamma. \tag{2.7}$$

By Newton,

$$F_{\mathsf{up}} = -F_{\mathsf{down}} \tag{2.8}$$

$$\implies \pi R^2 \beta = -2\pi R \frac{\delta H}{\delta R} \gamma. \tag{2.9}$$

So we arrive at an expression for β,

$$\beta = -\frac{2}{R_o} \frac{\delta H}{\delta R} \gamma. \tag{2.10}$$

For columns as seen in Tayebi et al. [56], with $R = 0.6\mu$m, $\delta R = 0.3\mu$m,

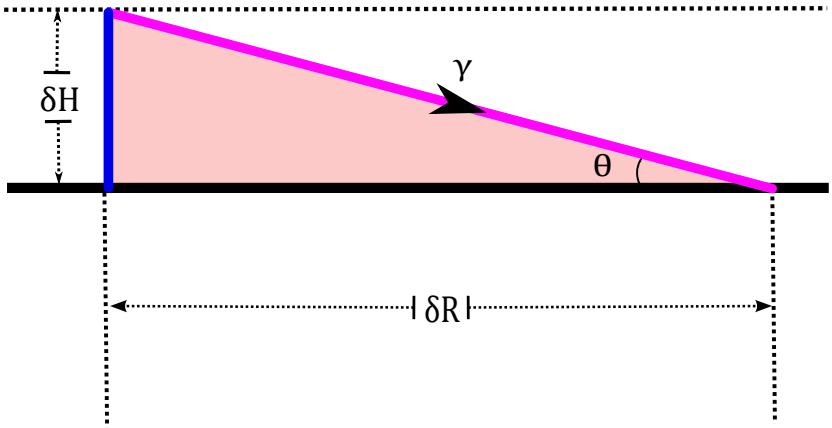

Figure 2.3: The force of the protruding column of L_o is balanced by a component of the surface tension, γ, which acts along the slope of the displaced L_d surface. We make the simplifying assumption that profile of the surface will be linear, at some constant angle Θ to the unperturbed L_d surface.

$\delta H = 0.011\mu$m, and $\gamma = 1.75 \times 10^7 k_B T \mu m^{-2}$[39], $\beta \approx 2.14 \times 10^6 k_B T \mu m^{-3}$.

We determine the compression modulus, B, by relating it to the coupling constant. We consider the energy per unit volume of smectic,

$$g_B = \frac{B}{2}\left(\partial_z u\right)^2 + \frac{K}{2}\left(\nabla_{||}^2 u\right)^2 + \beta\rho\partial_z u \tag{2.11}$$

We are interested in layer dilation, i.e. a change in $\partial_z u$,

$$\frac{\partial g_B}{\partial\left(\partial_z u\right)} = B\partial_z u + \beta\rho. \tag{2.12}$$

Minimising,

$$\frac{\partial g_B}{\partial(\partial_z u)} \stackrel{!}{=} 0 \implies \partial_z u = -\frac{\beta}{B}\rho. \tag{2.13}$$

We are looking at the dilation due to the L_o phase, so we set $\rho = 1$, and define $\delta d = \frac{d_{L_o} - d_{L_d}}{d_{L_o}}$ to be the fractional change in layer thickness between the L_o and L_d phases, so that

$$\beta = -\delta d\, B. \tag{2.14}$$

For the figures in Table 2.1, $\delta d \approx 0.13$, so giving $B \approx 1.66\times10^{7}\mathrm{k_B T}\mu\mathrm{m}^{-3}$.

As we have seen, the distortion caused by the inclusions we are considering amounts to no more than the equivalent of one or two additional layers across the entire height of the $\mathrm{L_o}$ column. The figures from Tayebi et al. [56] would also seem to suggest that the swelling arising from the increased thickness of the $\mathrm{L_o}$ phase causes too slight a bend for the error in using the linear form of the elastic free energy to be significant. Indeed, considering the size of the angle $\theta \approx 4 \times 10^{-4}$ encouragingly suggests the contribution from the omitted anharmonic correction to be at least an order of magnitude smaller than that of any of the other terms in the Hamiltonian.

We acknowledge that this is something of a rough approach, given the assumptions made in producing this expression, nonetheless it should be a reasonable approximation. We also feel that it is a more defensible approach to calculating β and B than using the continuum model, given the length scales we are working at. Our smectic layers are very thick compared to the thin water layer between them - this is potentially quite a different regime to that described by Helfrich theory, with its infinitesimal layers. However, we note that using the expression for B, Equation 1.48 given in Section 1.3.1, with the water gap, $s \approx 6.9$Å in place of d, gives $B \approx 2.854 \times 10^{7}\mathrm{k_B T}\mu\mathrm{m}^{-3}$. This is a figure within only a factor of 2 of our other estimate.

2.3 Results and discussion

2.3.1 A Bulk Geometry

We begin with the simplest case and consider the energies of an aligned stack of rafts in an infinite smectic. This is most similar to the situation considered by Sens et al. [49], and indeed, we will initially follow their procedure.

To determine the interaction potential, we will minimise this Hamiltonian, a procedure most easily carried out in Fourier Space. We define the three dimensional forward Fourier transform as follows,

$$f_{\mathbf{q}} = \int d^3\mathbf{r} f(\mathbf{r}) e^{i\mathbf{q}\cdot\mathbf{r}}; \tag{2.15}$$

with the reverse transform

$$f(\mathbf{r}) = \frac{1}{(2\pi)^3} \int d^3\mathbf{q} f_{\mathbf{q}} e^{-i\mathbf{q}\cdot\mathbf{r}}. \tag{2.16}$$

. Under this transformation, our adapted smectic Hamiltonian can be rewritten as

$$\mathcal{H} = \frac{1}{2(2\pi)^3} \int d^3\mathbf{q} \left(\left(B q_z^2 + K q_{||}^4 \right) u_{\mathbf{q}} u_{-\mathbf{q}} + i\beta q_z \left(\rho_{\mathbf{q}} u_{-\mathbf{q}} - \rho_{-\mathbf{q}} u_{\mathbf{q}} \right) \right). \tag{2.17}$$

This Hamiltonian can be minimised, as seen in Sens et al. [49], to yield a Green's function which describes the interaction potential between two infinitesimal parts of the smectic. The equilibrium smectic distortion field is given by

$$u_{\mathbf{q}} = \frac{-i\beta q_z}{B q_z^2 + K q_{||}^4} \rho_{\mathbf{q}}, \tag{2.18}$$

The equilibrium energy is then

$$\mathcal{H} = \frac{1}{2(2\pi)^3} \int d^3\mathbf{q} \frac{-\beta^2 q_z^2}{B q_z^2 + K q_{||}^4} \rho_{\mathbf{q}} \rho_{-\mathbf{q}}. \tag{2.19}$$

From (2.19), we extract the Green's function:

$$G_{\mathbf{q}} = \frac{-\beta^2}{2B} \frac{q_z^2}{q_z^2 + \lambda^2 q_{||}^4}. \tag{2.20}$$

Here, $\lambda = \sqrt{\frac{K}{B}}$ is the smectic penetration length of the order of the layer spacing.

Now we must consider the density term, $\rho_{\mathbf{q}}$ in Fourier space. The phase-separated lamellar body is comprised of ordered domains surrounded by more fluid smectic. Inside the ordered domains, where there are saturated phospholipids present, the lipids are more closely packed than outside of these domains, where where the unsaturated phospholipids are. We think of these L_o regions as having a greater lipid "density". For ease of calculation, we will use a

normalised density given by 1 inside of an ordered domain, and 0 outside of it. Studies have shown that near equilibrium, domains are radially symmetric - we therefore consider a radially symmetric domain of height (in z) L, and with a radial extent from its azimuthal axis of R_0. We can therefore write the density in real space as

$$\rho(\mathbf{r}) = \Theta\left(R_0 - r_{||}\right)\Theta\left(\frac{L}{2} - |z|\right), \tag{2.21}$$

where $\Theta(x)$ is the Heaviside Step function. In Fourier space this becomes

$$\rho_{\mathbf{q}} = \frac{4\pi R_0 J_1(q_{||}R_0)}{q_{||}q_z}\sin\left(q_z\frac{L}{2}\right). \tag{2.22}$$

It is worth remarking here that this construction makes clear our reference state is one without an inclusion. We have minimised the free energy by the expression for the equilibrium smectic distortion field $u_{\mathbf{q}}$, perturbed with the inclusion $\rho_{\mathbf{q}}$, to arrive at our integral expression for the system energy. One can see that $\rho_{\mathbf{q}} = 0$ if R_0 and or $L = 0$, and that this yields $\mathcal{H} = 0$. Ergo the state against which we compare the energy of the columnar inclusions is the state of a homogeneous smectic in which no phase separation of lipids has occurred.

We are now in a position to integrate for $\mathcal{H}$, and so find an expression for the energy of the inclusion. We recall that our integral reads

$$\mathcal{H} = \frac{1}{(2\pi)^3}\int d^3\mathbf{q} G_{\mathbf{q}}\rho_{\mathbf{q}}\rho_{-\mathbf{q}}. \tag{2.23}$$

We compute the q_θ and q_z integrals, and renormalise according to $\nu = q_{||}R_0$, and $\tau = \frac{L\lambda}{R_0^2}$, both dimensionless quantities, and also defining $\varepsilon_1 = \frac{L^2\lambda\beta^2\pi}{B}$, which has units of energy. This gives us

$$\mathcal{H} = -\varepsilon\int_0^\infty d\nu \frac{J_1^2(\nu)\left(1 - e^{-\tau\nu^2}\right)}{\tau^2\nu^3}. \tag{2.24}$$

This integral evaluates to the following, for $\tau > 0$, as is the case here,

$$\mathcal{H} = \frac{-A_1}{32\tau^3}\left({}_3F_3\left(\left\{1,1,\tfrac{5}{2}\right\},\{2,3,4\},-\tfrac{1}{\tau}\right) + 2\tau\left(1-2\gamma+\log(16)+2\log(\tau)\right)\right), \tag{2.25}$$

where ${}_3F_3$ is a hypergeometric function, and γ is the Euler-Mascheroni constant.

We can expand 2.25 for both large and small values of τ. The series expansion for the energy density $\frac{\mathcal{H}}{V}$ for $\tau \ll 1$ yields

$$\frac{\mathcal{H}}{V} \approx \frac{-\beta^2}{2B}\left(1 - \frac{4\sqrt{\tau}}{3\sqrt{\pi}}\right) \tag{2.26}$$

The limit of $\frac{\mathcal{H}}{V}$ tends to $\frac{-\beta^2}{2B}$ (the energy of a pointlike inclusion [62]) as $\tau \to 0$, reflecting the fact that there is no distortion outside the L_o phase. Meanwhile, the series expansion about for $\frac{1}{\tau} \ll 1$ yields

$$\frac{\mathcal{H}}{V} = -\frac{\beta^2}{B}\left(\frac{1-2\gamma+\log(16)-2\log\left(\frac{1}{\tau}\right)}{16\tau} + \frac{1}{32\tau^2} - \frac{5}{1536\tau^3} + O\left[\frac{1}{\tau^4}\right]\right). \tag{2.27}$$

The limit of $\frac{\mathcal{H}}{V}$ goes to 0 as $\tau \to \infty$, reflecting the fact that the L_o phase has the same layer spacing as the L_d phase in this limit. Plotting these expansions against the full expression, we see that they agree nicely in their respective domains. The aspect ratio of the columns in Taybei's paper [56] is about 1, hence these columns are in the $\tau \ll 1$ regime, as $R_o \gg \lambda$.

We now have an idea of the smectic free energy associated with one of the observed inclusions. Up until this point, however, we have yet to consider the surface energy.

The total energy is given by

$$\mathcal{H}_{Tot} = \mathcal{H}_B + E_S, \tag{2.28}$$

where we call the smectic energy of the L_o column in the bulk $\mathcal{H}_B$, which is is as in (2.26), and E_S is the energy associated with the surface of the cylindrical inclusion. Whilst there may be an energy associated with the radial surface of the column (σ_r in (2.1)), we will neglect this and focus instead on the faces of

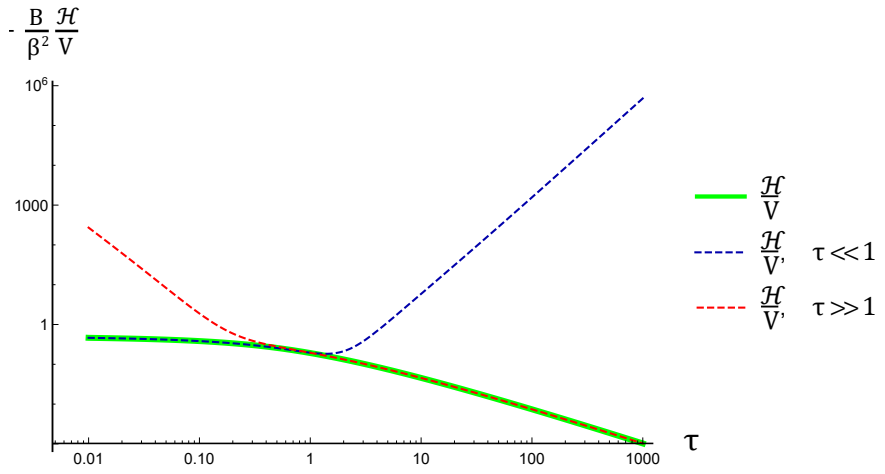

Figure 2.4: A plot to show the agreement of the expansions for $\tau \ll 1$ (blue) and $\frac{1}{\tau} \ll 1$ (red), for $\frac{H}{V}$, with the analytic expression (green). See that both agree very well within their respective domains, but rapidly diverge outside.

the inclusion at $z = \pm\frac{L}{2}$ (corresponding to σ_z in (2.1)) as an interfacial energy associated with these faces was proposed by Tayebi et al. [56] as a candidate for the formation of stable $L_o$columns. E_S can thus be written as

$$E_S = \sigma_z 2\pi R^2, \tag{2.29}$$

the product of an energy per area term, σ_z, and the total area of the two faces.

The surface energy per unit volume written in terms of the volume, V, and our control parameter τ, is

$$\frac{E_S}{V} = 2\sigma_z\sqrt{\frac{\pi\lambda}{V\tau}}. \tag{2.30}$$

We want to minimise the total energy with respect to τ, to find an expression

for σ_z that minimises $\mathcal{H}_{Tot}$ for a given value for τ.

$$\frac{\partial}{\partial\tau}\frac{\mathcal{H}_{Tot}}{V} = \frac{\partial}{\partial\tau}\left(\frac{-\beta^2}{2B}\left(1-\frac{4\sqrt{\tau}}{3\sqrt{\pi}}\right)\right) + \frac{\partial}{\partial\tau}2\sigma_z\sqrt{\frac{\pi\lambda}{V\tau}} \tag{2.31}$$

$$= \frac{\beta^2}{3B\sqrt{\pi\tau}} - \sigma_z\sqrt{\frac{\pi\lambda}{V\tau^3}}. \tag{2.32}$$

Minimising:

$$\frac{\partial}{\partial\tau}\frac{\mathcal{H}_{Tot}}{V} \stackrel{!}{=} 0 \implies \sigma_z\sqrt{\frac{\pi\lambda}{V\tau^3}} = \frac{\beta^2}{3B\sqrt{\pi\tau}} \tag{2.33}$$

$$\implies \sigma_z = \frac{\tau\beta^2}{3\pi B}\sqrt{\frac{V}{\lambda}}. \tag{2.34}$$

(2.34) gives us an expression for the surface energy, per unit area, that will minimise $\mathcal{H}_{Tot}$ for a column with a given volume, V, and for a certain $\tau = \frac{L\lambda}{R_0^2}$. For a L_o inclusion, of the dimensions of such a column seen in Tayebi (2012) [56], $R_0^2 = 2.25\mu\text{m}^2$, $L = 2.4\mu\text{m}$, this gives a value of $\sigma_z = 2.65 \times 10^4 k_B T\mu\text{m}^2$. We note that this is quite small, chemically speaking.

2.3.2 A Semi-infinite Slab

We now have an idea of the energy required to form a stable column of L_o in the bulk. It is relatively straightforward to examine the case of an inclusion on a substrate. We observe that for a columnar ordered domain in the bulk, the distortion field is symmetric about the middle of the column. The layers in the middle of the column will be flat, experiencing no distortion, with the L_o-induced layer swelling increasing with distance from this middle. This is identical to the middle layers being in contact with a flat substrate. Ergo, the energy of a column in a semi-infinite system is equivalent to that of half a column in a bulk system. However, we note that by halving the smectic energy, we are also only considering half of the inclusion itself. For a true comparison between a column in the bulk and one in a semi-infinite slab, we must examine columns of the same dimensions. To account for this, we will use an inclusion of length $2L$ in our semi-infinite description, so that when halved it will be of the same length as the column in the bulk description.

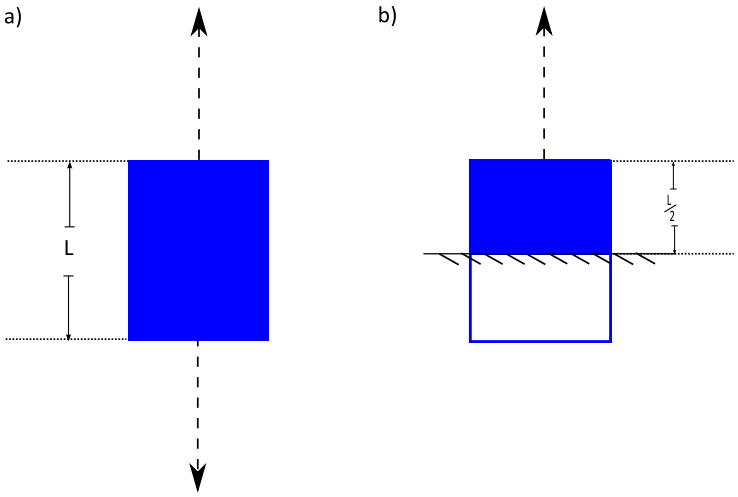

Figure 2.5: A side view of L_o columns in both an infinite bulk (a), and semi-infinite slab (b). The latter may be modelled by considering it to have the same properties and smectic energy as the former divided about its middle, where symmetry forces the layers to be flat.

So in (2.24), setting $L = 2L$, and halving, gives us the energy for a column of the same dimensions , but against a flat, rigid substrate, rather than in the bulk.

$$\mathcal{H}_{\text{semi-infinite}} = -\frac{\pi R_0^2 \beta^2}{2\lambda B} \int \frac{J_1^2\left(q_{||} R_0\right)}{q_{||}^3} \left(1 - e^{-\lambda 2 L q_{||}^2}\right) dq_{||}. \tag{2.35}$$

Integrating this, expanding and truncating as before, we see that

$$\frac{\mathcal{H}_{\text{semi-infinite}}}{V} \approx -\frac{\beta^2}{2B}\left(1 - \frac{4\sqrt{2L\lambda}}{3\sqrt{\pi R^2}}\right). \tag{2.36}$$

Comparing this to our earlier result for a column in the bulk, (2.26),

$$\frac{\mathcal{H}_{\text{infinite}}}{V} \approx -\frac{\beta^2}{2B}\left(1 - \frac{4\sqrt{L\lambda}}{3\sqrt{\pi R^2}}\right), \tag{2.37}$$

we see that though the two expressions are similar, the fact that the cost of the distortion does not grow linearly with column distance from an unperturbed

layer means that $\mathcal{H}_{\text{semi-infinite}} > \mathcal{H}_{\text{infinite}}$. It is perhaps easiest to think of this as arising because the column in the semi-infinite case has less deformable smectic around it, to evenly distribute the layer-mismatch distortion, than the column in the symmetric, uniform environment of the bulk.

2.3.3 A Finite Slab Geometry

We now consider a geometry with a periodicity in z. Previously we wrote the equilibrium energy, $\mathcal{H}$ in terms of its continuous Fourier Transform (2.15). We now seek to discretise its z-Fourier Transform, essentially replacing the integral transform with a Fourier Series.

Up until now our work has examined the case of a column of dense material in the bulk and at a single boundary. Whilst informative, such geometries are not typically found in nature and indeed the bulk of the experimental work carried out in this area has looked at a more thin-film geometry. In this section we will develop a model which will allow us to better analyse the energy cost of a columnar L_o inclusion between two flat substrates.

In the experimental work[57], the "thin film" is a slab of smectic upon a rigid substrate of silica, submerged in water (or K_2SO_4 for partial humidity). The surface tension at the smectic-air interface is close to that of water, ~ 70 mN m^{-1}, sufficiently great that the smectic is almost completely completely flat here (albeit with some minor deformation which we will disregard as negligible, for now). As such, we will model the columnar inclusion as though it is between two flat, rigid substrates, a distance H apart, its centre at some arbitrary distance, h, from the lower substrate.

We observe here, that this lower substrate, a place where the layers become identically flat, is equivalent to a situation in which a second inclusion, of the same dimensions and make up, is placed below the first, its centre at a distance of $2h$ from the centre of the original, with then a new substrate $H-h$ below that, so that the system has a reflective symmetry about the plane of the original lower substrate. We observe that at either substrate, the layers become identically flat. On symmetry grounds, rather than there being a substrate at some distance, h from the inclusion, this situation is equivalent to there being another inclusion at a distance $2h$, the respective distortions from

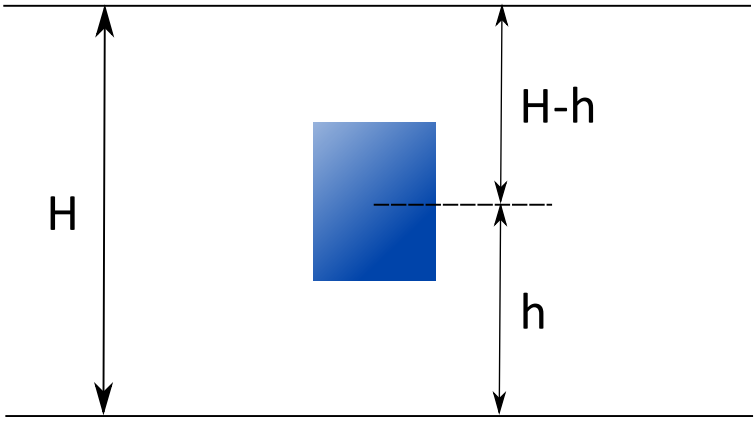

Figure 2.6: A columnar L_o inclusion, surrounded by L_d, and between two flat, rigid, substrates. The two substrates are a distance H apart, and the centre of the L_o column is a distance h from the lower substrate.

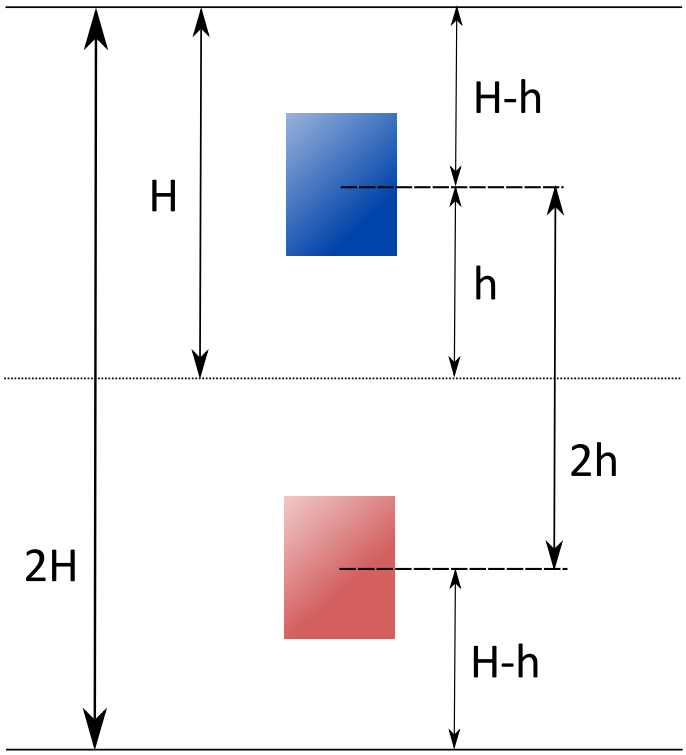

Figure 2.7: Having a flat, rigid substrate at a distance h is equivalent to having another, identical inclusion at a distance $2h$. At the midpoint between the two, the layers are as flat as if there was a substrate there.

each cancelling out to yield flat layers at the midpoint between them. This reasoning can be naturally extended, exploiting reflective symmetry in the system, without altering the energy. Thus, instead of modelling an inclusion positioned at an arbitrary point between two rigid substrates, we can model an infinite periodic system composed of repeating subunits of the symmetric two-inclusion geometry.

To apply this geometry we will employ a discrete Fourier transform in the z-axis, as opposed to the continuous Fourier transform used in the previous section. The forward transform given by

$$\tilde{f}_{\mathbf{q}_{||},n} = \int d^3\mathbf{r} f\left(\mathbf{r}\right) e^{i\mathbf{q}_{||}\cdot\mathbf{r}_{||}} \cos\left(\tfrac{n\pi z}{H}\right), \tag{2.38}$$

and the reverse:

$$f\left(\mathbf{r}\right) = \frac{2}{\left(2\pi\right)^2 H} \sum_n \int d^2\mathbf{q}_{||} \tilde{f}_{\mathbf{q}_{||},n} e^{-i\mathbf{q}_{||}\cdot\mathbf{r}_{||}} \cos\left(\tfrac{n\pi z}{H}\right). \tag{2.39}$$

Under this new transformation, the change in layer displacement, $\partial_z u$, can be written as

$$\partial_z u(z) = \frac{-2\pi}{(2\pi)^2 H} \sum_n \int d^2\mathbf{q}_{||} \tilde{u}_{\mathbf{q}_{||},n} n \cos\left(\tfrac{n\pi z}{H}\right) e^{-i\mathbf{q}_{||}\cdot\mathbf{r}_{||}}, \tag{2.40}$$

and so, in turn:

$$u(z) = \frac{-2}{(2\pi)^2} \sum_n \int d^2\mathbf{q}_{||} \tilde{u}_{\mathbf{q}_{||},n} \sin\left(\tfrac{n\pi z}{H}\right) e^{-i\mathbf{q}_{||}\cdot\mathbf{r}_{||}}, \tag{2.41}$$

$$\nabla_{||}^2 u(z) = \frac{2}{(2\pi)^2} \sum_n \int d^2\mathbf{q}_{||} \tilde{u}_{\mathbf{q}_{||},n} q_{||}^2 \sin\left(\tfrac{n\pi z}{H}\right) e^{-i\mathbf{q}_{||}\cdot\mathbf{r}_{||}}, \tag{2.42}$$

$$\rho(\mathbf{r}) = \frac{-2}{(2\pi)^2 H} \sum_n \int d^2\mathbf{q}_{||} \tilde{\rho}_{\mathbf{q}_{||},n} \cos\left(\tfrac{n\pi z}{H}\right) e^{-i\mathbf{q}_{||}\cdot\mathbf{r}_{||}}. \tag{2.43}$$

We recall our Hamiltonian

$$\mathcal{H} = \frac{1}{2} \int d^3\mathbf{r} \left(B\left(\partial_z u\right)^2 + K\left(\nabla_{||}^2 u\right)^2 + 2\beta\rho\partial_z u \right), \tag{2.44}$$

and rewrite it using the terms as defined above:

$$\begin{aligned}\mathcal{H} = &\sum_n \sum_{n'} \int d^3\mathbf{r} \int d^2\mathbf{q}_{||} \int d^2\mathbf{q}'_{||} \frac{2e^{-\left(\mathbf{q}_{||}+\mathbf{q}'_{||}\right)\cdot\mathbf{r}_{||}}}{\left(2\pi\right)^4} \times \\ &\left(\tilde{u}_{\mathbf{q}_{||},n} \tilde{u}_{\mathbf{q}'_{||},n'} \left(\tfrac{\pi^2 B n n'}{H^2} \cos\left(\tfrac{n\pi z}{H}\right) \cos\left(\tfrac{n'\pi z}{H}\right) + K q_{||}^2 q_{||}'^2 \sin\left(\tfrac{n\pi z}{H}\right) \sin\left(\tfrac{n'\pi z}{H}\right) \right) + \right. \\ &\left. \tfrac{2\pi\beta}{H^2} \left(\frac{\tilde{\rho}_{\mathbf{q}_{||},n} \tilde{u}_{\mathbf{q}'_{||},n'} n'}{2} \cos\left(\tfrac{n\pi z}{H}\right) \cos\left(\tfrac{n'\pi z}{H}\right) + \frac{\tilde{\rho}_{\mathbf{q}'_{||},n} \tilde{u}_{\mathbf{q}_{||},n} n}{2} \cos\left(\tfrac{n'\pi z}{H}\right) \cos\left(\tfrac{n\pi z}{H}\right) \right) \right).\end{aligned} \tag{2.45}$$

We compute the $\int d^2\mathbf{r}_{||}$ integral,

$$\begin{aligned}\mathcal{H} = &\sum_n \sum_{n'} \int dz \int d^2\mathbf{q}_{||} \int d^2\mathbf{q}'_{||} \frac{\delta^2\left(q_{||} + q'_{||}\right)}{2\left(2\pi\right)^4} \times \\ &\left(\tilde{u}_{\mathbf{q}_{||},n} \tilde{u}_{\mathbf{q}'_{||},n'} \left(\frac{\pi^2 B n n'}{H^2} \cos\left(\frac{n\pi z}{H}\right) \cos\left(\frac{n'\pi z}{H}\right) + K q_{||}^2 q_{||}'^2 \sin\left(\frac{n\pi z}{H}\right) \sin\left(\frac{n'\pi z}{H}\right) \right) + \right. \\ &\left. \frac{\pi\beta}{H^2} \left(\tilde{\rho}_{\mathbf{q}_{||},n} \tilde{u}_{\mathbf{q}'_{||},n} n' + \tilde{\rho}_{\mathbf{q}'_{||},n} \tilde{u}_{\mathbf{q}_{||},n} n \right) \cos\left(\frac{n\pi z}{H}\right) \cos\left(\frac{n'\pi z}{H}\right) \right).\end{aligned} \tag{2.46}$$

Sifting with the δ-functions yields

$$\begin{aligned}\mathcal{H} = &\sum_n \sum_{n'} \int dz \int d^2\mathbf{q}_{||} \frac{1}{2\left(2\pi\right)^4} \times \\ &\left(\tilde{u}_{\mathbf{q}_{||},n} \tilde{u}_{-\mathbf{q}_{||},n'} \left(\frac{\pi^2 B n n'}{H^2} \cos\left(\frac{n\pi z}{H}\right) \cos\left(\frac{n'\pi z}{H}\right) + K q_{||}^4 \sin\left(\frac{n\pi z}{H}\right) \sin\left(\frac{n'\pi z}{H}\right) \right) + \right. \\ &\left. \frac{\pi\beta}{H^2} \left(\tilde{\rho}_{\mathbf{q}_{||},n} \tilde{u}_{-\mathbf{q}_{||},n} n' + \tilde{\rho}_{-\mathbf{q}_{||},n} \tilde{u}_{\mathbf{q}_{||},n} n \right) \cos\left(\frac{n\pi z}{H}\right) \cos\left(\frac{n'\pi z}{H}\right) \right).\end{aligned} \tag{2.47}$$

We will now attempt to compute the dz integral. We will carry it out separately for each term that it hits:

$$\text{ⓘ} = \int_0^H dz C_1 n n' \cos\left(\frac{n\pi z}{H}\right) \cos\left(\frac{n'\pi z}{H}\right) \tag{2.48}$$

$$\text{ⓘⓘ} = \int_0^H dz C_2 \sin\left(\frac{n\pi z}{H}\right) \sin\left(\frac{n'\pi z}{H}\right) \tag{2.49}$$

$$\text{ⓘⓘⓘ} = \int_0^H dz \left(C_3 n' + C_4 n\right) \cos\left(\frac{n\pi z}{H}\right) \cos\left(\frac{n'\pi z}{H}\right) \tag{2.50}$$

We will make the substitution $t = z\frac{\pi}{H}$.

$$
\begin{aligned}
\text{(i)} &= \frac{C_1 H}{\pi}\int_0^\pi dt n n' \cos(nt)\cos(n't) \\
&= \begin{cases} 0 : \text{if } n \neq n' \\ \frac{C_1 H n^2}{2} : \text{if } n = n' \end{cases}. \\
\text{(ii)} &= \frac{C_2 H}{\pi}\int_0^\pi dt \sin(nt)\sin(n't) \\
&= \begin{cases} 0 : \text{if } n \neq n' \\ \frac{C_2 H}{2} : \text{if } n = n' \end{cases}. \\
\text{(iii)} &= \frac{H}{\pi}\int_0^\pi dt \left(C_3 n' + C_4 n\right)\cos(nt)\cos(n't) \\
&= \begin{cases} 0 : \text{if } n \neq n' \\ \frac{(C_3+C_4)Hn}{2} : \text{if } n = n' \end{cases}.
\end{aligned}
$$

So we can now rewrite the smectic Hamiltonian in our periodic geometry as

$$
\begin{aligned}
\mathcal{H} = \frac{1}{H(2\pi)^2}\sum_n \int d^2\mathbf{q}_{||} \Bigg(& \tilde{u}_{\mathbf{q}_{||},n}\tilde{u}_{-\mathbf{q}_{||},n'}\left(B(\pi n)^2 + H^2 K q_{||}^4\right) \\
& + \pi\beta n\left(\tilde{\rho}_{\mathbf{q}_{||},n}\tilde{u}_{-\mathbf{q}_{||},n} + \tilde{\rho}_{-\mathbf{q}_{||},n}\tilde{u}_{\mathbf{q}_{||},n}\right)\Bigg).
\end{aligned} \tag{2.51}
$$

We again minimise, this time choosing

$$
\tilde{u}_{\mathbf{q}_{||},n} = \frac{-\pi n\beta\tilde{\rho}_{\mathbf{q}_{||},n}}{B\left((\pi n)^2 + (H\lambda)^2 q_{||}^4\right)} \text{ or } \tilde{u}_{-\mathbf{q}_{||},n} = \frac{-\pi n\beta\tilde{\rho}_{-\mathbf{q}_{||},n}}{B\left((\pi n)^2 + (H\lambda)^2 q_{||}^4\right)}.
$$

With this minimisation we can write

$$
\mathcal{H} = \frac{1}{H(2\pi)^2}\sum_n \int d^2\mathbf{q}_{||} \frac{-(\pi n\beta)^2}{B\left((\pi n)^2 + H^2\lambda^2 q_{||}^4\right)}\tilde{\rho}_{\mathbf{q}_{||},n}\tilde{\rho}_{-\mathbf{q}_{||},n}, \tag{2.52}
$$

an equation analogous to (2.19), for the semi-infinite geometry.

We now seek an expression for the density function, $\tilde{\rho}_{\mathbf{q}_{||},n}$. We shall

begin by defining the function in real space, before applying our z-discrete Fourier Transform to describe it in our periodic reciprocal space.

Our system sees an inclusion with its centre offset from $z = 0$ by some distance, h. As for the bulk system, the density function will be describing a cylindrical domain of radius R_0 and length (in z) of L. We shall define it using Heaviside functions as follows:

$$\rho(\mathbf{r}) = \Theta\left(R_0\right)\Theta\left(z - \left(h - \tfrac{L}{2}\right)\right)\Theta\left(\left(h + \tfrac{L}{2}\right) - z\right). \tag{2.53}$$

Applying the forward transform to the density function, we note that the Heaviside functions serve to restrict the domain of integration for the transform.

$$\begin{aligned}\tilde{\rho}_{\mathbf{q}_{||},n} &= \int d^3\mathbf{r}\rho\left(\mathbf{r}\right)e^{i\mathbf{q}_{||}\cdot\mathbf{r}_{||}}\cos\left(\tfrac{n\pi z}{H}\right) \\ &= \int_0^{2\pi} d\theta \int_0^{R_0} r_{||}dr_{||}\int_{h-\frac{L}{2}}^{h+\frac{L}{2}} dz\left(e^{iq_{||}r_{||}\cos\theta}\cos\left(\tfrac{n\pi z}{H}\right)\right).\end{aligned} \tag{2.54}$$

Computing the $d\theta$ integral via a Hankel transform yields

$$\tilde{\rho}_{\mathbf{q}_{||},n} = 2\pi\int_0^{R_0} r_{||}dr_{||}\int_{h-\frac{L}{2}}^{h+\frac{L}{2}} dzJ_0\left(q_{||}r_{||}\right)\cos\left(\tfrac{n\pi z}{H}\right). \tag{2.55}$$

To perform the $dr_{||}$ integral, we must make use of the Bessel Recursion formula (Lebedev, 5.2.4 [17]):

$$\frac{d}{ds}s^nJ_n(s) = s^nJ_{n-1}(s). \tag{2.56}$$

We integrate this directly,

$$\int\frac{d}{ds}s^nJ_n(s)ds = \int s^nJ_{n-1}(s)ds \tag{2.57}$$

$$\implies s^nJ_n(s) + K = \int s^nJ_{n-1}(s)ds. \tag{2.58}$$

So, for $n = 1$ and $s = r_{||}$, we are able to proceed,

$$\tilde{\rho}_{\mathbf{q}_{||},n} = 2\pi \int_0^{R_0} \left(r_{||} J_0 \left(q_{||} r_{||} \right) \right) dr_{||} \int_{h-\frac{L}{2}}^{h+\frac{L}{2}} dz \cos\left(\tfrac{n\pi z}{H}\right) \tag{2.59}$$

$$= 2\pi \left(\frac{R_0}{q_{||}} J_1 \left(q_{||} R_0 \right) \right) \int_{h-\frac{L}{2}}^{h+\frac{L}{2}} dz \cos\left(\tfrac{n\pi z}{H}\right). \tag{2.60}$$

It now just remains to integrate dz,

$$\tilde{\rho}_{\mathbf{q}_{||},n} = \frac{2\pi R_0}{q_{||}} J_1 \left(q_{||} R_0 \right) \int_{h-\frac{L}{2}}^{h+\frac{L}{2}} \left(\cos\left(\tfrac{n\pi z}{H}\right) \right) dz \tag{2.61}$$

$$= \frac{2\pi R_0}{q_{||}} J_1 \left(q_{||} R_0 \right) \frac{H}{n\pi} \left(\sin\left(\tfrac{n\pi}{H}\left(h+\tfrac{L}{2}\right)\right) - \sin\left(\tfrac{n\pi}{H}\left(h-\tfrac{L}{2}\right)\right) \right). \tag{2.62}$$

So, following some small rearrangement,

$$\tilde{\rho}_{\mathbf{q}_{||},n} = \frac{4R_0 H}{q_{||} n} J_1 \left(q_{||} R_0 \right) \sin\left(\tfrac{n\pi L}{2H}\right) \cos\left(\tfrac{n\pi h}{H}\right). \tag{2.63}$$

We note there that if $L = H$ and $h = \frac{H}{2}$, a situation wherein an inclusion spans the full height of the finite slab, then $\tilde{\rho}_{\mathbf{q}_{||},n} = 0$, meaning that there can be no height mismatch as the layer spacing in both phases would have to be the same, ergo there could be no local layer deformation.

Computing the infinite sum, and the q_z integral of (2.52), and renormalising with $\nu = q_{||} R_0$, $\tau = \frac{L\lambda}{R_0^2}$, $\varepsilon_2 = \frac{\pi L H \lambda \beta^2}{B}$, we can express the energy as

$$\begin{aligned} \mathcal{H} = &- A_2 \int d\nu \frac{J_1^2(\nu)}{\tau^2 \nu^3} \Bigg(\coth\left(\tfrac{H}{L}\tau\nu^2\right) \times \\ &\times \Big(1 - \cosh\left(\tau\nu^2\right) + \cosh\left(\tfrac{2h}{L}\tau\nu^2\right) \left(1 - \cosh\left(\tau\nu^2\right)\right) \Big) + . \\ &+ \sinh\left(\tau\nu^2\right) - \sinh\left(\tfrac{2h}{L}\tau\nu^2\right) \left(1 - \cosh\left(\tau\nu^2\right)\right) \Bigg) \end{aligned} \tag{2.64}$$

Whilst this integral is analytically intractable, it is continuous and convergent

L (μm)	R^2 (μm^2)	V (μm^3)	H(μm)
2.4	1.5	16.96	7

Table 2.2: Dimensions of a columnar L_o inclusion in a finite slab of L_d [57]

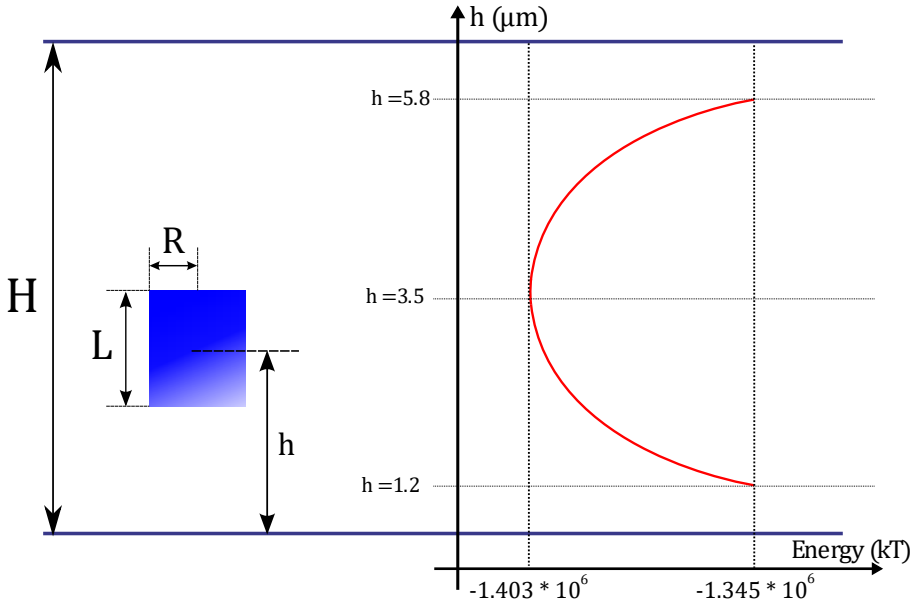

Figure 2.8: Energy ($\mathcal{H}$) of an inclusion at different positions (h) in the smectic. The dimensions of the column are given in Table 2.2.

in both limits of $q_{||} \in [0, \infty)$, ergo we can evaluate it numerically, for a given set of parameters. Fixing a value for the height of the lamellar stack, H, and the domain size, (L, R_o) inspired by the literature [56], we will numerically integrate equation (2.64) for a range of positions in the stack, so showing how the energy of the system, $\mathcal{H}$ varies with with respect to h. It is worth remarking that in the limit $H \to \infty$, (2.64) converges to (2.24) for $h = \frac{H}{2}$, and to (2.35) for $h = \frac{L}{2}$. From these systems, then, we already have the limit cases of an inclusion on an edge, and in the middle of a stack. We would expect to see the energy tend from a value near the latter to one nearer the former as h increases across the range $[\frac{L}{2}, \frac{H}{2}]$.

We note, firstly, that the energy of this inclusion, across all positions, is, as expected, similar, if slightly grater than the energy of the inclusions studied in the infinite and semi-infinite systems. For an inclusion of the dimensions

given in Table 2.2, (2.36) and (2.37) give us the energies for such an inclusion in a semi-infinite, $-1.813 \times 10^6 \mathrm{k_B T}$, and bulk, $-1.969 \times 10^6 \mathrm{k_B T}$, respectively.

The second thing to note from this figure is that it is more favourable for an inclusion to be in the centre of the smectic, with the energy associated with it being lower the further the inclusion is from either wall of the slab. This makes sense, as each wall appears like a mirror to the inclusion, in which it sees phantom inclusions at distances $2h - L$ and $2(H - h) - L$ from itself. The most energy efficient arrangement, this suggests, is with the maximum distance between the inclusion and its neighbours. This again agrees with our previous results, as we have seen that the energy of an inclusion in the bulk is less than that of an inclusion in a semi-infinite system.

In Tayebi (2012)[56], it was seen that the liquid-ordered stacks appear to form at the edges of the slab, rather than in the centre. To account for this discrepancy with our results here, we should note that we have neglected to consider the surface energy associated with the domains. For our bulk model, we calculated a surface energy, E_s, required to favour the formation of columns with the observed aspect ratio. We recall that (2.34) for an inclusion of the dimensions in Table 2.2, $\sigma_z = 2.65 \times 10^4 \mathrm{k_B T} \mu\mathrm{m}^2$, so giving us a value of $E_s = 3.75 \times 10^5 \mathrm{k_B T}$ for a column with two exposed faces.

A column at the boundary of the finite slab has only one face exposed to $\mathrm{L_d}$. As such the surface energy associated with such an inclusion is half that of one not in contact with the boundary, $\frac{E_s}{2} = 1.88 \times 10^5 \mathrm{k_B T}$. As such, the total energy of an inclusion at the boundary is

$$\mathcal{H}_{\text{boundary}} = -1.34 \times 10^6 + 1.88 \times 10^5 \mathrm{k_B T} = -1.16 \times 10^6 \mathrm{k_B T},$$

whilst the total energy of a domain in the centre of the stack is

$$\mathcal{H}_{\text{centre}} = -1.40298 \times 10^6 + 3.75 \times 10^5 \mathrm{k_B T} = -1.03 \times 10^6 \mathrm{k_B T}.$$

The total energy for a domain at the boundary, then, is less than that for one in the centre of the slab, ergo this surface energy is sufficient to compel $\mathrm{L_o}$ domains to form there, rather than elsewhere in the stack.

As we computed this surface energy for an inclusion in the bulk, it can only be an estimated lower bound for the inter-facial energy necessary

for an inclusion of such dimensions in a finite slab, so the true figure may well be higher, favouring even more the boundary prospect. Can we lend any provenance to such an energy, though?

We have determined that a surface energy of at least $\sigma_z = 2.65 \times 10^4 \mathrm{k_B T}\mu\mathrm{m}^2$ is required to have stable columnar $\mathrm{L_o}$ inclusions. The density of lipids in the $\mathrm{L_o}$ phase is markedly greater than that in the $\mathrm{L_d}$ phase, with an area per lipid of ~ 49.5Å in the $\mathrm{L_o}$ phase, and ~ 60 Å in the $\mathrm{L_d}$ phase [40, 42]. This gives $\sim 3 \times 10^5$ lipids $\mu\mathrm{m}^{-2}$ more in the $\mathrm{L_o}$ phase than the $\mathrm{L_d}$. We note that should $\mathrm{L_o}$ phases in neighbouring layers be able to form $\sim 1 \times 10^4$ extra hydrogen bonds $\mu\mathrm{m}^{-2}$ between them, than between $\mathrm{L_o}$ and $\mathrm{L_d}$, this would be equivalent to an energy of the order of σ_z. This equates to the formation of an extra hydrogen bond per 30 lipids, which is reasonable given the probability of transient hydrogen bond formation in such a scenario [36, 31]. This is, as such, not an implausible candidate for the energy required to form stable columnar liquid-ordered inclusions in lamellar bodies.

Chapter 3

Swimmers in Smectics

3.1 Introduction

Collective motion has been observed in many natural systems across all biological scales and a great range of environments [25, 12, 3, 38]. From the macroscopic: shoals of fish[30], flocks of starlings[6], and herds of sheep[22], to the microscopic: swarming krill[27], bioconvecting phytoplankton[41], and swimming bacteria[68]. These examples are striking as they represent the development of long-range order in a system of agents, arising from their interactions as a group, not from any external driving influence, field or force, nor through the actions of some leader. Over the years, many models have been developed describing collective motion in one form or another, though for the majority of living systems, the phenomenon has resisted a satisfactory explanation.

The seminal work by Vicsek et al. [66] constructed a limited model, in which long range orientational order was shown to arise in a system of agents obeying simple rules. In the original Vicsek model, a group of identical agents moved off-lattice, within a periodic box. The positions of the agents were updated following discrete interval time-steps in which an agent would move a prescribed distance. At each update, each agent would have its direction of travel changed to equal the average direction of all agents within a fixed radius neighbourhood. They found that above a critical density of agents, collective motion would occur with the spontaneous breaking of symmetry, and uniform global orientation of the agents. This order was observed to be

resilient to small amounts of noise (added as a white-noise angular error to agents' updating their direction of motion), but that broke down to random uncorrelated motion above a certain noise threshold. Grégoire and Chaté [25] later showed that the noise-induced phase transition, between the ordered and disordered states observed in Vicsek (and indeed any model of locally interacting active particles in 2D), is discontinuous, but subject to "strong finite-size effects".

Since Vicsek, various other minimal models have been developed which exhibit collective motion of self-propelled particles. Toner and Tu [61, 26] considered the situation from a continuum perspective, developing hydrodynamic equations to describe polar active matter. Other models have since related agent-based hydrodynamic models of interacting, self-propelled particles to their macroscopic description[26]. Meanwhile, much work has been done extending the discrete-time Vicsek model with different reorientation rules for agents, having agents directly interact, and taking into account the medium within which the agents move [12, 3, 15, 6].

Smectic A liquid crystals are comprised of molecules arranged into layers, with the orientation of the molecule normal to the plane of the layer. Within the layers, the molecules are free to move around within the plane of the layer, so each behaves as a 2D liquid. The discrete layers of molecules are organised into stacks, with a uniform spacing between neighbouring layers [16]. Examples of such objects include the lamellar phase of surfactant bilayer membranes, diblock co-polymer melts, as well as many others in chemistry [49, 48, 63].

It is known that the presence of impurities such as colloidal inclusions between the smectic layers can disturb the ordering of those layers [62, 43]. This can, in turn, lead to the inclusions being induced to change their relative positions within the smectic, to reduce the overall deformation to the layers. In effect, this results in an interaction potential between inclusions, which can be both repulsive or attractive over different length scales, and decays more rapidly within the plane than across layers. Practically, there is the prospect of strong non-trivial interactions between particles embedded within different layers of a smectic-phase.

Whilst there has been much interest, recently, on active nematics, ac-

tive smectics remain relatively unexplored. Work on active liquid crystals can broadly be split into two schema. The first are those systems wherein the liquid crystal is composed of active constituent molecules, such as the microtubule/kinesin systems of active nematics [20] or the smectic "Live Soap" system of Adhypak et al. [2]. Here the movement of the active molecules along their directors leads to the dynamics and phase transitions in these systems. The second are those wherein active elements move through a liquid crystal medium. Here the motion of the active particles is affected by, and affects, the director of the liquid-crystal molecules, such as bacteria swimming in lyotropic chromonic [69] or a smectic medium [21], aligning themselves with the molecular director leading to collective dynamics.

No work has yet examined active agents obliged to move perpendicular to the director in a smectic. We are interested in how swimmers, such as bacteria, embedded in and confined to the inter-layer space of a smectic liquid crystal, such as a lamellar stack of bilayers, might have their collective behaviour affected by interactions mediated by their distorting the smectic.

We build a minimal model to describe this situation, and run simulations to explore its behaviour. We observe that under certain circumstances (with a balance between the size and speed of micro-swimmers, and the stiffness of the smectic layers) the smectic-mediated interaction between the embedded swimmers is sufficient for the development of collective motion. The effect of noise on the robustness of the co-aligned motion is examined, and a phase transition from the ordered state to a disordered state is identified.

3.2 Methods and Theory

3.2.1 The Smectic-Mediated Force

Colloids embedded between layers of a smectic liquid crystal with a diameter slightly greater than the mean smectic layer spacing will distort the smectic. This distortion has an associated energy cost.

By perturbing the layer-structure of the smectic, micro-swimmers embedded in the smectic interact with one-another. The loss of symmetry with multiple inclusions in the smectic, each locally contributing to the distortion

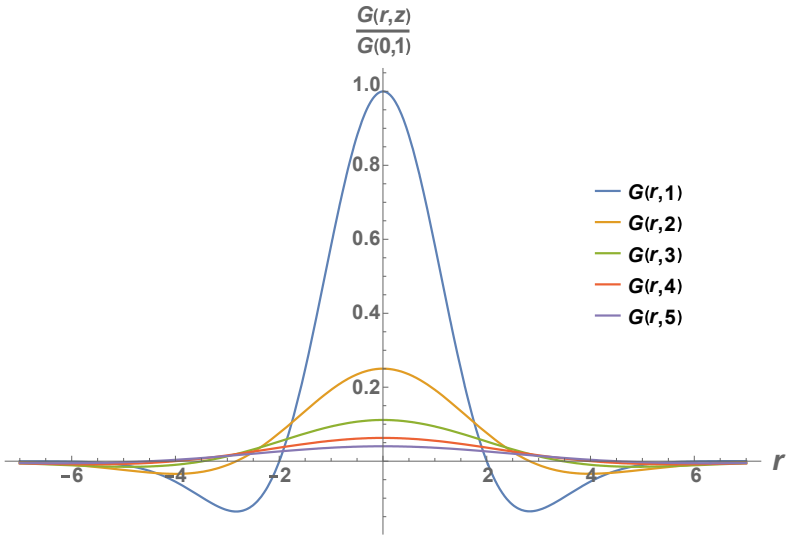

Figure 3.1: Plot of the interaction potential between two similar inclusions in a smectic phase, as a function of their separation. The plot is for $r_{||}$, the radial separation, in units of λ, the layer spacing. We plot $G(\mathbf{r})$, for $z \in \{1, 2, 3, 4, 5\}$. The potential has a maximum at $r_{||} = 0$, decaying rapidly to a minimum at $r_{||} = \sqrt{8\lambda|z|}$. The interaction is repulsive at short range, and attractive at long range. Note that it decays in $r_{||}$ much faster than in z.

field, makes for a system where some arrangements of agents distort the smectic less and so are more energetically favourable than other arrangements. We can understand this energy landscape in terms of the two-body interaction potentials between pairs of swimmers, and so the consequent forces that the swimmers experience as they are induced to move into positions which minimise the total distortion to the smectic.

We follow the approach by Sens, Turner et al. in determining the interaction potential between particles embedded in a smectic liquid crystal [49, 48, 63].

We make use of the Landau-de Gennes Hamiltonian for a smectic liquid crystal [16]. This description is concerned with the displacement, u, in the direction normal to the plane (which we will henceforth refer to as the z direction, in contrast to the x, y-plane of the layer) of layers from an average flat state. As well as the standard terms dealing with compression or dilation of layers ($B(\partial_z u)^2$), and bending of layers ($K(\nabla_{||}^2 u)^2$), we must also consider the effect of the swimmers distorting layers. To do this we will include an

additional term to the standard Hamiltonian, $\beta\rho\partial_z u$:

$$\mathcal{H} = \frac{1}{2}\int d^3\mathbf{r}\left(B\left(\partial_z u\right)^2 + K\left(\nabla_{||}^2 u\right)^2 + 2\beta\rho\partial_z u\right) \tag{3.1}$$

where B (dimensions of energy length^{-3}) and K (dimensions of energy length^{-1}) are respectively the compression and bending moduli, ρ is the density of the colloidal inclusions at a point. β is a coupling constant which determines the magnitude of the layer deformation caused by a unit density of swimmers.

Minimising the Hamiltonian yields the interaction potential between a pair of inclusions with a separation $\mathbf{r} = \mathbf{r} - \mathbf{r}'$:

$$G(\mathbf{r}) = \frac{\beta^2}{16\pi\lambda B z^2} e^{-\frac{r_{||}^2}{4|z|\lambda}}\left(1 - \frac{r_{||}^2}{4|z|\lambda}\right), \tag{3.2}$$

We note here that (3.2) is not well behaved in the limit $z \to 0$. This is a consequence of our using a continuum approach, which breaks down over small lengthscales. Although some theoretical work [49] suggests that inclusions in the same layer will experience a monotonic attraction, there also exists experimental work suggesting the reverse[43]. Both may indeed be true, as the former deals with inclusions of diameter $d \approx \lambda$, whilst the latter of diameter $d \gtrsim \lambda$. The exact crossover between them is not clear and has resisted our attempts to calculate it. As such, we will make a significant simplification in our model, and neglect any direct smectic-mediated interaction between swimmers in the same layer.

The smectic mediated force is thus given by the derivative of (3.2). We do not allow swimmers to move between layers, so we will set the z-component of this force to zero. So the smectic mediated-force exerted on one swimmer by another at a separation $\mathbf{r}$ is, in Cartesian coordinates,

$$\mathbf{F}_{\mathrm{Sm}} = -\nabla G(\mathbf{r}) = -\frac{\beta^2}{16\pi\lambda B} e^{-\frac{x^2+y^2}{4|z|\lambda}} \begin{pmatrix} \frac{x^3+xy^2}{8z^4\lambda^2} - \frac{x}{|z|\lambda z^2} \\ \frac{y^3+yx^2}{8z^4\lambda^2} - \frac{y}{|z|\lambda z^2} \\ 0 \end{pmatrix} \tag{3.3}$$

In a system of N swimmers, the force on a particular swimmer (i) will be the sum of the forces exerted on it by all the other swimmers (j) in the system:

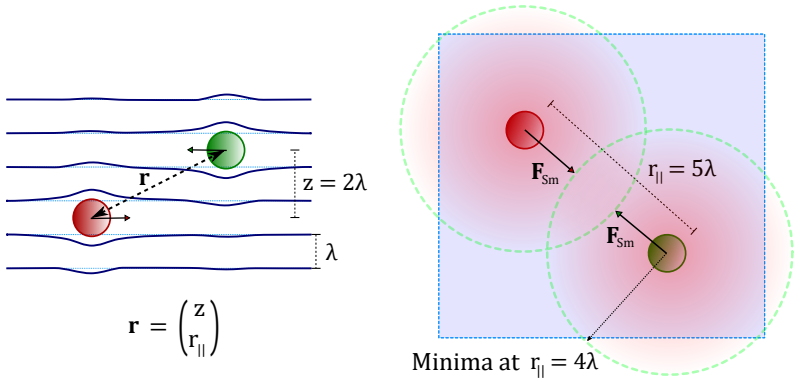

Figure 3.2: Colloidal inclusions in the smectic locally distort the layers. This distortion has an associated potential which results in a force, $\mathbf{F}_{\mathrm{Sm}}$, that moves the inclusions to their relative energetic minima at $r_{||} = \sqrt{8\lambda|z|}$, indicated by the dashed green radius.

$$\mathbf{F}_{\mathrm{Sm}i} = \sum_{j=1}^{N-1} -\nabla G(\mathbf{r}_i - \mathbf{r}_j) \tag{3.4}$$

3.2.2 Swimmer Reorientation

A micro-swimmer, in the absence of any smectic-mediated force, will travel with a self-propulsion velocity

$$\mathbf{v_{sp}} = |\mathbf{v_{sp}}|\mathbf{p} \tag{3.5}$$

Where the unit vector $\mathbf{p} = (\cos\psi, \sin\psi, 0)$ is the swimming direction. In the presence of the smectic-mediated force, this swimming direction may change as the swimmer is reorientated by the torques acting upon it.

In a deterministic system, reorientation can only occur due to some broken symmetry in the swimmer which causes it to have an orientational preference due to the anisotropy of the smectic force. Our swimmers are constrained to only move in two dimensions by the smectic layers that they are confined between. In this 2D plane, they can only orient themselves with

respect to the direction at which the smectic-induced force acts upon them. In the absence of this force they would not reorient, as the medium they are swimming through is presumed to be isotropic, and we are neglecting any hydrodynamic interactions between the swimmers themselves, or the confining smectic. Considering only orientation about an axis normal to the smectic layers, let us define the swimming direction of our motile particle to be

$$\mathbf{p} = \begin{pmatrix} \cos\psi \\ \sin\psi \end{pmatrix}, \tag{3.6}$$

with ψ measured relative to some arbitrary axis in the smectic plane. We shall also write our previously defined smectic-mediated force, (3.4), as

$$\mathbf{F}_{\mathrm{Sm}} = |\mathrm{F}_{\mathrm{Sm}}| \begin{pmatrix} \cos\phi \\ \sin\phi \end{pmatrix}, \tag{3.7}$$

which acts to move the swimmer in the direction ϕ, measured relative to the same axis as ψ.

Irrespective of their shape, our swimmers will have some centre of hydrodynamic stress [9] where the hydrodynamic force arising by their motion through the fluid may be considered to be acting. All automotile agents will have a hydrodynamic centre to their swimming motion. We shall call this point c_H. Any force acting on a point offset from c_H will effect some rotation on the swimmer. Of course, applying a force on the point c_H would result in no rotation.

For simplicity, we shall only consider an offset from c_H along the axis of the swimming direction vector, $\mathbf{p}$. This is not such a huge assumption, as it is a condition satisfied simply by our swimmers being radially symmetric about their swimming direction vector. Now, we shall call the point upon which the smectic-mediated force acts upon our swimmer c_{Sm}, and we shall define the offset

$$\delta = c_{\mathrm{Sm}} - c_H. \tag{3.8}$$

We note that there are two cases to consider here: that of a positive offset ($c_{\mathrm{Sm}} > c_H \implies \delta > 0$), like a typical "pusher", and that of a negative offset

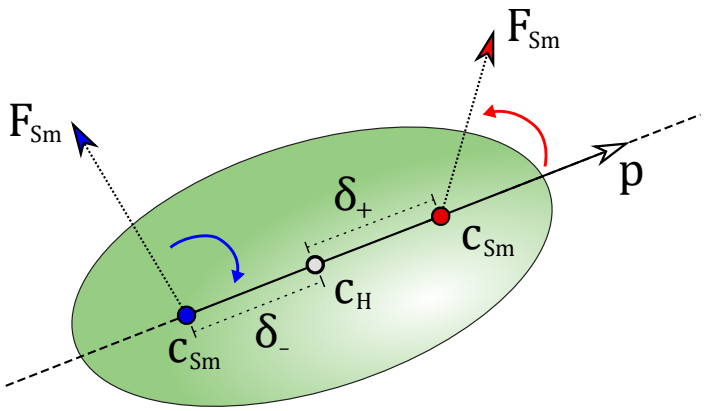

Figure 3.3: The offset, δ, of the point the smectic force acts on, c_{Sm}, from the centre of hydrodynamic stress, c_{H}, can result in a change in the agent's swimming direction, $\mathbf{p}$. If $\delta > 0$ (δ_+), the resultant torque will minimise the angle between $\mathbf{p}$ and $\mathbf{F}_{\mathrm{Sm}}$, aligning the swimming direction with the smectic force (red). If $\delta < 0$ (δ_-), the swimmer will anti-align, to swim against the pull of the smectic force (blue).

($c_{\mathrm{Sm}} < c_H \implies \delta < 0$), like a typical "puller".

It now remains for us to describe the induced reorientation of our swimmers. We shall do so by considering those torques that act upon the swimmer to effect or inhibit changes in orientation.

We define the smectic torque, which results from the action of the smectic-induced force upon the offset point, as

$$\mathbf{T}_{\mathrm{Sm}} = \delta \left(\mathbf{p} \wedge \mathbf{F}_{\mathrm{Sm}} \right). \tag{3.9}$$

This torque acts to increase the angle between $\mathbf{p}$ and $\mathbf{F}_{\mathrm{Sm}}$ if δ is negative, and to decrease it if δ is positive. This is to say, that it acts to align the swimmer with the direction of the smectic force if the swimmer is a pusher, and to anti-align it if a puller. The torque is scaled by the magnitude of $\mathbf{F}_{\mathrm{Sm}}$ and δ, so if there is no force, or no offset, then there is no torque to induce reorientation.

A micro-swimmer will also experience a drag-based resistance to changes in direction: a torque arising from viscosity and serves to impede changes in

direction. This viscous torque will depend on the shape of the swimmer. For a spherical swimmer, the viscous torque due to Stokes' drag is well known from Faxen's Laws: $\mathbf{T} = 8\pi\mu a^3 (\dot{\mathbf{p}} \wedge \mathbf{p})$, which assumes no vorticity or turning of the swimmer about its long axis, nor any distortion caused by other swimmers. However, for a generic swimmer

$$\mathbf{T}_V = c_1 \mu (\dot{\mathbf{p}} \wedge \mathbf{p}), \tag{3.10}$$

where μ is the dynamic viscosity, and c_1 is a geometric parameter ($\sim [\mathrm{L}]^3$) dependent on the shape of the swimmer. By Newton, we balance the torques such that

$$\mathbf{T}_V + \mathbf{T}_{\mathrm{Sm}} = 0, \tag{3.11}$$

ergo,

$$c_1 \mu (\mathbf{p} \wedge \dot{\mathbf{p}}) = \delta (\mathbf{p} \wedge \mathbf{F}_{\mathrm{Sm}}), \tag{3.12}$$

$$\implies \quad \mathbf{p} \wedge \dot{\mathbf{p}} = \frac{\delta}{c_1 \mu} (\mathbf{p} \wedge \mathbf{F}_{\mathrm{Sm}}), \tag{3.13}$$

$$\implies \quad \dot{\mathbf{p}} = \frac{\delta}{c_1 \mu} (\mathbf{p} \wedge \mathbf{F}_{\mathrm{Sm}} \wedge \mathbf{p}). \tag{3.14}$$

We recall that

$$\dot{\mathbf{p}} = \frac{\partial}{\partial t}\mathbf{p} = \dot{\psi} \begin{pmatrix} -\sin\psi \\ \cos\psi \end{pmatrix}. \tag{3.15}$$

And so, equating (3.14) and (3.15), we have the following system:

$$\begin{cases} -\dot{\psi}\sin\psi &= \frac{\delta |\mathrm{F}_{\mathrm{Sm}}|}{c_1 \mu} \sin\psi (\sin\psi\cos\phi - \cos\psi\sin\phi), \\ \dot{\psi}\cos\psi &= \frac{\delta |\mathrm{F}_{\mathrm{Sm}}|}{c_1 \mu} \cos\psi (\cos\psi\sin\phi - \sin\psi\cos\phi). \end{cases} \tag{3.16}$$

Dividing by $-\sin\phi$ or $\cos\phi$, respectively, and rewriting $\cos\psi\sin\phi - \sin\psi\cos\phi = \sin(\psi - \phi)$, we arrive at an expression for the change in swimming direction due to the action of the smectic-mediated force upon the swimmer:

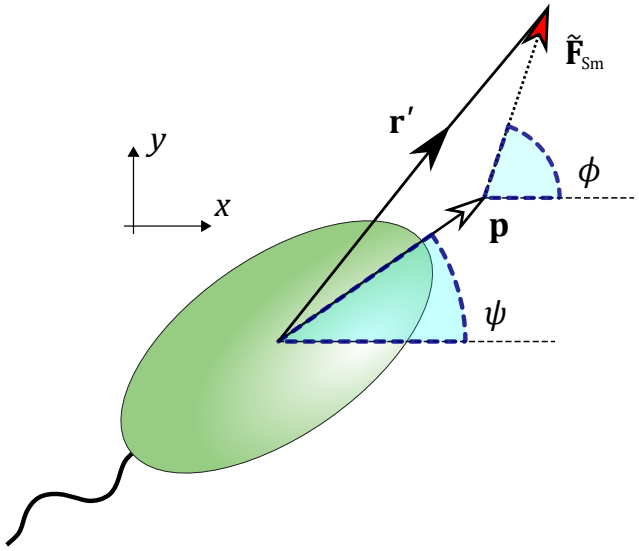

Figure 3.4: A swimmer moves in the plane as a result of the combination of its own motility ($\mathbf{p} = (\cos\psi, \sin\psi)$) and the smectic force ($\tilde{\mathbf{F}}_{\mathrm{Sm}} = |\tilde{\mathrm{F}}_{\mathrm{Sm}}|\,(\cos\phi, \sin\phi)$).

$$\dot{\psi} = \frac{\delta|\mathrm{F}_{\mathrm{Sm}}|}{c_1\mu}\sin(\phi - \psi). \tag{3.17}$$

3.2.3 A Dimensionless Model

A swimmer's position, $\mathbf{r}$, in its smectic layer will change over time through a combination of its own motility, and the force it experiences via the smectic. Stokes tells us that a sphere of radius a in a fluid, acted upon by a force will move with a velocity $\mathbf{v} = \frac{\mathbf{F}}{6\pi\mu a}$ where μ is the dynamic viscosity. Our swimmers are of a more general shape, though, so their velocity due to the action of the smectic-mediated force will be $\frac{\mathbf{F}_{\mathrm{Sm}}}{c_2\mu}$, where c_2 is a length parameter dependent on the shape of the swimmer. Consequently we can state its change in position simply as

$$\dot{\mathbf{r}} = \mathbf{v_{sp}} + \frac{1}{c_2\mu}\mathbf{F}_{\mathrm{Sm}}, \tag{3.18}$$

Equations (3.4), (3.17) and (3.18), comprise our model.

Scaling our lengths by λ, so $\tilde{\mathbf{r}} = \frac{1}{\lambda}\mathbf{r}$, and time so that $\tilde{t} = \frac{|\mathrm{v}_{sp}|}{\lambda}t$, we are in a position to nondimensionalise our equations.

We note that

$$\dot{\mathbf{r}} = \frac{d\mathbf{r}}{dt} = \frac{|\mathrm{v}_{sp}|\lambda}{\lambda}\frac{d\tilde{\mathbf{r}}}{d\tilde{t}} = \tilde{\mathbf{r}}' \cdot |\mathrm{v}_{sp}| \tag{3.19}$$

so

$$\tilde{\mathbf{r}}' = \mathbf{p} + \frac{\mathbf{F}_{\mathrm{Sm}}}{|\mathrm{v}_{sp}|c_2\mu}. \tag{3.20}$$

We now write

$$\tilde{\mathbf{F}}_{\mathrm{Sm}} = \frac{\mathbf{F}_{\mathrm{Sm}}}{|\mathrm{v}_{sp}|c_2\mu} = S\sum_i \sigma(\mathbf{r} - \mathbf{r}_i) \tag{3.21}$$

where

$$S = \frac{\beta^2}{16\pi\lambda^4 B|\mathrm{v}_{sp}|c_2\mu}, \tag{3.22}$$

is a dimensionless parameter characterising the strength of the smectic interaction, and

$$\sigma(\mathbf{r}) = -e^{-\frac{x^2+y^2}{4|z|}} \begin{pmatrix} \frac{(x^3+xy^2)}{8z^4} - \frac{x}{|z|z^2} \\ \frac{(y^3+yx^2)}{8z^4} - \frac{y}{|z|z^2} \\ 0 \end{pmatrix}. \tag{3.23}$$

Similarly, for reorientation,

$$\dot{\psi} = \frac{d\psi}{dt} = \frac{|\mathrm{v}_{sp}|}{\lambda}\frac{d\psi}{d\tilde{t}} = \frac{|\mathrm{v}_{sp}|}{\lambda}\psi'. \tag{3.24}$$

So we have

$$\psi' = \frac{\lambda}{|\mathrm{v}_{sp}|}\frac{\delta|\mathrm{F}_{\mathrm{Sm}}|}{c_1\mu}\sin(\phi - \psi), \tag{3.25}$$

$$= \frac{\lambda}{|\mathrm{v}_{sp}|}\frac{\delta}{c_1\mu}|\mathrm{v}_{sp}|c_2\mu|\tilde{\mathrm{F}}_{\mathrm{Sm}}|\sin(\phi - \psi), \tag{3.26}$$

$$= \frac{\delta\lambda c_2}{c_1}|\tilde{\mathrm{F}}_{\mathrm{Sm}}|\sin(\phi - \psi). \tag{3.27}$$

Defining $\tau = \frac{c_1}{\delta\lambda c_2}$, a dimensionless parameter characterising the time for a swimmer to reorient, we can write a dimensionless expression for reorientation:

$$\psi' = \frac{|\tilde{\mathrm{F}}_{\mathrm{Sm}}|}{\tau} \sin(\phi - \psi). \tag{3.28}$$

So we have two dimensionless control parameters, τ and S, as well as the equations (3.20), (3.21) and (3.28), comprising a dimensionless model.

3.2.4 Simulation Details

To explore the behaviour of a system of micro-swimmers in a smectic liquid crystal we will simulate swimmers governed by our model equations. We are interested in potential order that such a system may evidence, driven by the smectic-mediated interaction between agents.

Our simulations will involve a periodic box, comprising ten smectic layers (and thus ten inter-layer gaps), each 50λ by 50λ, where λ is the mean distance between layers. A box of this size was chosen to reduce the impact of ipsitropic effects in the first instance and through one or more other swimmers (in a smaller box, the strength of the inter-agent interaction could be sufficient for the swimmer to feel it's own influence, or for other swimmers to be acted upon by the swimmer and it's periodic phantom). A five layer difference reduces the maximum magnitude of the potential by over an order of magnitude, ten by two. Similarly, a $(50\lambda)^2$ box was found to be sufficient to ensure agents had freedom to move, without being restricted by the box size and proximity to neighbours through the periodicity, but not so great that the agents failed to interact in reasonable simulation time. Into the box are placed 100 agents, 10 per layer, with their positions and orientations within the layer randomly determined for each simulation.

We chose a timestep size of $0.001\frac{\lambda}{|\mathrm{v}_{sp}|}$. This value well compromises between reduction of computational noise (inherent in any discrete-time approximation of a continuous process) and efficiency. It also allows a reasonable comparison with the original Vicsek model [66] which runs on a similar chronal resolution, in the "small velocity regime".

Microswimmers, being self-propelled and thus force-free, are considered to swim by a hydrodynamic force dipole generating a flow field about the particle decaying as $\frac{1}{r^2}$ in a bulk fluid [53], and swimmers can interact hydrodynamically with one another and with boundaries by means of this flow field.

Such an interaction clearly has the potential to be long ranged and capable of having a much greater impact on the the dynamics of our system than the smectic-mediated interaction. With such a decay, even for a hydrodynamic interaction of a similar order to the smectic interaction at short range, for more distant swimmers the the hydrodynamic interaction will dominate.

It has been observed that the flow of fluid adjacent to a lyotropic membrane can induce a corresponding flow in the membrane itself, consequently capable of transmitting the flow to the fluid on the other side of the membrane [47, 67]. In practice this raises the possibility that in some systems the swimmers might be capable of hydrodynamically interacting across layers. We will assume a system where we have selected a smectic make-up such that any hydrodynamic interaction is sufficiently screened by the membranes to have a negligible impact in neighbouring layers, so that the only interlayer interaction in our model will be via the smectic-mediated interaction.

The hydrodynamic interaction of microswimmers confined to two-dimensional geometries is still currently a rich area of research [58, 35]. Different means of swimming (for instance puller versus pusher) have very different flow fields associated with them which influences whether they attract or repel, align or diverge, at different configurations. A thorough examination of potential intra-layer hydrodynamic interactions between swimmers is beyond the scope of this work, and any choice will dominate the dynamics of our simulations. As such we feel that the best choice is to make the somewhat unreasonable approach of omitting any intra-layer hydrodynamic interaction between our agents.

Our swimmers are modelled as point particles with no direct interaction with other agents in the same layer (though three-body interactions via both agents in the same layer interacting with an intermediary in another layer are possible). As such, the situation can arise that swimmers in the same layer could occupy the same co-ordinates. In practice this occurs frequently in the simulations, and with both agents resting in the same potential well they will be inclined to remain stuck in this configuration. Whilst this unrealistic situation could be avoided by the inclusion in our model of some repulsive same-layer interaction (for instance a Lennard-Jones potential), we chose not to do this for two main reasons: firstly, that we are uncertain what the best

in-layer interaction should be; and secondly, that we want to construct a simplified model entirely driven by our reasoned smectic-mediated effect rather than a combination of this and some other phenomenon.

Where we added noise to our simulations to examine the impact this had on any emergent order, this was done in the form of an orientational noise. This was done by including an additional term to our reorientation expression, (3.17), with $\Delta\phi$, randomly drawn from the continuous interval $[-\eta\pi, \eta\pi]$, with $\eta \in [0, 1000]$ determining the strength of the noise. With noise, our expression for reorientation is given by

$$\phi' = \frac{|\tilde{\mathrm{F}}_{\mathrm{Sm}}|}{\tau} \sin(\phi - \psi) + \Delta\phi. \tag{3.29}$$

1000 is the upper limit for η as this corresponds to a potential maximum change in angle of π in a single time-step (recalling that in realising the model in a simulation, any change in orientation angle must be multiplied by our time-step size, here of 0.001 dimensionless model time units).

3.2.5 Order Parameters

To characterise the amount of order in the system, we will measure two order parameters in our simulations. There are two types of order that we are interested in quantifying. The first is the extent to which we have alignment of swimmers - a measure of how effective (or not) the torque resultant from the smectic-mediated interaction has been in co-aligning agents. The second is the extent to which our swimmers have arranged themselves to sit on the minima in the smectic energy landscape.

For the first, we will take inspiration from Vicsek [66] and utilise the centre of mass speed of our swimmers. This is defined as

$$\Phi(t) = \frac{1}{N} \left| \sum_{i}^{N} \mathbf{p}_i(t) \right|, \tag{3.30}$$

where $\mathbf{p}_i$ is the swimming direction of swimmer i. The value of Φ characterises the extent to which the system displays global orientational order. A disordered system, with agents swimming in different direction will have a value

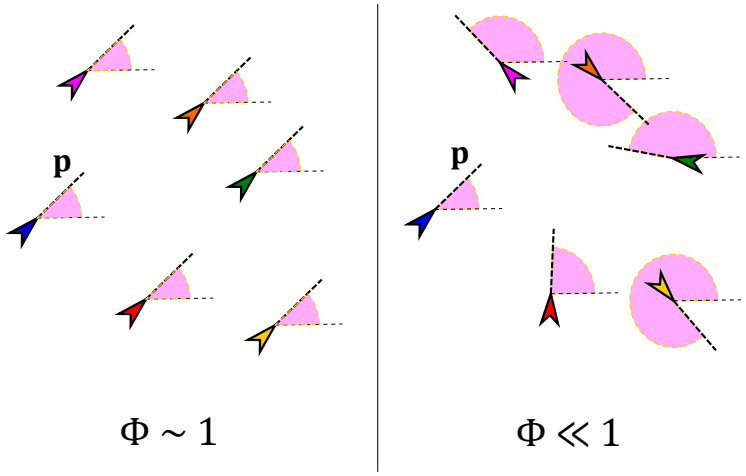

Figure 3.5: A system with agents with very different swimming direction vectors ($\mathbf{p}$) will have a low centre of mass speed, $\Phi \ll 1$, whilst a system with agents swimming in the same direction will have a high centre of mass speed $\Phi \approx 1$. Different colours are to indicate the swimmers being in different layers. Recall that our model is scaled so that $|\mathrm{v_{sp}}| = 1[\lambda\text{per unit model time}]$.

for Φ close to 0, with this number increasing as the system exhibits greater order. $\Phi = 1$ means that all the agents are travelling in the same direction.

For the second order parameter, we wish to characterise the extent to which the system has relaxed, with our agents having arranged themselves on the interlayer lattice of smectic-mediated potential minima. This will be a proxy measure for the extent to which the system displays positional order. We note that as more swimmers find these minima, relative to the other agents, then the system energy will drop. We will, therefore, compute the system energy. We rewrite (3.2) as

$$G(\mathbf{r}) = \overbrace{(\lambda|\mathrm{v_{sp}}|c_2\mu)S}^{\xi} \underbrace{\tfrac{1}{z^2} e^{-\frac{r_{||}^2}{4|z|}} \left(1 - \frac{r_{||}^2}{4|z|}\right)}_{g(\mathbf{r})}, \tag{3.31}$$

where (x, y, z) are those rescaled by $\frac{1}{\lambda}$. So for each swimmer i,

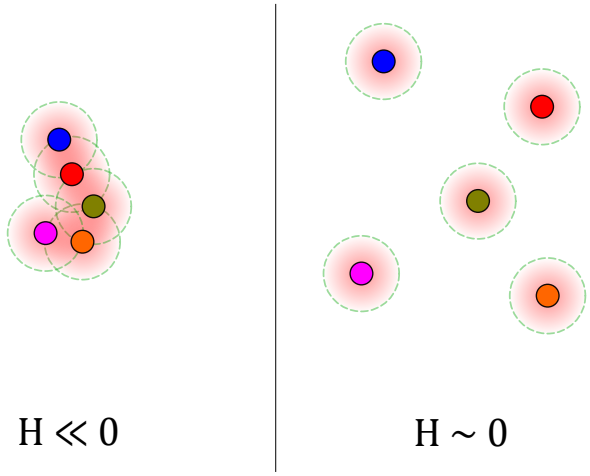

Figure 3.6: A system with the swimmers highly separated will have a system energy H close to 0. As the swimmers get closer to one-another, they will get closer to their respective minima at $r_{||} = \sqrt{8\lambda|z|}$. With more swimmers at these minima, the positional order will be high, and the system energy will be lower.

$$g_i(\mathbf{r}(t)) = \sum_{j \neq i}^{N-1} g\left(\mathbf{r}_i(t) - \mathbf{r}_j(t)\right). \tag{3.32}$$

This energy which will stand in for a positional order parameter, then, is given by

$$\mathrm{H}(t) = \frac{1}{N} \sum_{i}^{N} g_i. \tag{3.33}$$

We have rescaled H to remove ξ from this quantity, because as a constant, it proportionally scales the magnitude of H, and as we are only interested in the *relative* value of H, we would gain little from its inclusion.

We note that $\mathrm{H}(t)$ will become more negative, as the positional order increases. The theoretical limit to the value of H is $-\frac{5197}{180}\exp(-2) \approx -3.91$. This value being achieved only if all swimmers find their respective minima at $r_{||} = \sqrt{8\lambda|z|}$ to all other swimmers in the system. Such a configuration may be impossible in practice, as it is infeasible to satisfy the positional requirements of agents across the different layers. We observe, however, that the

contribution of swimmers in neighbouring layers dominates this figure, adding $20\exp(-2) \approx -2.71$. It is important, also, to consider that the very strong short range repulsive and attractive interactions between agents, will make it difficult for them to fully explore all configurations of their space, and that they are likely to become trapped in a state of partial frustration, unable to access the global minima. As such, we would expect to see this order parameter's value to plateau, short of the true minima.

3.3 Results and Discussion

3.3.1 No Added Noise

We will begin with the simplest case and examine a deterministic system with no added orientational noise.

Considering our expression for reorientation, (3.17), we clearly have two cases to address: $\delta > 0$ - agents who co-align due to the smectic-mediated force ("pushers" such as *E. coli*), and $\delta < 0$ - agents who anti-align ("pullers" such as *C. reinhardtii*), as well as the trivial case of no-realignment. These correspond to positive and negative value for τ, respectively. We shall look at each case separately, beginning with that of co-alignment.

Deterministic Co-alignment: General Behaviour

Our aim is to understand the behaviour of a collection of co-aligning swimmers in a smectic liquid crystal for a range of values of τ - the parameter which controls the rate at which swimmers change swimming direction, and S - the parameter which controls the strength of the smectic interaction.

Using a simulation written in Python we ran simulations for

$$S, \tau \in \{0.001, 0.01, 0.1, 1, 10, 100, 1000\}.$$

Position and orientation data was collected for all agents in the simulation, for 10000 time-steps following a burn-in of 150000 time-steps (sufficient time for a swimmer to traverse the length of the 50λ box three times[1]). From the

[1]Simulation runtime was a limited resource, and running the simulation with very long

position and orientation data for each parameter set, we made movies to show the behaviour qualitatively and constructed three histograms, each to address a different question:

1. Given that the smectic-interaction favours a two-particle separation of $r_{||} = \sqrt{8\lambda|z|}$, are swimmers more likely to be found at particular distances from one-another?

2. As a result of smectic-induced co-alignment, do swimmers with a particular separation move in the same direction?

3. Should the combination of the first two effects induce swimmers to orbit one-another in any sense, is there any respective rotation between swimmers of a given separation?

As such these histograms are to highlight any correlation that might exist between density and separation $|\mathrm{r}_{ij}| = |\mathbf{r}_j - \mathbf{r}_i|$; separation and co-orientation, $\mathbf{p}_i \cdot \mathbf{p}_j$; and separation and vorticity, $|\omega_{ij}| = |\mathbf{r}_{ij} \wedge \mathbf{p}_j - \mathbf{r}_{ij} \wedge \mathbf{p}_i|$.

The full set of histograms can be found in Appendices, whilst the movies may be found in the SI. Selected examples are presented below.

The quasi-phase diagram in Figure 3.7 summarises the different behaviours observed in our simulations. There are two principle regions of note in the (S, τ) phase space shown in the diagram. In the first, broadly covering low S and higher τ, and so covering systems of particles with weak or slow interaction, we have "ballistic" behaviour. Examples of this type of behaviour can be seen in Figures 3.8, 3.9 and 3.10. Here, where the smectic interaction is small (or non-existent, in the case of $S = 0$), agents neither get pulled into or trapped in respective potential wells, nor do they co-align, so swimming directions remain random. We see no grouping of particles, nor changes in trajectory. This contrasts with the second, which broadly covers higher S and low τ, so stronger interactions and rapid reorientation. This is where we have "collective motion": groups of co-aligned particles moving together. Examples

equilibration times was prohibitive. It was assumed that 150000 time-steps would be sufficient to reach a steady state, but in fact true a steady state was not achieved in many of these simulations. Instead we would argue that these simulation results represent a sort of quasi-steady state. This will be discussed in more detail later.

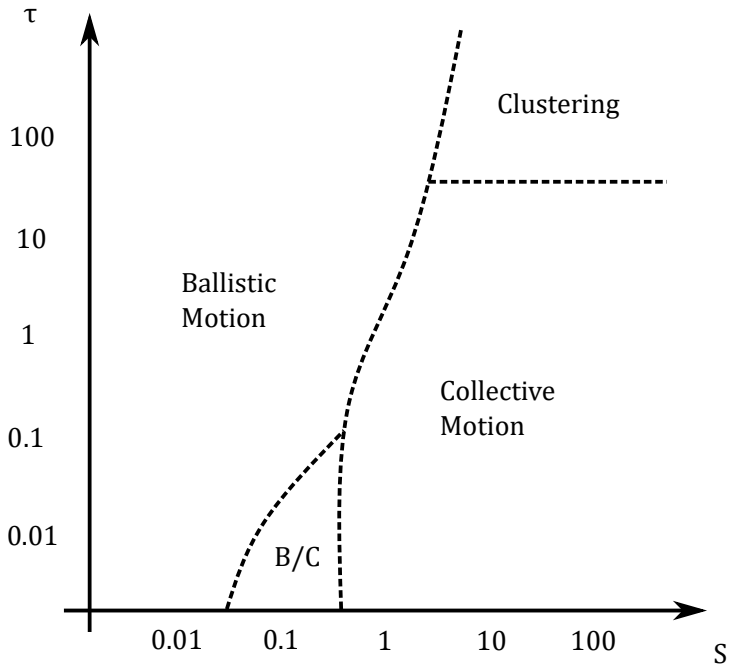

Figure 3.7: Rough sketch of the phase diagram. Indicates the behaviour one would observe in a system of swimmers in smectics for a range of smectic interaction magnitudes (S) and reorientation times τ, after a moderate length of time.
The dashed lines are only present to indicate approximate boundaries between the different observed qualitative behaviours, rather than representing distinct quantified cut-offs.
"Ballistic behaviour" refers to agents who act like non-interacting particles, developing no order in the system. 'Collective motion" refers to agents arranging themselves into co-aligned flocks, moving together - a highly ordered system. "Clustering" refers to situations in which agents have become closely grouped, via the smectic interaction, but remain unaligned, due to slow reorientation. The groups drift slowly in the mean swimming direction of their members, or may not move at all. "B/C" refers to situations where the agents are on the transition from "ballistic" to "collective" behaviour.
This diagram represents a "quasi-steady state", true steady state behaviour taking orders of magnitude more simulation time to reach. We conjecture that with more time, the line separating "Ballistic" and "Collective motion" will move to the left, and the line between "Clustering" and "Collective motion" will move up - collective motion being the only stable long-term behaviour in a deterministic system such as this.

of this behaviour can be seen in Figures 3.11, 3.12, and 3.13. Along the line dividing the "ballistic" and "collective motion", the observed behaviour is a mix of the two states. With a longer run time, we would expect this more erratic behaviour to condense into the collective motion state, as the agents would further relax into smectic-interaction minima, eventually coming together into one group with a uniform swimming direction - this being a lower energy state for the system. Indeed, for finite τ, we conjecture that given a sufficiently long runtime, because this system is deterministic it must eventually reach collective motion so long as $S > 0$. S and τ can only influence the timescale over which the system finds a minimal state.

The emergence of collective motion in these simulations is very noteworthy. Our model lacks any explicit co-alignment of agents, as seen in the traditional Vicsek model [66], rather the collective motion seen here has arisen through swimmers experiencing a force (due to the smectic-distorting presence of swimmers in other layers), whose action upon their asymmetric bodies has effect a torque to change their swimming direction. This external effect, experienced by the cohort, then yields collective motion as a consequence.

Deterministic Co-alignment: Measuring Order

We now report on our investigation as to how the orientational ($\Phi(t)$) and positional ($\mathrm{H}(t)$) order change with time for different S and τ parameter choices. Rather than compute these order parameters for the whole phase space, which would have a heavy computational cost, we will focus our attention on eight cases, along the $S = 1$ and $\tau = 1$ trajectories:

$$(S, \tau) \in \{(1, 0.01), (1, 0.1), (1, 10), (1, 100), (0.01, 1), (0.1, 1), (1, 1), (1, 10)\},$$

which are marked in Figure 3.14. The results of these can be seen in Figures 3.15 and 3.16.

We see from these results that the choice of parameters has a huge impact on the time it takes the system to relax. The case of $(\tau, S) = (10, 1)$ is of particular note, as it demonstrates that even for $\tau > 1$, the system does tend to an ordered state, albeit over a much longer time-scale - we see no reason to think this would not also be observed for $\tau = 100$, given a simulation length a

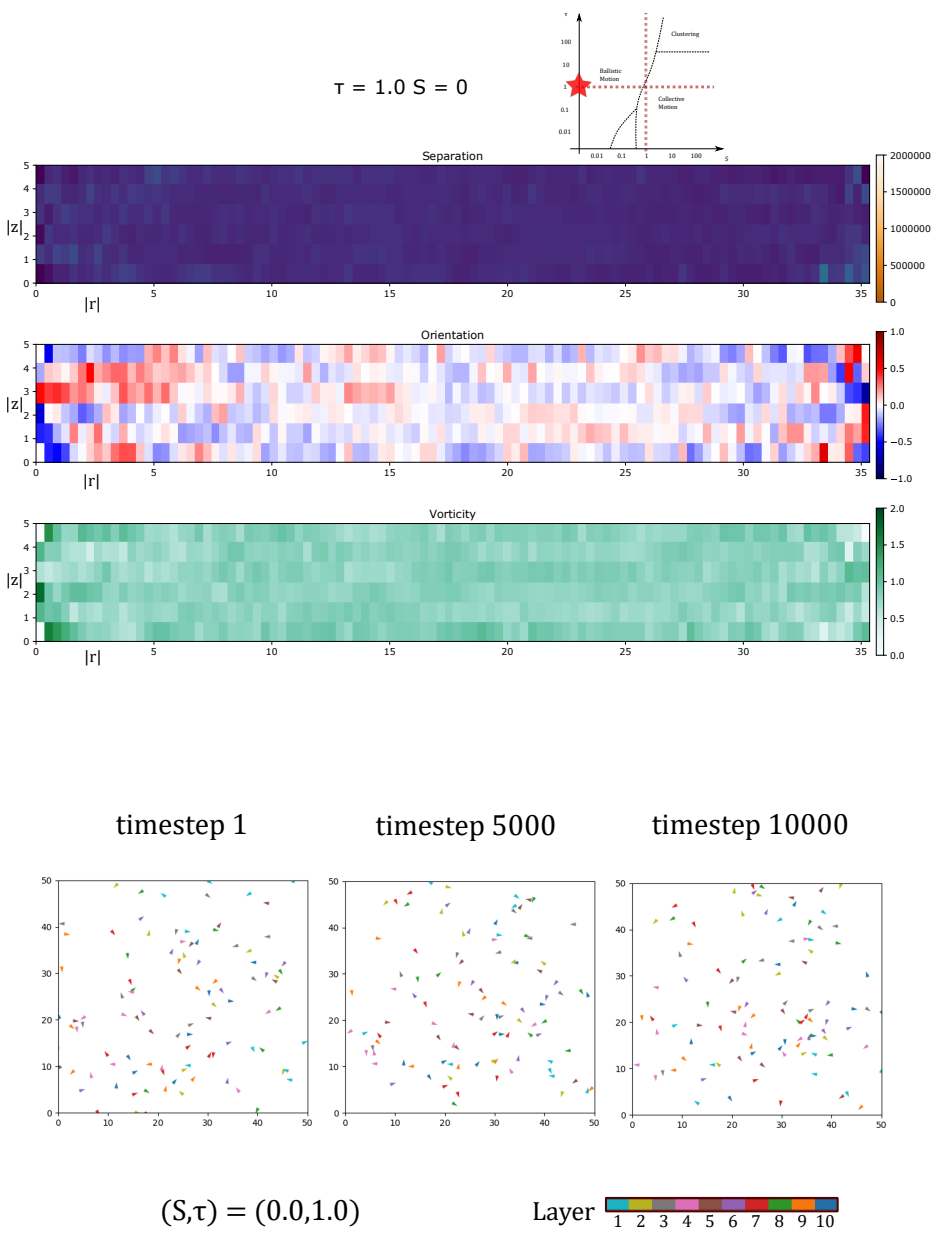

Figure 3.8:]
Above: correlation plots for a realisation of $(S, \tau) = (0, 1)$. Below: three snapshots of the same realisation at the beginning, middle and end of the data collection part of the simulation run. With $S = 0$, there is no smectic-mediated interaction between agents, nor can there be alignment. This is born out in the histograms which show no correlation between particles, and the movie snapshots in which one can see no structure to the arrangement of the particles. This is our trivial ballistic scenario.

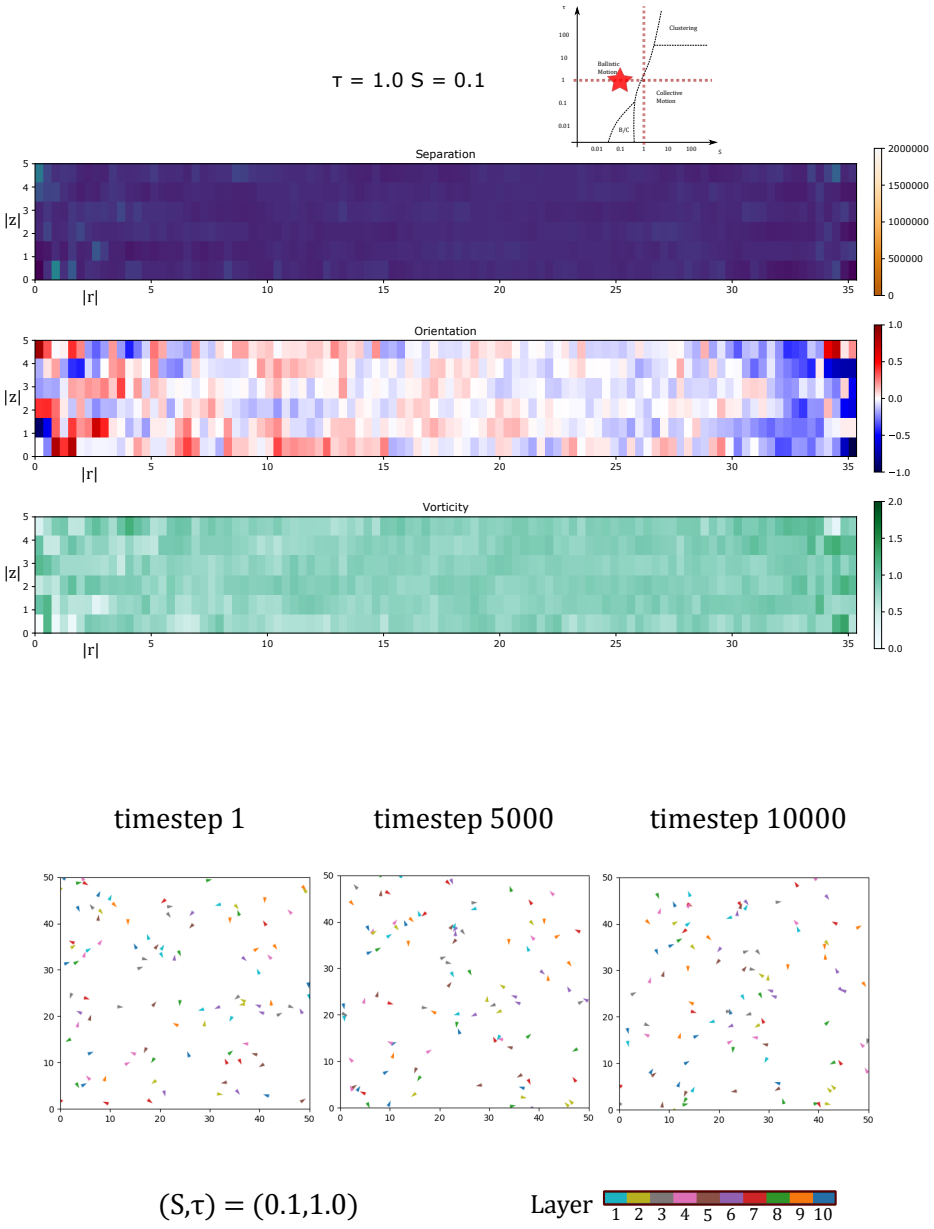

Figure 3.9: Correlation plots for $(S, \tau) = (0.1, 1)$. Here the smectic interaction is low. Over the timeframe that the model has been run, no strong signals have developed in the histograms. Particles remain almost completely unaligned, with no seperation correlation. This is very similar to the uninteracting case. Ballistic behaviour.

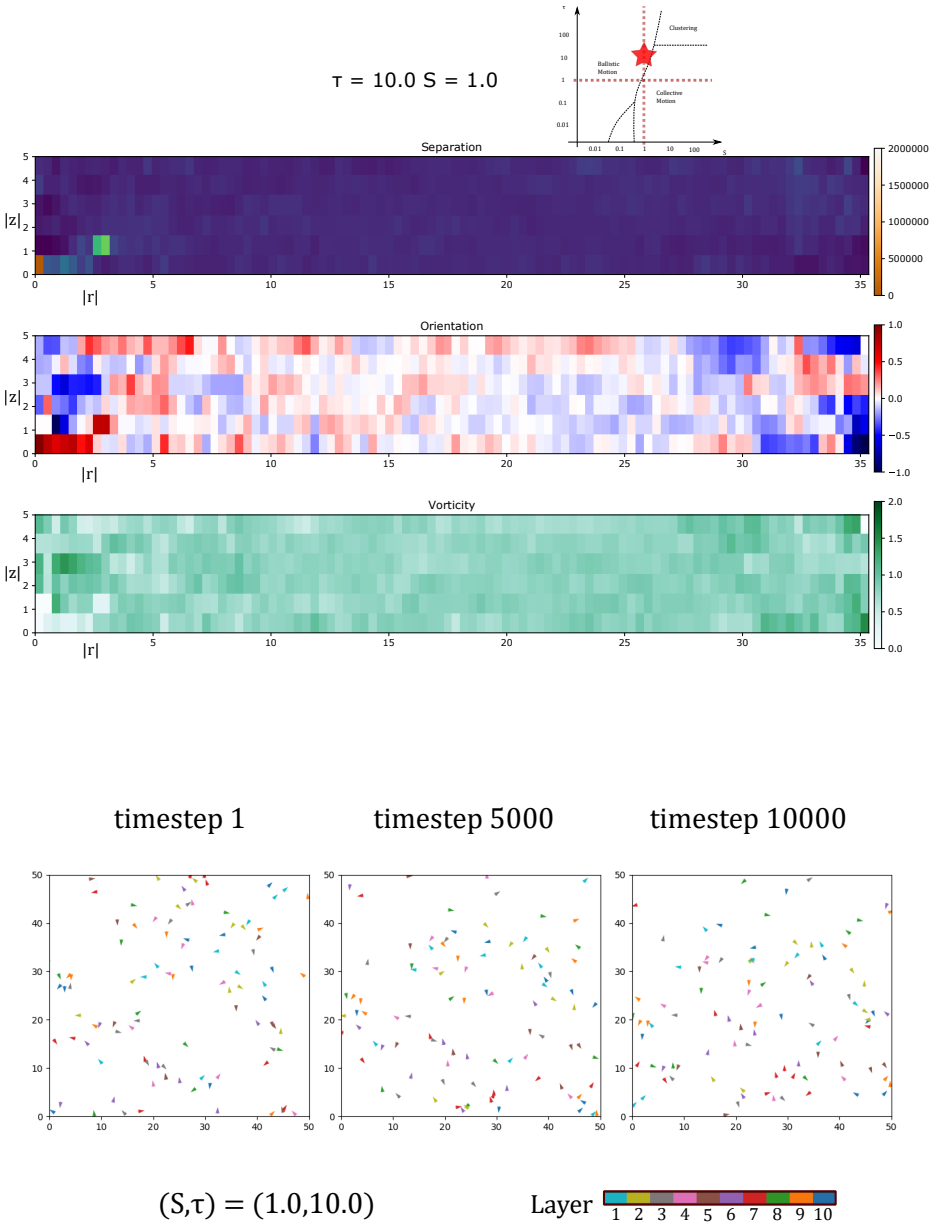

Figure 3.10: Correlation plots for $(S, \tau) = (1, 10)$. The smectic interaction is reasonable, but swimmers are slow to reorient. We see a small signal in the seperation correlation histogram, showing that some swimmers have been attracted to the energy minima for swimmers in neighbouring layers and by thier interactions with these, have been influenced to get close to swimmers in the same layer, via a three-body interaction. However, whilst there is some small corresponding co-alignment between these near neighbours, no long-range order has yet developed. The behaviour is essentially ballistic.

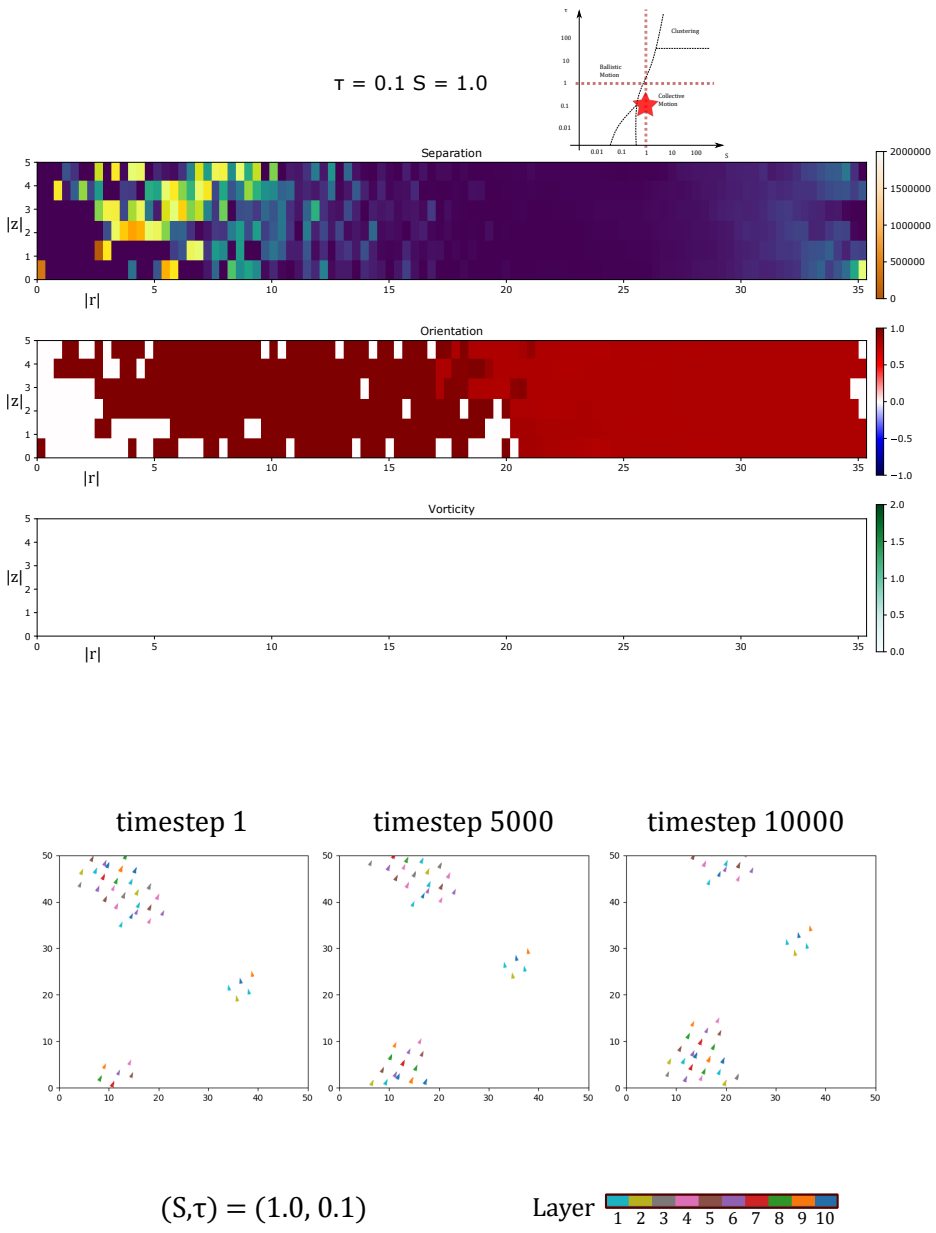

Figure 3.11: Correlation plots for $(S, \tau) = (1, 0.1)$. The smectic interaction is moderate, and swimmers reorient quickly. We have clear collective motion in the screenshots, with two groups of co-aligned, closely arranged swimmers. This is borne out in the histograms, where we see a strong signal in the seperation plot, and almost complete swimmer alignment in the orientation plot. Note that in the screenshots, swimmers appear arranged on a lattice, with nearest neighbours in $r_{||}$ being from neighbouring layers in z. Observe also that the peaks on the seperation plot correspond to the minima at $r_{||} = \sqrt{8\lambda|z|}$.

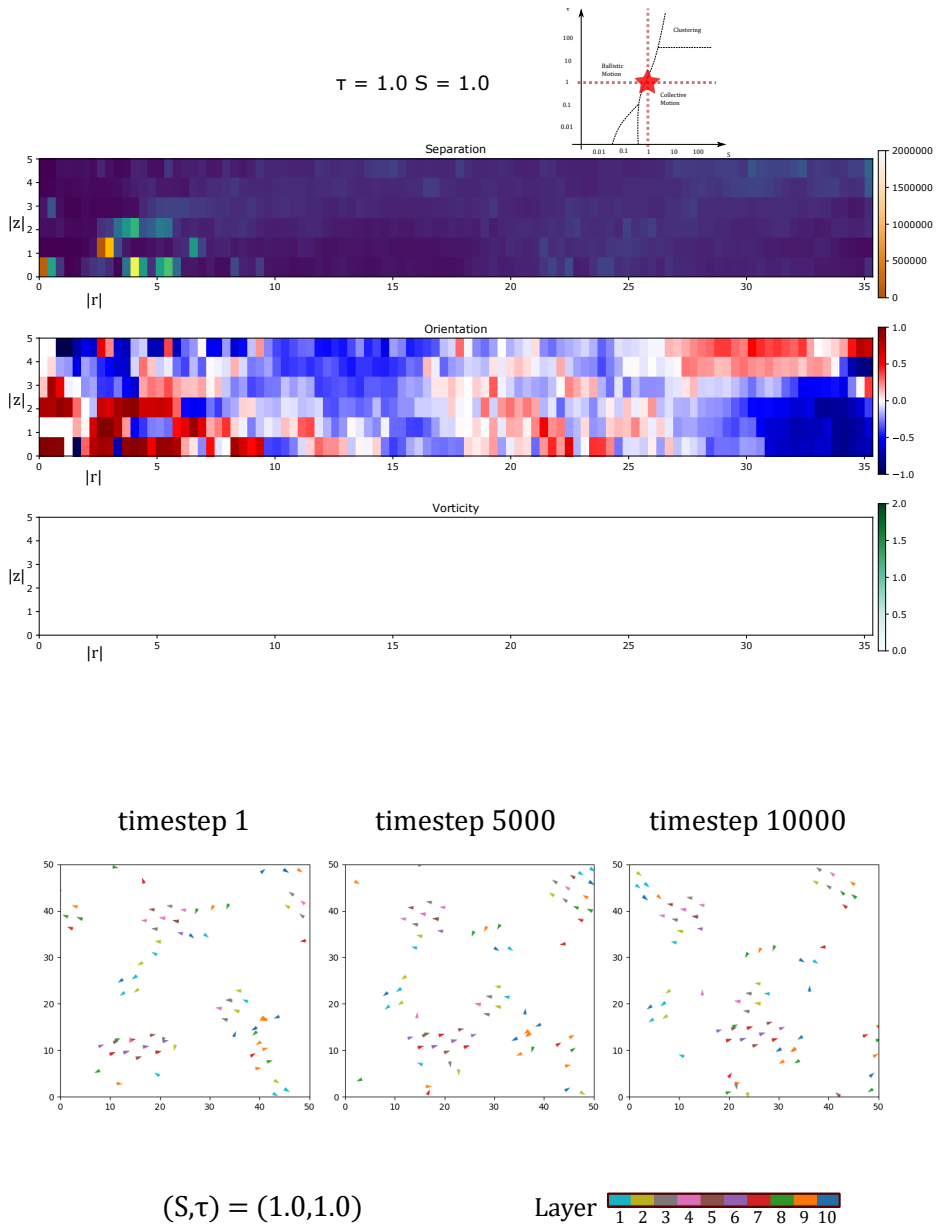

Figure 3.12: Correlation plots for $(S, \tau) = (1, 1)$. For moderate values of both S and τ, we observe collective motion, evident in the movie screenshots. However, over the timescale that the model has been run for, we have only incomplete global alignment - several groups of aligned swimmers. The seperation plot clearly shows that we have only order at short range, whilst the banding in the orientation and vorticity plots indicates alignment only with near neighbours.

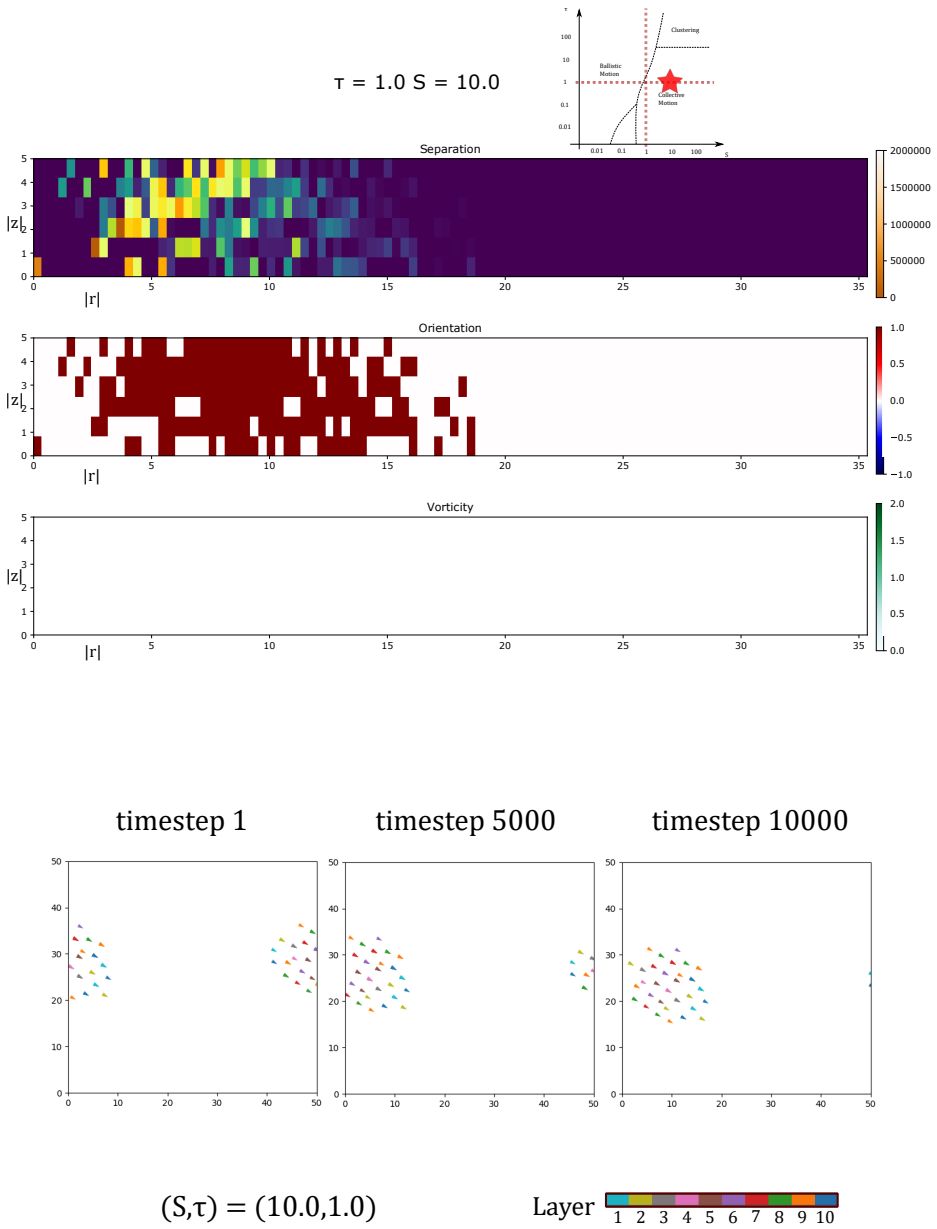

Figure 3.13: Correlation plots for $(S, \tau) = (10, 1)$ With a strong smectic interaction and reorientation occuring over a moderate timescale, we observe colletive motion. All swimmers are aligned and moving as part of one group. Within each layer, three-body interactions have forced agents to overlap. In the seperation plot, there are strong peaks corresponding to the smectic minima. The correlation and vorticity plots show complete global alignment of swimmers.

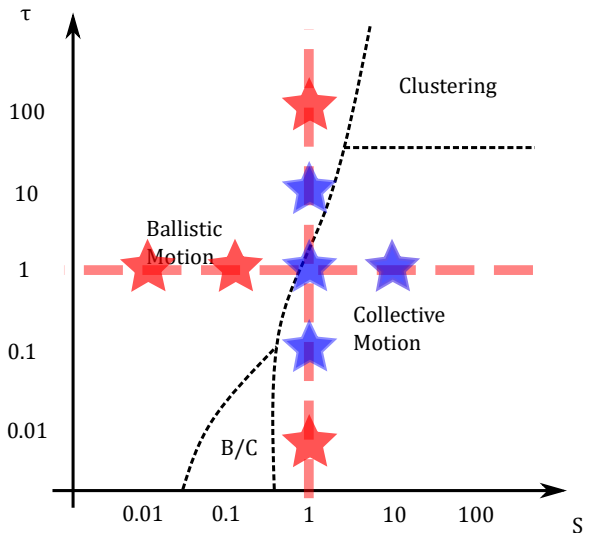

Figure 3.14: Marked with stars are the parameter choices for which we will look at change in order with model run time. Marked with blue stars are those parameter choices for which we will examine the effect of noise on the order of the system. These values are chosen as they cover a range of interesting S and τ cases.

corresponding order of magnitude greater, or indeed for any finite value for τ. In Figure 3.15 we have the plot for $(\tau, S) = (1, 0.1)$, here again we have small (but discernible) increases in system order. Once again we must infer that given a suitable span of time, this and other $0 < S < 1$ systems will eventually reach an ordered state. However, it is clear that to see evidence of order (and so collective motion), over a biologically relevant span of time (that in which a swimmer might travel a distance two orders of magnitude its body length), generally requires $\frac{S}{\tau} > 1$.

Looking at the plots for H(t), we see that no simulation reached our theoretical limit, with all seeming to stabilise in a frustrated state. We observe that rapid reorientation lead to higher values of H being reached, and that these were also cases where there were more upsets in orientational order accompanied by increases in positional order - the frustrated system finding a new minima and briefly disrupting the alignment of the agents. These systems remain frustrated as a result of the strong short-range smectic interaction making it very difficult for deterministically driven swimmers to escape poten-

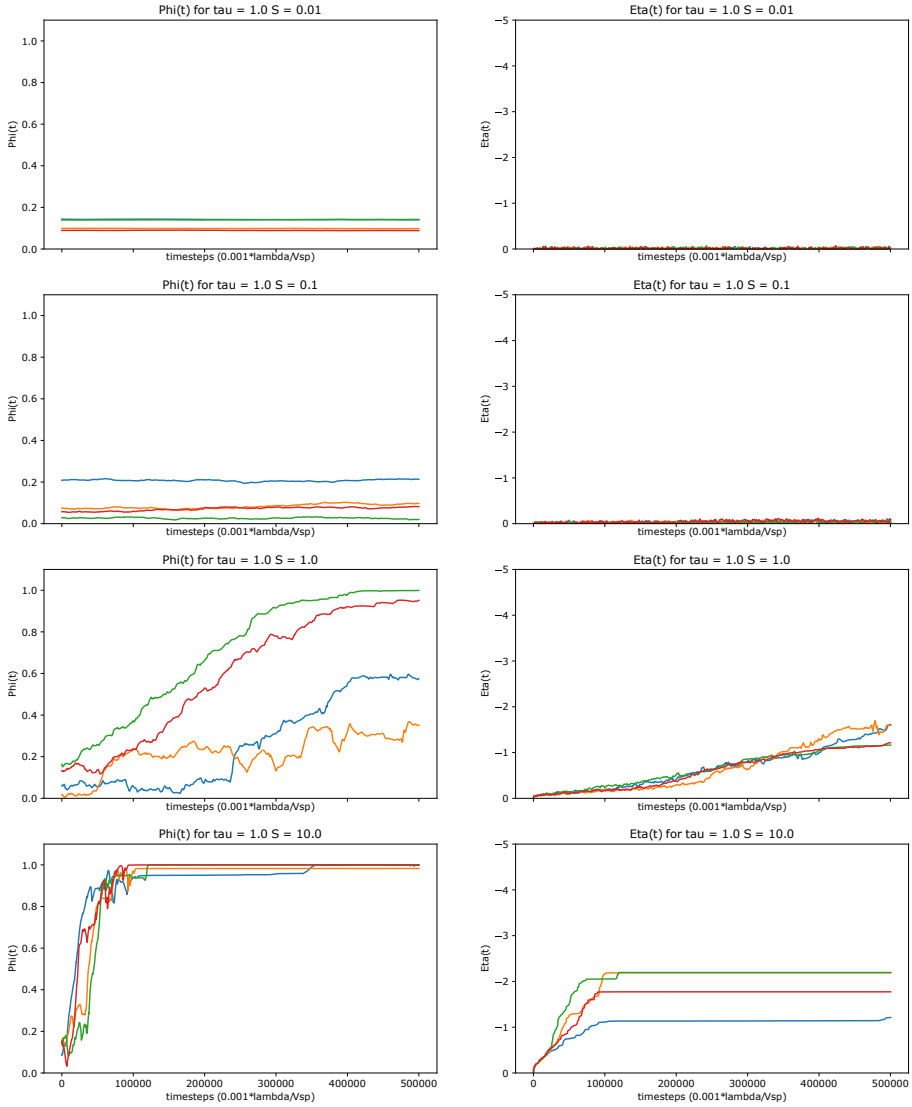

Figure 3.15: Plots of $\Phi(t)$ and $\mathrm{H}(t)$ for $(\tau, S) \in \{(1, 0.01), (1, 0.1), (1, 1), (1, 10)\}$ across 500000 model timesteps (equivalent to the time it would take a swimmer to traverse the box 100 times), each with four realisations from different random initial conditions. Note that for $S < 1$ there is little change in orientational or positional order, whilst for $S \geq 1$ the order does increase, and significantly faster for $S = 10$ than for $S = 1$, where only one of the four realisations reached a centre of mass speed of 1 in the simulation time. We also note that the positional order for $S = 10$ reached different seemingly stable values for H, all below the theoretical limit, $\mathrm{H} \approx 3.91$.

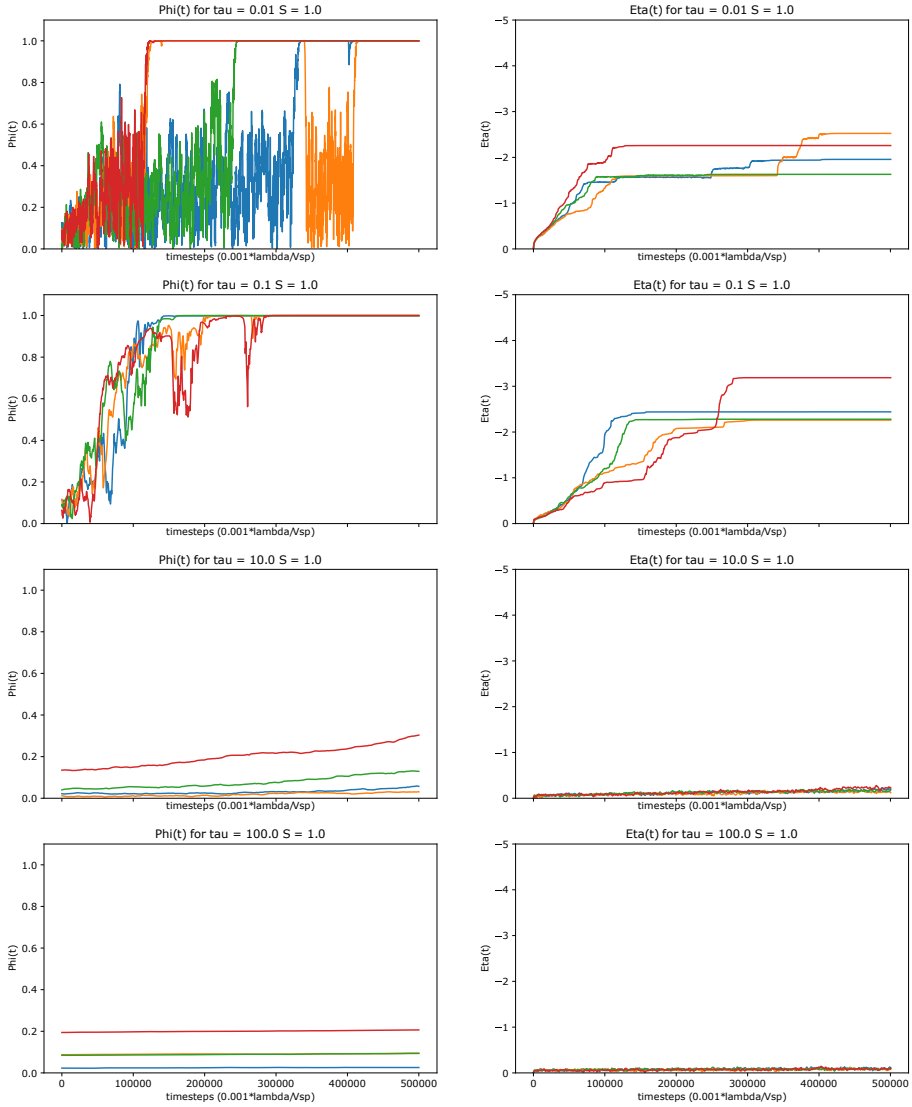

Figure 3.16: Plots of $\Phi(t)$ and $\mathrm{H}(t)$ for $(\tau, S) \in \{(0.01, 1), (0.1, 1), (10, 1), (100, 1)\}$ across 500000 model time-steps, each with four realisations from different random initial conditions. Note that for $\tau < 1$, a high degree of orientational order and positional order are found, whereas this occurs only very slowly for $\tau = 10$, and no change in order is seen at all for $\tau = 100$ over this time-frame. See that increases in the positional order are accompanied by temporary drops in orientational order. Also worth noting is that the orientational order signal for $\tau = 0.01$ is very noisy. We attribute this to the small relative time-step size (0.001 model time), to the reorientation time - a smaller time-step size would yield a cleaner signal, but would be much more computationally expensive.

tial wells and find new minima. Once they find a relaxed state, they lack the energy to leave and find a further, more relaxed one.

Deterministic Anti-alignment

We now turn to the case of swimmer for whom the point of action of the smectic interaction is negatively offset from their centre of hydrodynamic stress. We will examine the behaviour of anti-aligning swimmers by looking at the change in order with respect to time, for the same set of parameters as considered for the co-aligning swimmers, albeit with the values for τ multiplied by -1:

$$(S, \tau) \in \{(1, -0.01), (1, -0.1), (1, -10), (1, -100), (0.01, -1), (0.1, -1), (1, -1), (1, -10)\}.$$

This will allow us to make a direct comparison between these two types of swimmer. The results are presented in Figures 3.17 and 3.18.

In one sense, these results are unsurprising. Experiencing a torque that turns them to swim against the pull experienced by the smectic-mediated force drives the agents to swim away from one-another, resulting in the development of low orientational order. The positional order is more interesting, however. For $S > 1$ we see that swimmers are still dragged into interaction minima, though then align themselves facing away from their neighbours. Hence some small positional order and $\Phi \approx 0$. For $S = 1$, $\tau < 1$ we see the system again develops some positional order, but now with H > 0. This is agents positioning themselves in regions where the smectic-interaction is repulsive, and $G(\mathbf{r})$ is positive. These realisations also have extremely varied values for Φ. The explanation is that these rapidly reorienting swimmers are caught continually in the repulsive region of their neighbours, but are changing their swimming direction to swim against this repulsion - back towards the high potential - more rapidly than they can be thrown out. The smectic interaction is also weak enough that their own motility is sufficient for them to overcome a certain degree of repulsion and so move into the high potential region. Our model swimmers have a constant motility, and a limitless internal battery to propel themselves, but for real swimmers one must imagine that such a situation must get tiring.

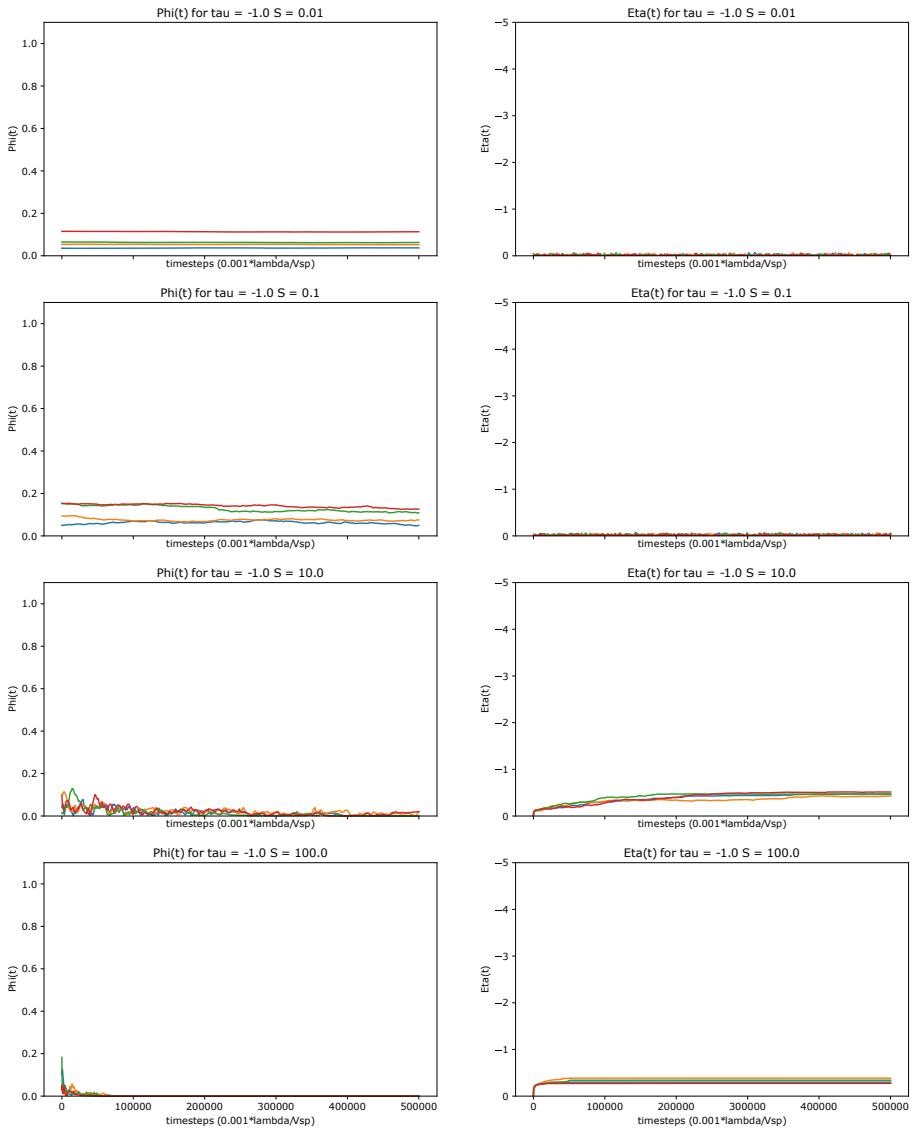

Figure 3.17:
Plots of $\Phi(t)$ and $\mathrm{H}(t)$ for $(\tau, S) \in \{(-1, 0.01), (-1, 0.1), (-1, 1), (-1, 10)\}$ across 500000 model timesteps, each with four realisations. Note that there is no increase in orientational order, and that it rapidly decays to 0, for $S \geq 1$. See also that for the same S, we have a small increase in H, indicating some development of positional order.

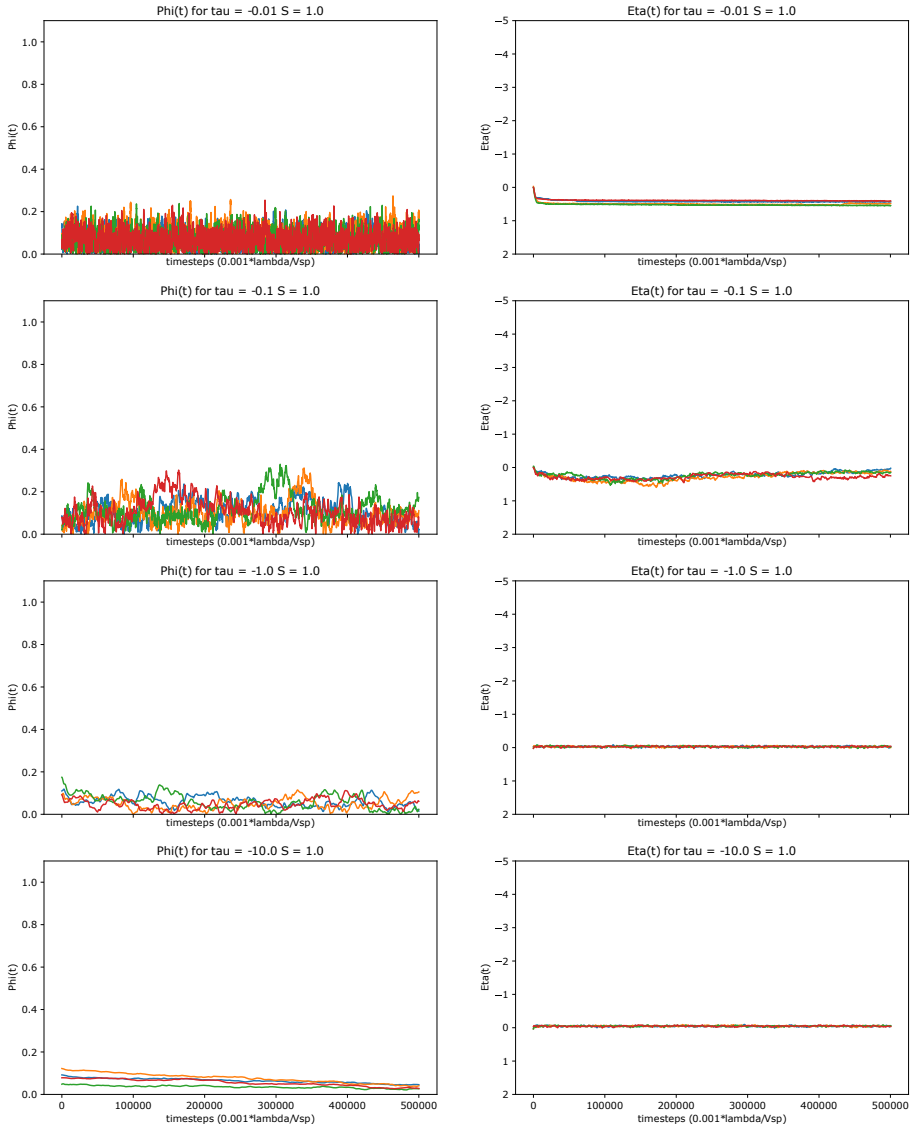

Figure 3.18:
Plots of $\Phi(t)$ and $\mathrm{H}(t)$ for $(\tau, S) \in \{(-0.01, 1), (-0.1, 1), (-10, 1), (-100, 1)\}$ across 500000 model timesteps, each with four realisations (each shown in a different colour in the plot). Note the extremely noisy signal for Φ for $\tau < 1$, and that it does not increase for any value of τ (even decreasing for $\tau > 1$). Whilst for $\tau > 1$, H remains ~ 0, for $\tau < 1$ we see $\mathrm{H} > 0$. This means that agents are actively moving into regions where $G(\mathbf{r})$ is repulsive - a higher energy state.

3.3.2 Noise

Here we shall look at the effect of noise on ordered systems. We have seen that a deterministic system of agents in a smectic, who co-align in response to a smectic-mediated force, become ordered and develop collective motion. We now add orientational noise to the system, akin to increasing the temperature of our agents as it will allow them to explore more states. For a subset of the parameter choices that we measure the order for, we will see how the order changes as we increase the amount of noise. The S and τ values we examine are

$$(\tau, S) \in \{(0.1, 1), (1, 1), (10, 1), (1, 10)\},$$

as can be seen in Figure 3.14. These values were chosen as they have minimal computational noise (being quantities at least two orders of magnitude larger than the timestep size), and exhibited some extent of order in our deterministic simulations. The plots of change in time-averaged order with respect to noise can be seen in Figure 3.19.

Let us first consider the case of $(\tau, S) = (10, 1)$. In the deterministic system, we saw that given enough time, there was an increase in order, see Figure 3.15. The addition of a small amount of noise does not seem to have helped the system achieve greater order any faster, as the time-averaged order parameter remains low, only reaching the same value of $\sim \frac{1}{\sqrt{N}}$ that one would expect from random swimmer orientation in system of N swimmers, and as is seen in all the cases. It is possible that noise might help the system achieve a steady state faster, for noise values below the threshold necessary to break order. In the future it might be possible to run the simulations for long enough to confirm this.

For those parameter choices where order could develop, we see that the addition of noise disrupts this. All of our plots show order generally decreasing as noise is increased. For $(\tau, S) = (1, 1)$, we see much lower values of $\bar{\Phi}$ and $\bar{\mathrm{H}}$ at low noise, and a more pronounced drop in these values as η is increased, than the other two parameter sets. This can be attributed to the system not having reached a steady state when the order parameters were collected. Nonetheless, the system displays similar characteristics to the steady state systems, in that high order was observed for low noise, which then dropped as the noise was

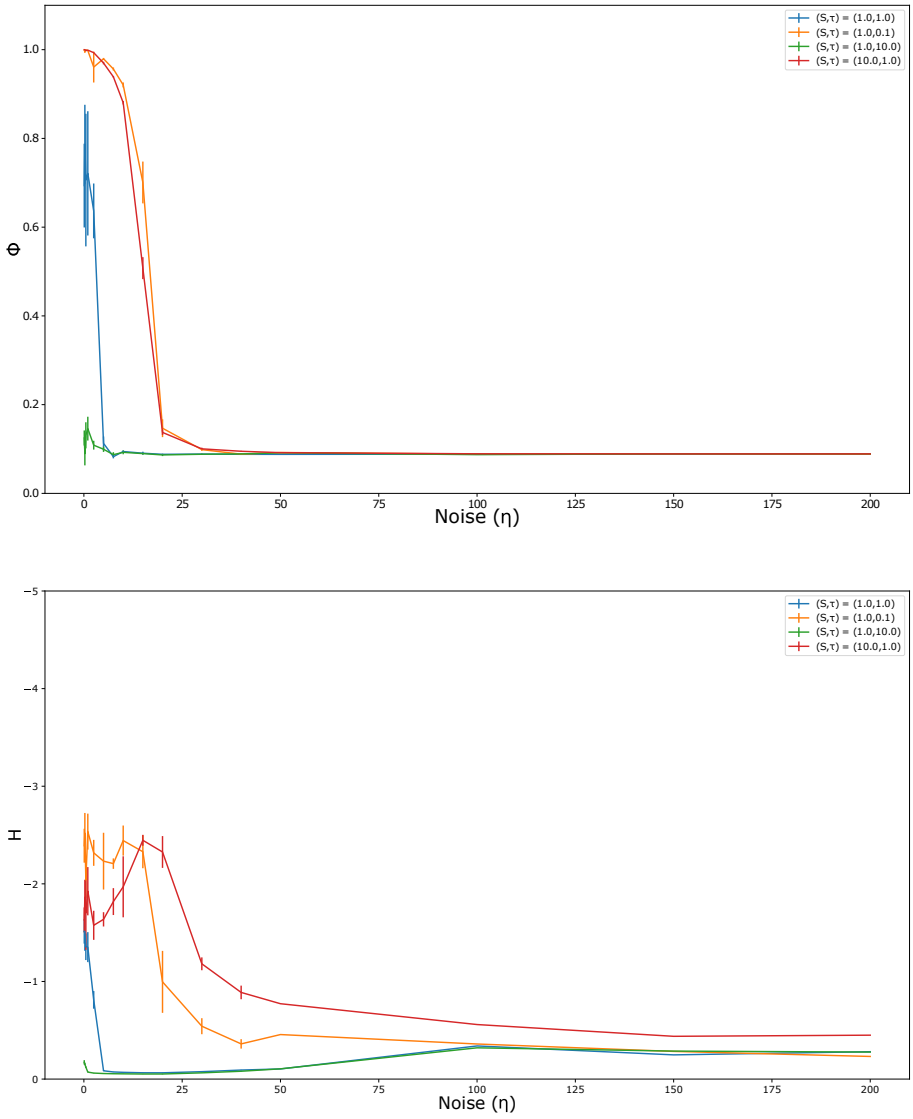

Figure 3.19: Plots of the change in time-averaged system order, $\bar{\Phi}$ and $\bar{\mathrm{H}}$, with increase in orientational noise, η, for $(\tau, S) \in \{(0.1, 1), (1, 1), (10, 1), (1, 10)\}$. Each plot is the mean of four realisations, of which each simulation was run for 300000 time-steps (to allow time for them to reach a steady state), then the order parameters time-averaged over 200000 time-steps. Error bars show the mean standard error. Firstly we see that for $(\tau, S) = (10, 1)$ we see no orientational order for any noise value, but we do observe a small increase in positional order as the noise is increased. For the other parameter choices, note that at low noise we see a high degree of order, whilst at high noise, the order is lost. This is most marked for $\bar{\Phi}$ where there is a sharp reducton over a small range of η, whilst the drop-off occurs over a larger range of η for $\bar{\mathrm{H}}$.

increased.

So, considering now the two cases where steady state behaviour was reached, and changed as noise was added to the system: $(\tau, S) \in \{(1, 10), (0.1, 1)\}$. For very low noise the orientational order, $\bar{\Phi}$, was ~ 1, however we observed a gradual then rapid decline in order as η increased, reaching the minimum of $\sim \frac{1}{10}$ by $\eta = 50$. This is a continuous phase transition, of the same character as seen in Vicsek [66], which is unsurprising given that the form of noise we have added is the same. For both cases, the critical transition occurs between $\eta = 10$ and $\eta = 20$. Striking different behaviour is seen for the positional order, $\bar{\mathrm{H}}$. Here, we again see a decrease in order as η increases, but the profile of the transition is very different. The order does not reach a minimum until well past the point at which orientational order has broken down, at $\eta = 100$, and the gradient of the transition is much shallower. This suggests that this positional order is more robust to orientational noise. We also note that the minimum value for the positional order seems to depend on the value for S, with all those cases for $S = 1$ settling to the same lower value for $\bar{\mathrm{H}}$ than that for $S = 10$.

Whilst more work must be done to properly describe these phase transitions, and to ascertain the relationship between choice of S and τ and the system's reaction to increasing noise, we have demonstrated that systems of swimmers embedded in a smectic liquid crystal can exhibit collective motion, and that this ordered state undergoes a continuous phase transition as orientational noise is added to the system.

Chapter 4

Conclusions

Summary and Outlook

In Chapter 2, we looked at columnar structures formed by interacting ordered domains in a stack of bilayer membranes. We modelled the aligned liquid-ordered microdomains as a single large inclusion in a smectic liquid crystal. We showed that from a standpoint of considering the elastic energies of the system, such an arrangement of these domains is not favourable.

Beginning by examining a columnar inclusion of this sort in a bulk geometry, we fixed a volume but allowed its aspect ratio to vary (via the control parameter τ). We could then determine what interfacial energy was necessary to favour the development of inclusions of a given aspect ratio. This took the form of a surface energy which penalised the flat faces of the column.

Extending our description to a slab-like geometry, more reminiscent of that investigated by Tayebi et al., we showed that the energy cost of a columnar inclusion depended on its position in the slab. Considering the inclusion energy, it should be more favourable for inclusions to form in the centre of the smectic film, and increasingly less favourable towards the edges, contrary to the observations [56]. Applying the interfacial energy we calculated for the bulk case at only the liquid-ordered / liquid-disordered smectic interface, and not at the smectic/substrate interface was sufficient to favour the presence of the columnar inclusions at this boundary. In reality there should be non-zero energy associated with the smectic/substrate interface, but given that glass substrates typically carry a slight negative charge, setting this energy to zero

is a conservative assumption.

Looking at the magnitude of the interfacial energy computed for inclusions of the dimensions seen in Tayebi et al. we observed that the suggestion the authors made, of the effect of the liquid-ordered domains on the hydrogen bond network favouring liquid-ordered domain alignment, was sensible given the magnitude of the energies involved.

We employed a linear theory in this work, omitting the anharmonic correction to the elastic free energy from the Hamiltonian we used. A linear theory has significant advantages in its usability, compared to the non-linear theory, and indeed this simplification enabled us to achieve an analytical result for the energy of the bulk column, and to formulate a model for a column in a finite slab. We justified our use of the linear theory by our system being in a small deformation regime. However, despite our estimation of the magnitude of the distortion we are not certain of the exact profile of the deformation at the L_o interface. A sharp enough layer deformation could result in a situation where non-linear effects make a significant contribution to the energy density [8]. This could be of particular importance if edge dislocations were to occur in our system.

The total distortion over the larger columns we examined amounted to the equivalent of a couple of layer thicknesses. This does suggest that the system could achieve a lower energy by adopting a configuration with edge dislocations on the radial L_o/L_d interface. There is no clear evidence for the existence of edge dislocations in this system, though they could explain why the height difference between the ordered domain column and the surrounding layers does not appear to scale linearly with the height of the column [56]. Whether the stresses in the system are sufficient to drive the creation of edge dislocations to ease the distortion, and exactly what impact they would have on the system energy are important questions, and ones that can only be answered properly with use of a fully non-linear theory [8].

The work we undertook looked only at a single, already formed and aligned column in a smectic. An obvious next step might be to extend this to look at a system of multiple interacting columns. In practice we found that more than one inclusion made the calculations involved unwieldy, so declined to pursue them. We also attempted to investigate aligned domains of different

shapes. Cone-shaped inclusions were of particular interest to us as a means to consider the energy of a partially formed column, these seeming to be observable in the experimental work [56]. We constructed the integral expression for the energy but found it to be intractable, resisting our attempts to evaluate it analytically or numerically. Finally we note that our work here included no dynamics, and that this is also a potentially interesting avenue for future research.

Chapter 3 saw us turn our attention to a system of motile inclusions embedded in a smectic phase. We constructed a minimal model with two control parameters: S which described the relative strength of the smectic-mediated particle-particle interaction, and τ describing the relative time taken for the swimmers to reorient themselves when subject to torques. Simulations were run with a periodic smectic box of 10 layers each with 10 swimmers.

We began by trying to characterise the behaviour of the deterministic system across the (S, τ) phase-space. This proved challenging as reaching a true steady state took in excess of the computation time we had allocated to the problem. The author also made the decision to sacrifice a depth of results for a breadth. It would have perhaps given more useful insight to run multiple realisations of fewer cases in the deterministic model, so allowing averaging over multiple samples. This would give cleaner averages in the correlation plots. However, we did qualitatively characterise the behaviour of the system and so produced a rough sketch of a phase diagram indicative of the type of behaviour one could observe in such a system, for particular parameter choices over a short, biologically relevant timescale. In doing so we identified two very different types of behaviour for systems with $\tau > 0$: ballistic swimming of unaligned, weakly interacting agents; and collective motion, of aligned groups of agents moving together. The latter was observed for stronger smectic interactions, and the former for weaker. We conjectured that given long enough timescales the system must eventually relax into collective motion. This is a lower energy state than the ballistic one, and even a weak interaction should eventually give rise to stable collective motion. Further work to support or disprove this conjecture should be carried out. For systems with $\tau < 0$, no collective motion was observed.

We note that this difference between positive and negative τ, corre-

sponding to pusher-type swimmers and puller-type respectively, is biologically relevant. It suggests that for swimmers in a smectic system, only pushers are capable of naturally undergoing collective motion, whilst pullers are capable of clustering. This could have implications for different survival strategies in nature and may merit further investigation.

We made the decision to omit any hydrodynamic interaction between agents from our model. This was done to keep our model as simple and general as possible, and to ensure our results could be attributed to the smectic-mediated interaction alone, rather than some other inter-agent interaction or combination of interactions. This said, such an omission is difficult to justify on the grounds that few, if any, realisable systems will be free of a significant hydrodynamic interaction of some kind.

Hydrodynamic interactions by swimmers in a quasi-two dimensional fluid between two confining walls can be screened by the walls to decay as $\frac{1}{r^3}$ [53] which still represents a significant long-range interaction relative to the smectic-mediated interaction. It has been reported that such interactions can cause swimmers to align and attract if they are positioned at certain angles to one-another, but to repel otherwise, leading to unstable collective effects [58, 35]. Such in-layer interactions could in turn make the intralayer collective motion we see in our model unstable by disrupting the in-layer alignment of swimmers. However, the interplay between in-layer hydrodynamic interactions, and intralayer smectic-mediated interactions certainly has the potential to offer rich, complex behaviour in appropriately realised.

Having observed the development of order in the system, in the form of collectively moving aligned agents, we sought to understand what impact the introduction of orientational noise would have on this order. In this, we took inspiration from the highly cited Vicsek model [66], applying the same form of noise to test whether a comparable order-disorder phase transition might be observed. We measured two order parameters: Φ, a measure of global co-alignment; and H, a measure of system energy and so a proxy for positional order. We observed that for (S, τ) choices which produced highly ordered systems with collective motion at a steady state for low noise, as the noise was increased a Vicsek-like phase transition to disorder occurred in the measure of orientational order. This then is a potentially realisable

system with Vicsek qualities: bottom-up natural collective motion. It would be well worth attempting to recreate this experimentally, to see if we can incite collective motion in a microscopic system, given appropriate choice of smectic medium, and of swimming organism.

From a theoretical and computational standpoint, we would hope to further interrogate this phase transition, and to explore how the results might differ in an infinite rather than periodic system. In the short term, however, more work must be carried out to improve the quality of the order-disorder plots, and to drive the out of steady state case ($S = 1, \tau = 1$) to a true steady state before attempting to observe its phase transition, in order to better compare it to the moderate S and small τ cases. We anticipate that the character of the transition should be the same.

Finally we note that the physics describing inclusions in smectics is not drastically different from the dual case of a columnar phase raising the possibility of comparable results in that different environment.

This is an apparently rich area with much still to be explored. Continuum models offer a powerful tool for describing these systems. We hope to see more work on inclusions in smectics and similar environments employing these tools in the future.

Bibliography

[1] Milton Abramowitz, Irene A. Stegun, and Robert H. Romer. Handbook of Mathematical Functions with Formulas, Graphs, and Mathematical Tables. *American Journal of Physics*, 56(10):958–958, oct 1988. ISSN 0002-9505. doi: 10.1119/1.15378. URL `http://aapt.scitation.org/doi/10.1119/1.15378`.

[2] Tapan Chandra Adhyapak, Sriram Ramaswamy, and John Toner. Live soap: Stability, order, and fluctuations in apolar active smectics. *Physical Review Letters*, 110(11):118102, mar 2013. ISSN 00319007. doi: 10.1103/PhysRevLett.110.118102.

[3] R. Aditi Simha and Sriram Ramaswamy. Hydrodynamic fluctuations and instabilities in ordered suspensions of self-propelled particles. *Physical review letters*, 89(5):058101, jul 2002. ISSN 00319007. doi: 10.1103/PhysRevLett.89.058101.

[4] Bruce Alberts, Alexander Johnson, Julian Lewis, Martin Raff, Keith Roberts, and Peter Walter. *Molecular biology of the cell*. Garland Pub, 1994. ISBN 0815316194.

[5] Paulo F F Almeida. Thermodynamics of lipid interactions in complex bilayers, jan 2009. ISSN 00052736.

[6] M. Ballerini, N. Cabibbo, R. Candelier, A. Cavagna, E. Cisbani, I. Giardina, V. Lecomte, A. Orlandi, G. Parisi, A. Procaccini, M. Viale, and V. Zdravkovic. Interaction ruling animal collective behavior depends on topological rather than metric distance: Evidence from a field study. *Proceedings of the National Academy of Sciences of the United*

States of America, 105(4):1232–1237, jan 2008. ISSN 10916490. doi: 10.1073/pnas.0711437105.

[7] Burkhard Bechinger. Lipid multilayers: Domains stack up, 2012. ISSN 14764660.

[8] E A Brener and V I Marchenko. Nonlinear theory of dislocations in smectic crystals: an exact solution. *Physical review. E, Statistical physics, plasmas, fluids, and related interdisciplinary topics*, 59(5 Pt A):R4752–3, may 1999. ISSN 1063-651X. doi: 10.1103/physreve.59.r4752. URL `http://www.ncbi.nlm.nih.gov/pubmed/11969511`.

[9] H. Brenner. The Stokes resistance of an arbitrary particle. *Chemical Engineering Science*, 18(1):1–25, 1963. ISSN 00092509. doi: 10.1016/0009-2509(63)80001-9.

[10] P. M. Chaikin and T. C. Lubensky. *Principles of Condensed Matter Physics*. Cambridge University Press, jun 1995. doi: 10.1017/cbo9780511813467.

[11] S. Chandrasekhar. *Liquid Crystals*. Cambridge University Press, Cambridge, second edi edition, 1992. ISBN 9780511622496. doi: 10.1017/CBO9780511622496. URL `http://dx.doi.org/10.1017/CBO9780511622496`.

[12] H. Chaté, F. Ginelli, G. Grégoire, F. Peruani, and F. Raynaud. Modeling collective motion: Variations on the Vicsek model. *European Physical Journal B*, 64(3-4):451–456, aug 2008. ISSN 14346028. doi: 10.1140/epjb/e2008-00275-9.

[13] Blanca Climent-Ezquerra and Francisco Guillén-González. A review of mathematical analysis of nematic and smectic-A liquid crystal models: A survey in mathematics for industry, 2014. ISSN 14694425.

[14] Peter J. Collings and J. W. G. Goodby. *Introduction to liquid crystals : chemistry and physics*. ISBN 9781138298767.

[15] Abdallah Daddi-Moussa-Ider and Andreas M. Menzel. Dynamics of a simple model microswimmer in an anisotropic fluid: Implications

for alignment behavior and active transport in a nematic liquid crystal. *Physical Review Fluids*, 3(9), sep 2018. ISSN 2469990X. doi: 10.1103/PhysRevFluids.3.094102.

[16] Pierre-Gilles De Gennes and Jacques Prost. *The Physics of Liquid Crystals*. Oxford University Press, second edition, 1993. ISBN 0198517858.

[17] David Dickinson, N. N. Lebedev, and R. A. Silverman. *Special Functions and their Applications*. 1965. doi: 10.2307/2314530.

[18] Ingo. Dierking. *Textures of liquid crystals*. Wiley-VCH, 2003. ISBN 9783527307258.

[19] C Dietrich, L A Bagatolli, Z N Volovyk, N L Thompson, M Levi, K Jacobson, and E Gratton. Lipid rafts reconstituted in model membranes. *Biophysical Journal*, 80(3):1417–1428, 2001. ISSN 00063495. doi: 10.1016/S0006-3495(01)76114-0.

[20] Amin Doostmohammadi, Jordi Ignés-Mullol, Julia M. Yeomans, and Francesc Sagués. Active nematics. *Nature Communications*, 9(1):1–13, dec 2018. ISSN 20411723. doi: 10.1038/s41467-018-05666-8.

[21] Claudia Ferreiro-Córdova, John Toner, Hartmut Löwen, and Henricus H. Wensink. Long-time anomalous swimmer diffusion in smectic liquid crystals. *Physical Review E*, 97(6), jun 2018. ISSN 24700053. doi: 10.1103/PhysRevE.97.062606.

[22] Francesco Ginelli, Fernando Peruani, Marie Helène Pillot, Hugues Chaté, Guy Theraulaz, and Richard Bon. Intermittent collective dynamics emerge from conflicting imperatives in sheep herds. *Proceedings of the National Academy of Sciences of the United States of America*, 112(41): 12729–12734, oct 2015. ISSN 10916490. doi: 10.1073/pnas.1503749112.

[23] Ursula W. Goodenough and L. Andrew Staehelin. Structural differentiation of stacked and unstacked chloroplastmembranes: Freeze-etch electron microscopy of wild-type and mutant strains of Chlamydomonas. *Journal of Cell Biology*, 48(3):594–619, mar 1971. ISSN 15408140. doi: 10.1083/jcb.48.3.594.

[24] I. S. (Izrail Solomonovich) Gradshtein, I. M. (Iosif Moiseevich) Ryzhik, and Alan. Jeffrey. *Table of integrals, series, and products*. Academic Press, 1980. ISBN 1483265641.

[25] Guillaume Grégoire and Hugues Chaté. Onset of Collective and Cohesive Motion. *Physical Review Letters*, 92(2):025702, jan 2004. ISSN 0031-9007. doi: 10.1103/PhysRevLett.92.025702. URL `https://link.aps.org/doi/10.1103/PhysRevLett.92.025702`.

[26] R. Großmann, L. Schimansky-Geier, and P. Romanczuk. Self-propelled particles with selective attraction-repulsion interaction: From microscopic dynamics to coarse-grained theories. *New Journal of Physics*, 15, aug 2013. ISSN 13672630. doi: 10.1088/1367-2630/15/8/085014.

[27] William M Hamner and Peggy P Hamner. Behavior of Antarctic krill (Euphausia superba): schooling, foraging, and antipredatory behavior. *Canadian Journal of Fisheries and Aquatic Sciences*, 57(S3):192–202, dec 2000. ISSN 0706-652X. doi: 10.1139/f00-195. URL `http://www.nrcresearchpress.com/doi/10.1139/f00-195`.

[28] W. Helfrich. Steric Interaction of Fluid Membranes in Multilayer Systems. *Zeitschrift fur Naturforschung - Section A Journal of Physical Sciences*, 33(3):305–315, mar 1978. ISSN 18657109. doi: 10.1515/zna-1978-0308.

[29] Takuma Hoshino, Shigeyuki Komura, and David Andelman. Correlated lateral phase separations in stacks of lipid membranes. *Journal of Chemical Physics*, 143(24), dec 2015. ISSN 00219606. doi: 10.1063/1.4934984.

[30] Andreas Huth and Christian Wissel. The Movement of Fish Schools: A Simulation Model. pages 577–595. 1990. doi: 10.1007/978-3-642-51664-1_39.

[31] Jianjun Jiang, Weixin Li, Liang Zhao, Yuanyan Wu, Peng Xiu, Guoning Tang, and Yusong Tu. Water-phospholipid interactions at the interface of lipid membranes: comparison of different force fields. feb 2018. URL `http://arxiv.org/abs/1602.08554`.

[32] Alexander M. Jones, Yuanhu Xuan, Meng Xu, Rui Sheng Wang, Cheng Hsun Ho, Sylvie Lalonde, Chang Hun You, Maria I. Sardi, Saman A. Parsa, Erika Smith-Valle, Tianying Su, Keith A. Frazer, Guillaume Pilot, Réjane Pratelli, Guido Grossmann, Biswa R. Acharya, Heng Cheng Hu, Cawas Engineer, Florent Villiers, Chuanli Ju, Kouji Takeda, Zhao Su, Qunfeng Dong, Sarah M. Assmann, Jin Chen, June M. Kwak, Julian I. Schroeder, Reka Albert, Seung Y. Rhee, and Wolf B. Frommer. Border control - A membrane-linked interactome of Arabidopsis. *Science*, 344(6185):711–716, 2014. ISSN 10959203. doi: 10.1126/science.1251358.

[33] Randall D. Kamien and Christian D. Santangelo. Smectic liquid crystals: Materials with one-dimensional, periodic order. *Geometriae Dedicata*, 120 (1):229–240, jun 2006. ISSN 00465755. doi: 10.1007/s10711-006-9075-y.

[34] Norbert Kučerka, Frederick A. Heberle, Jianjun Pan, and John Katsaras. Structural significance of lipid diversity as studied by small angle neutron and X-ray scattering, sep 2015. ISSN 20770375.

[35] Ye Li, He Zhai, Sandra Sanchez, Daniel B. Kearns, and Yilin Wu. Noncontact Cohesive Swimming of Bacteria in Two-Dimensional Liquid Films. *Physical Review Letters*, 119(1), jul 2017. ISSN 10797114. doi: 10.1103/PhysRevLett.119.018101.

[36] Carlos F Lopez, Steve O Nielsen, Michael L Klein, and Preston B Moore. Hydrogen bonding structure and dynamics of water at the dimyristoylphosphatidylcholine lipid bilayer surface from a molecular dynamics simulation. *Journal of Physical Chemistry B*, 108(21):6603–6610, 2004. ISSN 15206106. doi: 10.1021/jp037618q. URL `www.cmm.upenn.edu//`.

[37] Yicong Ma, Sajal K. Ghosh, Sambhunath Bera, Zhang Jiang, Christian M. Schlepütz, Evguenia Karapetrova, Laurence B. Lurio, and Sunil K. Sinha. Anomalous partitioning of water in coexisting liquid phases of lipid multilayers near 100% relative humidity. *Physical Chemistry Chemical Physics*, 18(2):1225–1232, 2016. ISSN 14639076. doi: 10.1039/c5cp04703j.

[38] Akira Okubo, Daniel Grünbaum, and Leah Edelstein-Keshet. The Dynamics of Animal Grouping. pages 197–237. 2001. doi: 10.1007/978-1-4757-4978-6_7.

[39] N. R. Pallas and Y. Harrison. An automated drop shape apparatus and the surface tension of pure water. *Colloids and Surfaces*, 43(2):169–194, 1990. ISSN 01666622. doi: 10.1016/0166-6622(90)80287-E.

[40] Sagar A. Pandit, S. Vasudevan, S. W. Chiu, R. Jay Mashl, Eric Jakobsson, and H. L. Scott. Sphingomyelin-cholesterol domains in phospholipid membranes: Atomistic simulation. *Biophysical Journal*, 87(2):1092–1100, 2004. ISSN 00063495. doi: 10.1529/biophysj.104.041939.

[41] T J Pedley and J O Kessler. Hydrodynamic Phenomena in Suspensions of Swimming Microorganisms. *Annual Review of Fluid Mechanics*, 24(1): 313–358, jan 1992. ISSN 0066-4189. doi: 10.1146/annurev.fl.24.010192.001525. URL `http://www.annualreviews.org/doi/10.1146/annurev.fl.24.010192.001525`.

[42] Horia I. Petrache, Steven W. Dodd, and Michael F. Brown. Area per lipid and acyl length distributions in fluid phosphatidylcholines determined by 2H NMR spectroscopy. *Biophysical Journal*, 79(6):3172–3192, 2000. ISSN 00063495. doi: 10.1016/S0006-3495(00)76551-9.

[43] R. Pratibha, W. Park, and I. I. Smalyukh. Colloidal gold nanosphere dispersions in smectic liquid crystals and thin nanoparticle-decorated smectic films. In *Journal of Applied Physics*, volume 107, 2010. doi: 10.1063/1.3330678.

[44] Hilde A. Rinia and Ben De Kruijff. Imaging domains in model membranes with atomic force microscopy. In *FEBS Letters*, volume 504, pages 194–199, aug 2001. doi: 10.1016/S0014-5793(01)02704-1.

[45] Safran and S. A. Statistical Thermodynamics of Surfaces. *Interfaces, and Membranes*, 1994.

[46] Christian D. Santangelo. Geometry and the nonlinear elasticity of defects in smectic liquid crystals. *Liquid Crystals Today*, 15(3):11–18, sep 2006.

ISSN 1358-314X. doi: 10.1080/14645180601168117. URL http://www.tandfonline.com/doi/abs/10.1080/14645180601168117.

[47] Bernhard Sebastian, Tobias Favero, and Petra S. Dittrich. The Effects of Shear Force Transmission Across Vesicle Membranes. *Journal of Physical Chemistry Letters*, 8(24):6128–6134, dec 2017. ISSN 19487185. doi: 10.1021/acs.jpclett.7b02676.

[48] P. Sens and M. S. Turner. Inclusions in Thin Smectic Films. *Journal de Physique II*, 7(12):1855–1870, dec 1997. ISSN 1155-4312. doi: 10.1051/jp2:1997218. URL http://www.edpsciences.org/10.1051/jp2:1997218.

[49] P. Sens, M. S. Turner, and P. Pincus. Particulate inclusions in a lamellar phase. *Physical Review E - Statistical Physics, Plasmas, Fluids, and Related Interdisciplinary Topics*, 55(4):4394–4405, 1997. ISSN 1063651X. doi: 10.1103/PhysRevE.55.4394.

[50] Kai Simons and Winchil L C Vaz. Model systems, lipid rafts, and cell membranes. *Annual review of biophysics and biomolecular structure*, 33:269–95, 2004. ISSN 1056-8700. doi: 10.1146/annurev.biophys.32.110601.141803. URL http://www.ncbi.nlm.nih.gov/pubmed/15139814.

[51] S. J. Singer and Garth L. Nicolson. The fluid mosaic model of the structure of cell membranes. *Science*, 175(4023):720–731, 1972. ISSN 00368075. doi: 10.1126/science.175.4023.720.

[52] Shri Singh and Professor David A Dunmur. *Liquid Crystals: Fundamentals*. WORLD SCIENTIFIC, nov 2002. ISBN 978-981-02-4250-3. doi: 10.1142/4369.

[53] Andrey Sokolov and Igor S. Aranson. Physical properties of collective motion in suspensions of bacteria. *Physical Review Letters*, 109(24):248109, dec 2012. ISSN 00319007. doi: 10.1103/PhysRevLett.109.248109.

[54] Stephen Lower. Liquid Crystals, 2019. URL https://chem.libretexts.org/Bookshelves/Physical{_}and{_}Theoretical{_}Chemistry{_}Textbook{_}Maps/Supplemental{_}Modules{_

}(Physical{_}and{_}Theoretical{_}Chemistry)/Physical{_}Properties{_}of{_}Matter/States{_}of{_}Matter/Liquid{_}Crystals.

[55] Robert J. Stokes and D. Fennell. Evans. *Fundamentals of interfacial engineering*. Wiley-VCH, 1997. ISBN 9780471186472.

[56] Lobat Tayebi, Yicong Ma, Daryoosh Vashaee, Gang Chen, Sunil K. Sinha, and Atul N. Parikh. Long-range interlayer alignment of intralayer domains in stacked lipid bilayers. *Nature Materials*, 11(12):1074–1080, dec 2012. ISSN 14761122. doi: 10.1038/nmat3451.

[57] Lobat Tayebi, Atul N. Parikh, and Daryoosh Vashaee. Interlamellar organization of phase separated domains in multi-component lipid multilayers: Energetic considerations. *International Journal of Molecular Sciences*, 14 (2):3824–3833, feb 2013. ISSN 16616596. doi: 10.3390/ijms14023824.

[58] Mario Theers, Elmar Westphal, Gerhard Gompper, and Roland G. Winkler. Modeling a spheroidal microswimmer and cooperative swimming in a narrow slit. *Soft Matter*, 12(35):7372–7385, aug 2016. ISSN 17446848. doi: 10.1039/c6sm01424k.

[59] T E Thompson and T W Tillack. Organization of glycosphingolipids in bilayers and plasma membranes of mammalian cells. *Annual review of biophysics and biophysical chemistry*, 14:361–86, 1985. ISSN 0883-9182. doi: 10.1146/annurev.bb.14.060185.002045. URL http://www.ncbi.nlm.nih.gov/pubmed/2988578.

[60] Hans Wilhelm Trissl and Christian Wilhelm. Why do thylakoid membranes from higher plants form grana stacks? *Trends in Biochemical Sciences*, 18(11):415–419, 1993. ISSN 09680004. doi: 10.1016/0968-0004(93)90136-B.

[61] Yuhai Tu and John Toner. How birds fly together: Long-range order in a two-dimensional dynamical XY model. *Physical Review Letters*, 75(23): 11, dec 1995. ISSN 0031-9007. doi: 10.1103/PhysRevLett.75.4326. URL http://arxiv.org/abs/adap-org/9506001.

[62] M. S. Turner and P. Sens. Interactions between particulate inclusions in a smectic-A liquid crystal. *Physical Review E - Statistical Physics, Plasmas, Fluids, and Related Interdisciplinary Topics*, 55(2):R1275–R1278, 1997. ISSN 1063651X. doi: 10.1103/PhysRevE.55.R1275.

[63] M. S. Turner and P. Sens. Multipole expansion for inclusions in a lamellar phase. *Physical Review E - Statistical Physics, Plasmas, Fluids, and Related Interdisciplinary Topics*, 57(1):823–828, 1998. ISSN 1063651X. doi: 10.1103/PhysRevE.57.823.

[64] Matthew S. Turner and P. Sens. Inclusions on fluid membranes anchored to elastic media. *Biophysical Journal*, 76(1 I):564–572, jan 1999. ISSN 00063495. doi: 10.1016/S0006-3495(99)77224-3.

[65] Gerrit Van Meer, Dennis R. Voelker, and Gerald W. Feigenson. Membrane lipids: Where they are and how they behave, feb 2008. ISSN 14710072.

[66] Tams Vicsek, Andrs Czirk, Eshel Ben-Jacob, Inon Cohen, and Ofer Shochet. Novel type of phase transition in a system of self-driven particles. *Physical Review Letters*, 75(6):1226–1229, 1995. ISSN 00319007. doi: 10.1103/PhysRevLett.75.1226.

[67] Francis G. Woodhouse and Raymond E. Goldstein. Shear-driven circulation patterns in lipid membrane vesicles. *Journal of Fluid Mechanics*, 705:165–175, aug 2012. ISSN 00221120. doi: 10.1017/jfm.2012.118.

[68] Xiao-Lun Wu and Albert Libchaber. Particle Diffusion in a Quasi-Two-Dimensional Bacterial Bath. *Physical Review Letters*, 84(13):3017–3020, mar 2000. ISSN 0031-9007. doi: 10.1103/PhysRevLett.84.3017. URL `https://link.aps.org/doi/10.1103/PhysRevLett.84.3017`.

[69] Shuang Zhou, Andrey Sokolov, Oleg D. Lavrentovich, and Igor S. Aranson. Living liquid crystals. *Proceedings of the National Academy of Sciences of the United States of America*, 111(4):1265–1270, jan 2014. ISSN 00278424. doi: 10.1073/pnas.1321926111.